IEEE Access
Multidisciplinary | Rapid Review | Open Access Journal

Date of publication xxxx 00, 0000, date of current version xxxx 00, 0000.

Digital Object Identifier 10.1109/ACCESS.2019.DOI

Low-Density Spreading Codes for NOMA Systems and a Gaussian Separability Based Design

MICHEL KULHANDJIAN[1], *Senior Member, IEEE*, **HOVANNES KULHANDJIAN[2]**, *Senior Member, IEEE*, **CLAUDE D'AMOURS[1]**, *Member, IEEE* **and LAJOS HANZO[3]**, *Fellow, IEEE*

[1]School of Electrical Engineering and Computer Science, University of Ottawa, Ottawa, Ontario, K1N 6N5, Canada (e-mail: mkk6@buffalo.edu,cdamours@uottawa.ca)

[2]Department of Electrical and Computer Engineering, California State University, Fresno, Fresno, CA 93740, U.S.A. (e-mail: hkulhandjian@csufresno.edu)

[3]Electronics and Computer Science, University of Southampton, Southampton, SO17 1BJ, U.K. (e-mail: lh@ecs.soton.ac.uk)

Corresponding author: Michel Kulhandjian (e-mail: mkk6@buffalo.edu).

L. Hanzo would like to acknowledge the financial support of the Engineering and Physical Sciences Research Council projects EP/N004558/1, EP/P034284/1, EP/P034284/1, EP/P003990/1 (COALESCE), of the Royal Society's Global Challenges Research Fund Grant as well as of the European Research Council's Advanced Fellow Grant QuantCom.

This project was partially funded by C. D'Amours' NSERC Discovery Grant.

ABSTRACT Improved low-density spreading (LDS) code designs based on the Gaussian separability criterion are conceived. We show that the bit-error-rate (BER) hinges not only on the minimum distance criterion, but also on the average Gaussian separability margin. If two code sets have the same minimum distance, the code set having the highest Gaussian separability margin will lead to a lower BER. Based on the latter criterion, we develop an iterative algorithm that converges to the best known solution having the lowest BER. Our improved LDS code set outperforms the existing LDS designs in terms of its BER performance both for binary phase-shift keying (BPSK) and for quadrature amplitude modulation (QAM) transmissions. Furthermore, we use an appallingly low-complexity minimum mean-square estimation (MMSE) and parallel interference cancellation (PIC) (MMSE-PIC) technique, which is shown to have comparable BER performance to the potentially excessive-complexity maximum-likelihood (ML) detector. This MMSE-PIC algorithm has a much lower computational complexity than the message passing algorithm (MPA)[a].

[a]Code sets for MPA are designed similar to low-density parity-check (LDPC) codes to avoid cycles and to increase girth of the Tanner graph, code sets that are "optimal" for MMSE-PIC might not be optimal for MPA.

INDEX TERMS Non-orthogonal multiple-access (NOMA), low-density spreading signatures (LDS), sparse-code multiple-access (SCMA).

NOMENCLATURE

5G	The fifth generation
6G	The sixth generation
APP	A posteriori probability
AWGN	Additive white Gaussian noise
BBPSO	Bare-bone particle swarm optimization
BER	Bit-error-rate
BICM	Bit-interleaved coded modulation
BLER	Block error rate
BP	Believe propagation
BPSK	Binary phase-shift keying
CDMA	Code-division multiple access
CIR	Channel impulse response
CM	Coded modulation
D2D	Device-to-device
D2E	Device-to-everything
DE	Domain equalization
ED	Euclidean distance
EMB	Enhanced mobile broadband
EXIT	Extrinsic information transfer
FBMC	Filter-bank multicarrier
FDMA	Frequency division multiple access

FIR	Finite impulse response
GML	Global maximum likelihood detector
IoT	Internet-of-Things
IoV	Internet of Vehicles
IrLDS	Irregular low-density spreading
ITS	Intelligent transportation system
JSG	Joint sparse graph
LDPC	Low-density parity-check
LDS	Low-density spreading
LDSM	Low-density superposition modulation
LDSMA	Low-density spreading multiple access
LLR	Log-likelihood ratio
LRS	Large random spreading
LTE	Long-term evolution
M2M	Machine-to-machine
MAI	Multiple-access interference
MAP	Maximum a posteriori detector
MC	Multicarrier
MF	Matched filter
MIMO	Multiple-input multiple-output
ML	Maximum-likelihood
MLCM	Multilevel coded modulation
MMSE	Minimum mean-square estimation
mMTC	Massive machine-type-communications
mmWave	Millimeter-wave
MPA	Message passing algorithm
MS	Mobile station
MUD	Multiuser detection
MUSA	Multiuser shared access
MWBE	Maximum-Welch-bound-equality
NOMA	Non-orthogonal multiple access
OFDM	Orthogonal frequency-division multiplexing
OMA	Orthogonal multiple access
PDA	Probabilistic data association
PDMA	Pattern division multiple access
PEG	Progressive edge-growth
PIC	Parallel interference cancellation
QAM	Quadrature amplitude modulation
QLSS	Quasi-large sparse sequence
QPP	Quadratic permutation polynomial
QPSK	Quadrature phase-shift keying
RE	Resource element
SCDMA	Sparse code-division multiple-access
SCMA	Sparse code multiple access
SD	Sphere-decoding algorithm
SEP	Symbol error probability
SER	Symbol error rate
SFBC	Space-frequency block codes
SIC	Successive interference cancellation
SINR	Signal-to-interference-noise ratio
SISO	Soft-input soft-output
SM	Spatial modulation
SNR	Signal-to-noise ratio
SVE	Spreading vector extension
TCM	Trellis-coded modulation
TDMA	Time-division multiple access
TSC	Total squared correlation
TTCM	Turbo trellis-coded modulation
UD	Uniquely decodable
uRLLC	Ultra-reliable low-latency communications
VA	Viterbi algorithm
WBE	Welch-bound-equality
ZF	Zero-forcing filter

I. INTRODUCTION

High spectral- and power-efficiency, massive connectivity and low latency are among the requirements for next generation communications and these requirements are expected to increase in the future, as researchers turn their efforts towards sixth generation (6G) wireless communications. Enhanced mobile broadband (EMB), ultra-reliable low-latency communications (uRLLC) and massive machine-type communication (mMTC) support a suite of compelling applications driving these requirements. Massive multiple-input multiple-output (MIMO), non-orthogonal multiple access (NOMA) and millimeter-wave (mmWave) communications constitute promising techniques of addressing these stringent requirements [1].

In the previous generations spanning from 1G to 4G, the multiple access schemes were exclusively characterized by orthogonal multiple access (OMA) techniques, where users are assigned unique, user-specific resources in either frequency- (frequency-division multiple access (FDMA)), time- (time-division multiple access (TDMA)) or code-domain (code-division multiple access (CDMA)). However, the multiple access scheme of 5G is required to support a wide range of use cases, including a massive number of low-power Internet-of-Things (IoT) devices, device-to-device (D2D) communications, device-to-everything (D2E), the Internet of Vehicles (IoV), as well as seamless machine-to-machine (M2M) communications [2]–[6]. The mMTC mode includes, for example, e-health services, smart cities/villages, e-farms, and intelligent transportation systems (ITS) [7], [8]. They require improved connectivity compared to previous generations of wireless communications.

Supporting a large number of users communicating over a common channel may not be readily achievable by OMA techniques due to presence of multiple-access interference (MAI) in rank-deficient systems, where the number of users is higher than that of the resource blocks. To meet the demand of increased bandwidth efficiency in synchronous CDMA, a dense spreading NOMA CDMA concept was introduced in [9], which can support many more users for a given code length compared to traditional CDMA. A number of signature designs have been conceived [10]–[12], where low cross-correlation sequence sets are designed to minimize the overall MAI, which allows more users to simultaneously access the common channel. This in turn results in increased spectral efficiency.

Using low cross-correlation sequence sets might not be the best design policy for highly rank-deficient systems. One of the important design criteria in such rank-deficient systems is for the code set to be uniquely decodable (UD) [9]. By definition, the UD codes can be unambiguously decoded in a noiseless channel using linear recursive decoders [13]. Low-complexity linear decoders were introduced for these UD code sets using either binary $\{0,1\}$, or antipodal $\{\pm 1\}$, or alternatively ternary $\{0,\pm 1\}$ chips in [14]–[16]. Although these code set designs attain a substantial increase in system capacity even with the aid of low-complexity detectors, they only perform well for synchronous transmission over non-dispersive fading channels, such as additive white Gaussian noise (AWGN) channels. To satisfy the UD criterion, all the users have to rely on accurate transmit power control so that their signals are received with equal power. In practice, the wireless transmission channel exhibits, numerous impairments, such as frequency-selective multipath fading, and unequal received power. Another limitation of linear decoders is that they do not produce soft output decisions required by the channel decoders.

To combat the MAI at a reasonable cost, many researchers have proposed the construction of sparsely structured sequences for multiple access so as to take advantage of efficient sparse signal processing, relying for example on the message passing algorithm (MPA) for reducing to reducing the complexity of multiuser detection (MUD). These challenges can be addressed by the introduction of sparse spreading based NOMA techniques, which can be categorized into power-domain NOMA (PDM-NOMA) [1], [17]–[20] and code-domain NOMA (CDM-NOMA) [21]. A few of the strong contenders of CDM-NOMA are low-density spreading aided CDMA (LDS-CDMA) [22], low-density spreading assisted orthogonal frequency-division multiplexing (LDS-OFDM) [23], sparse code multiple access (SCMA) [24], [25], irregular LDS (IrLDS), pattern division multiple access (PDMA) [26] and multi-user shared access (MUSA) [27]. The LDS can be considered a special case of SCMA, which may also be characterized by sparse codebooks, each of which can be expressed as the Kronecker product of a sparse sequence denoted by $\mathbf{s}_j$, and a constellation set of order M. Specifically, we have:

$$\mathbf{X}_j = [\mathbf{s}_j\beta_1, \mathbf{s}_j\beta_2, \ldots, \mathbf{s}_j\beta_M], \tag{1}$$

where $\{\beta_1, \beta_2, \ldots, \beta_M\}$ indicates a constellation set. Hence, the rank of the users' LDS codebooks, $\mathbf{X}_j$, is equal to one. However, this is not the case for the users' SCMA codebooks. The rank of SCMA codebooks is higher than one and it is equal to the number of non-zero values in the SCMA waveforms. The comparison between direct sequence CDMA (DS-CDMA), multicarrier CDMA (MC-CDMA), LDS-OFDM and SCMA is illustrated in Fig. 1. Readers are referred to surveys of SCMA [28] and signature-based NOMA [29] for further reading.

CDM-NOMA offers flexible resource element (RE) allocation where the sparsity may be flexibly configured for handling time-variant user-loads. It performs well in terms of handling the MAI imposed by rank-deficient systems

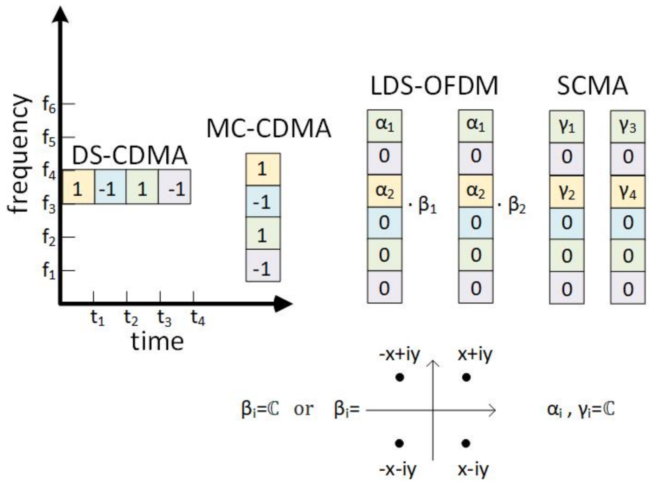

FIGURE 1. Multiple access technique comparisons.

and has low-complexity receivers compared to conventional dense spreading based CDMA. LDS, may also be appropriate for IoT communications [21] and it is also considered as a potential candidate for the uplink of mMTC [21].

There have been various criteria for the optimization of sparse spreading based NOMA [30]–[43], which maps the signals of users to REs in a sparse manner, whilst relying on the constellation shaping of non-zero entries [31], [32], and accurate power allocation for each spreading sequence [44]. The RE mapping methods can be broadly divided into two types; a) regular RE mapping, where the spreading densities of all users are the same, as in LDS-OFDM and b) irregular RE mapping, where the densities are non-identical, as in IrLDS and PDMA. Constellation shaping can be categorized into a) widely studied constellations $\{0,1\}$ [31], binary phase-shift keying (BPSK) [45], quadrature phase-shift keying (QPSK) [39], quadrature amplitude modulation (QAM) [39], etc., b) two-dimensional constellation bounded in unit circle [32], c) or any other constellations. The power allocation of each spreading sequence can be divided into two classes a) equal power, b) unequal power among all users.

A. RELATED LITERATURE

Spreading sequences of the low-density type containing many zeros were first introduced in [30] supporting low-complexity MUD. The introduction of cyclically shifted LDS design [30] allows maximum-likelihood (ML) detection to be carried out by computationally efficient methods, such as the Viterbi algorithm (VA) when BPSK modulation is used. It is widely recognized that finding the ML solution is generally NP-hard [46]. Various sub-optimal solutions can be applied such as sphere-decoding (SD) [47], probabilistic data association (PDA) [48], decision-feedback methods [49] etc. The problem, however, becomes more difficult if the system is rank-deficient. The complexity of the decoding process is crucial with the advent of iterative turbo detection, the so-called turbo MUD algorithm approximates the complex optimum joint detection scheme by iteratively exchanging soft decision variables between the multiuser detector and single-user soft-input soft-output (SISO) channel decoders. Based on this idea Hoshyar *et al.* [31] showed that iterative decoding is necessary for fully exploiting the LDS structure. To further exploit the lower complexity of iterative detection, sparse spreading sequences were conceived [22], [31], [32]. The family of low-density parity-check (LDPC) codes has been shown to be attractive due to its capacity-approaching capability and decoding simplicity, when using the MPA. This is why, Hoshyar *et al.* [31] proposed an LDS structure based on LDPC codes, where the user's symbol are arranged in such a way that the interference seen by each user at each chip is different. Explicitly, the specific choice of the non-zero entries is in perfect harmony with the particular choice of the LDPC indicator matrix that defines the structure of the LDS code matrix. As a further advance, a near-optimum chip-level SISO iterative MUD is developed in [22] for the LDS structure for transmission over AWGN channels. It was shown to yield promising performance for rank-deficient systems, especially, for BPSK modulation [22], where the emphasis was on the MUD structure, rather than on design of spreading sequences having particular structure, which were found by simple trial and error under a unit amplitude constraint. In contrast to [22] a structured approach focusing on the design of spreading sequences was proposed by Van de Beek and Popović [32] based on the LDPC indicator matrix. In general, signatures having a unity scalar magnitude are designed by maximizing their minimum distance. Moreover, Van de Beek and Popović advocated the so-called Latin-rectangular mappings, where not only the non-zero elements of each row are distinct, but also those in each column, because they are capable of significantly outperforming a randomly generated signature matrix, as a benefit of their high minimum distance.

It is widely recognized that the global search based maximum likelihood (GML) detector approaches the single-user bit-error-rate (BER), at high signal-to-noise ratios (SNR), when using long random spreading (LRS) sequence based CDMA [50]. Inspired by the LRS-CDMA concept, Sun and Xiao [45], [50] proposed the so-called quasi-large sparse sequence (QLSS) - CDMA concept by replacing the dense sequences of QLRS-CDMA by sparse sequences.

The specific constructions of LDS signatures found in [31], [32] have been inspired by classic LDPC code designs in order to facilitate the employment of the MPA algorithm. Safavi *et al.* [33] considered schemes, where the spreading and mapping to conventional QAM constellations are performed separately. Their proposed recursive matrix construction has been optimized for maximizing the Euclidean distance.

Apart from the fact that the multiple access sequences play a key role in NOMA for supporting low-complexity detection, they determine the achievable sum rate. Qi *et al.* [34] analyze the sparsity of the sum capacity-achieving sequences and propose a beneficial construction method with the aid of classic frame theory [51]. The particular low-density spreading sequence design that maximizes the sum rate based on frame theory for complex zero-mean Gaussian random variables is presented in [34], where each row has almost the same number of non-zero entries, forming a nearly regular sparse spreading sequences. In contrast to this design, Yu *et al.* [40] proposed the simultaneous optimization of the RE assignment and power allocation among REs, where the users employing the same radio resource have different channel gains. It was achieved by first formulating a sum-rate optimization problem subject to practical sparsity and power constraints.

In 2017, Qi *et al.* [37] formulated an optimization problem for specifically designing the sparsity of spreading sequences, while maximizing the efficiency of NOMA subject to the maximum tolerable symbol error rate (SER) as well as to the affordable detection complexity. Another challenge is the construction of the sparse matrix that optimizes the performance of the MPA detector, since there are no closed-form expressions for characterizing the detection performance of MPA for sparse sequences. Despite this shortcoming, Qi *et al.* [35] proposed a systematic technique for constructing the sparse sequences relying on a hierarchical method with the objective of optimizing the performance of MPA for BPSK modulation. For the given SNR and target factor graph girth, the algorithm produces the optimum sparsity. Based on the optimum sparsity and the minimum girth, the algorithm directly produces the position of non-zero entries in the matrix. Lastly, the particular values of non-zero entries are determined by specifically maximizing the minimum distance. Wang *et al.* [42] took a step further by combining multicarrier (MC) LDS and channel coding schemes into a joint sparse factor graph and quantified the average BER based on the mean and variance of the soft information distribution obtained. Explicitly, through their theoretical analysis, the average BER has been derived based on the mean and variance of the soft information distribution at the output of the joint sparse factor graph. The proposed design produces the optimal degree distribution of LDS spreading capable of approaching the theoretical capacity in terms of SNR.

The optimization of sparse matrices is typically carried out by assuming to have Gaussian input signal, which is suboptimal, for practical discrete constellations. Xiao *et al.* [52] proposed a codebook design for multicarrier-low-density spreading aided multiple access (MC-LDSCMA) based on the maximization of the minimal user rate for practical finite alphabet signalling.

Another LDS signature spreading vector extension (LDS-SVE) method is introduced by Zhang *et al.* [38] for uplink OFDM systems. Compared to LDS-OFDM, LDS-SVE jointly transforms and spreads a pair of modulated symbols across four subcarriers. This is achieved upon multiplying the real and imaginary parts of two modulated symbols by a transformation matrix, which is optimized by minimizing the single-user BER.

LDS designs that are based on the sparseness of the LDPC parity check matrix [31], [32] are typically considered as having a regular parity check matrix. By contrast, Jiang and Wu *et al.* [36] proposed a low-density superposition modulation (LDSM) scheme that is based on an irregular parity check matrix, which provides both diversity and coding gains, hence improving both the overall average performance as well as the cell-edge performance. The progressive edge-growth (PEG) algorithm is utilized to construct the LDSM matrix. A compelling systematic technique of designing the degree distribution of the LDSM signature matrices is proposed by Lu and Jiang in [43], which is based on the powerful extrinsic information transfer (EXIT) chart tool and the so-called bare-bone particle swarm optimization (BBPSO) algorithm they optimize the degree distribution of LDSM signature matrices. Their EXIT chart analysis in rightfully characterizes the resultant design. Similarly, Zhang *et al.* in [41] proposed a pair of sparse superposition matrices.

Similar to the minimum distance criterion based LDS code design of [35] developed for BPSK modulation, Song *et al.* address the maximization of the minimum Euclidean distance for QAM constellations in [39]. More explicitly, signature matrices having factor graphs exhibiting very few short cycles and large superposed signal constellation distances are designed by Song *et al.* In short, for a given factor graph structure the algorithm produces the optimal signature matrix associated with the maximum LDS code distance. The LDS code set of Song *et al.*, which are detected both by the MPA and the ML detector, exhibit an excellent performance.

By expanding the traditional direct sequence CDMA to NOMA, Liu *et al.* [53] developed a cyclic shift based multiple access scheme, where the in-phase and quadrature-phase channels are used for transmitting the data and pilots, respectively. In contrast to conventional SCMA, which is based on geometric shaping design, Jiang and Wang [54] combine both geometric and probability-based for increasing the channel capacity and reducing the BER. As a benefit of using a sparse spreading matrix, low-complexity iterative MUD can be employed. Song *et al.* [55] propose super-sparse on-off division multiple access using spreading waveforms based on idling. On the other hand, Ye *et al.* [56] resort to using a deep multi-task learning technique for optimizing an end-to-end NOMA system. As a further development, Xie *et al.* [57] design constellations for non-coherent reception of the signals arriving from multiple users, and reduce the SER simultaneously. Combinatorial structures relying on the so-called balanced incomplete block design have also been widely studies in the context of LDPC constructions. The designs of Lan *et al.* [58] used as sparse codes have better interference properties, hence they provide higher user/bandwidth efficiency and have the flexibility of creating variable code rates. Motivated by this fact, Wu *et al.* [59] proposed LDS designs based on Steiner codes [60], whose incidence matrix conviniently supports superposition based multiuser communications. By using algebraic code construction methods, Liu *et al.* in [44] proposed power-imbalanced LDS designs of the non-zero entries for a given factor graph with the aid of Eisenstein integers[i].

According to the above construction designs and studies, the sparsity of spreading sequences, significantly influences the performance of MUD due to its crucial impact on the MAI characteristics. Since the performance analysis of finite-size multiuser systems is mathematically intractable, the large-system limit based analysis was provided in [61]–[63]. By deriving a probability density model for the non-zero entries of sparse spreading sequences, a method based on statistical mechanics was proposed to analyze the optimal detection performance in [63] and the spectral efficiency of the scheme in [61].

The theoretical analysis of LDS systems in the presence of flat fading channel in terms of their spectral efficiency relying on both linear and non-linear optimum receivers (such as maximum *a posteriori* detector) was carried out in the large-system limit in [64]. Furthermore, the channel capacities of SCMA and low-density spreading multiple access (LDSMA) schemes are analyzed in [65] and compared to that of the Gaussian multiple access channel imposing random phase rotations and fast fading. The performance advantage of LDSMA, which exploits the high degree of flexibility of subcarrier allocation, has been demonstrated in [66]. The results showed that the diversity gain attained improves the link-level performance in terms of the achievable block error rate (BLER).

The capacity region of uncoded LDS schemes communicating over a multiple access channel is analysed in [77]. However, low-complexity of MPA decoding of LDS as a multiple access technique has a lower capacity than successive decoding [78]. For the coded LDS multiple access channel the mutual information transfer characteristics of turbo MUD applied to LDS-OFDM is studied using EXIT charts in [79].

The rigorous information-theoretic analysis of infinite graphs showed that having a regular user-to-RE allocation is advantageous [80]. However, increasing the pattern matrix dimensionality results in a significantly increased detection complexity. Moreover, the rigorous closed-form analytical expression of the spectral efficiency of regular sparse sequence based NOMA relying on optimum decoding in terms of spectral efficiency is derived in [81], for Gaussian signaling over non-fading channels in the asymptotic large-system limit.

The LDS concept was applied in various attractive communication systems. As an example, Hoshyar *et al.* [67] and Al-Imari *et al.* [82] used LDS structures for spreading the

[i]Eisenstein integers, also known as Eulerian integers, are complex numbers of the form $z = a + b\omega$, where $a, b \in \mathbb{N}$ and $\omega = \frac{-1+i\sqrt{3}}{2} = e^{\frac{2\pi i}{3}}$ constitute a primitive cube root of unity.

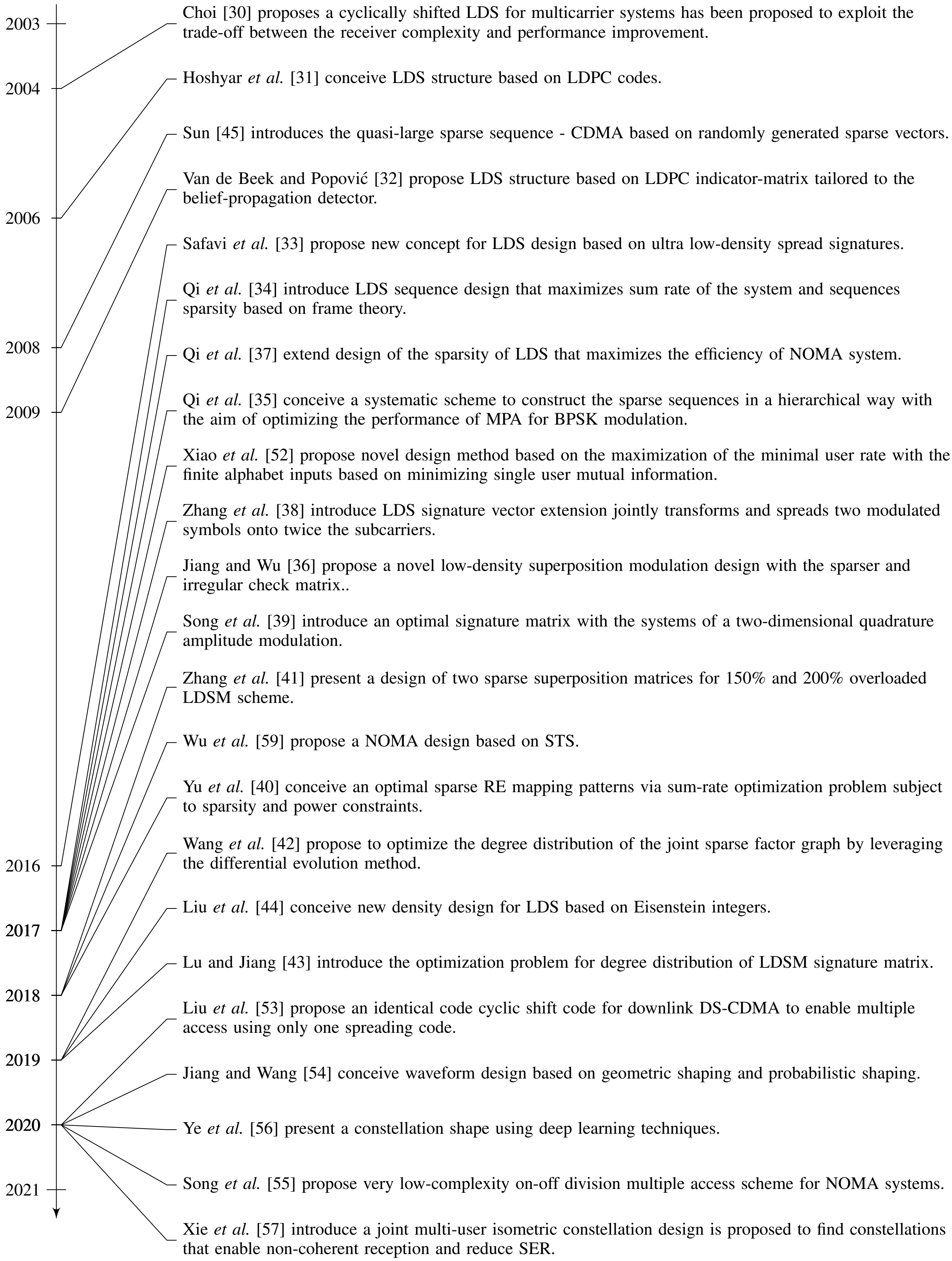

FIGURE 2. Timeline of LDS design contribution.

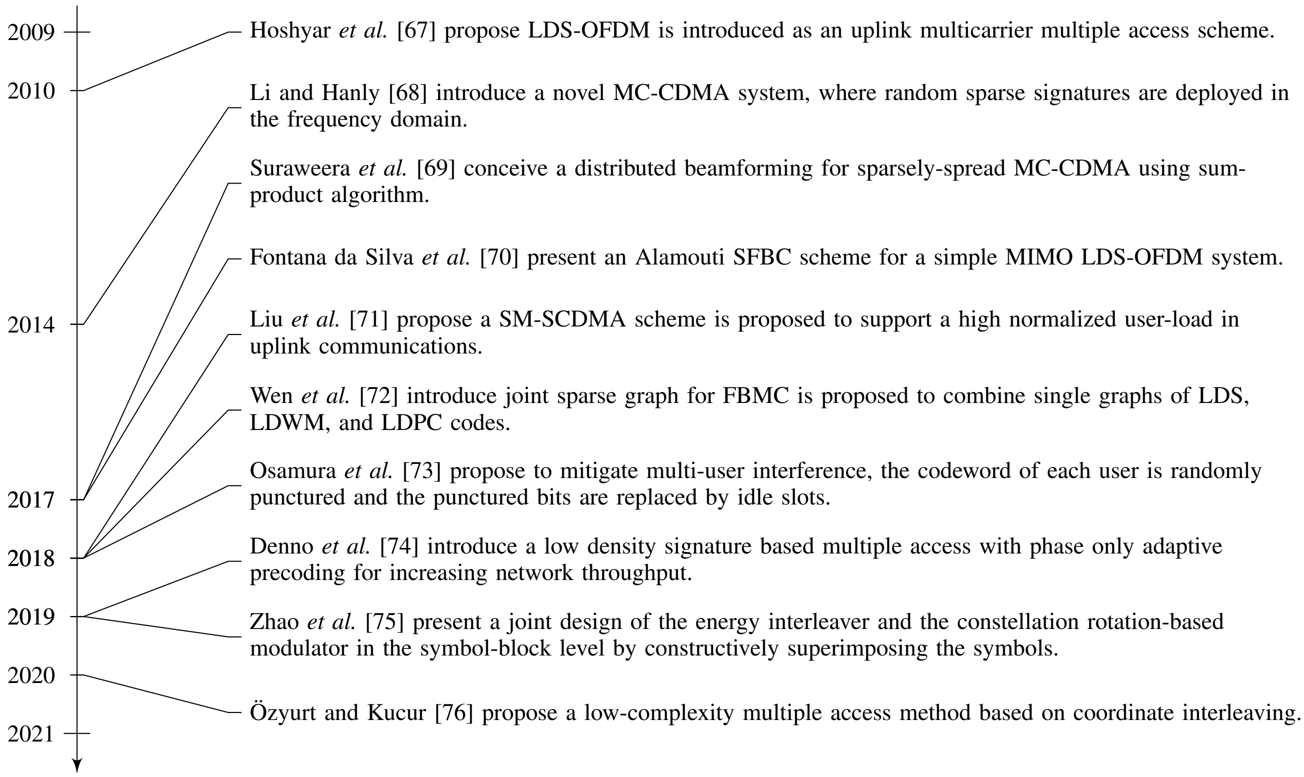

FIGURE 3. Timeline of LDS applied in applications.

TABLE 1. Contrasting our novel contributions to the state-of-the-art.

Contributions	This work	[56]	[53]	[40]	[39]	[35]	[34]	[33]	[32]
Minimum Euclidean distance	✓				✓				✓
Gaussian margin	✓								
Sum Capacity	✓			✓					
Maximum SINR per user	✓								
Adaptive to number of users	✓	✓	✓	✓	✓	✓	✓	✓	✓
Joint RE and constellation shaping	✓	✓				✓	✓	✓	✓
BER approach single user at $K/L = 2$	✓								

symbols across the frequency domain, hence their technique was termed as LDS-OFDM. Li and Hanly [68] and Li *et al.* [83] introduced MC-CDMA for downlink communication, where sparse random signatures are deployed in the frequency domain. A power-efficient non-linear transmit precoder weight optimization problem is formulated, while satisfying the maximum tolerable symbol error probability (SEP) targets at the mobile stations (MSs). Suraweera *et al.* [69] approached this problem by conceiving a distributed linear beamforming technique for the multicell MC-CDMA downlink by using the sum-product algorithm for detecting the sparse signatures. LDS spreading has also been proposed for MIMO systems by da Silva *et al.* [70]. Their proposed technique relies on Alamouti's space-frequency block codes (SFBC) conceived for low-complexity MIMO LDS-OFDM systems. As a parallel development in MIMO systems, spatial modulation (SM) has drawn a lot of research attention in recent years. Liu *et al.* [71] have proposed a sparse code-division multiple-access (SCDMA) scheme for supporting a high normalized user-load in uplink communications. Recently, filter-bank multicarrier (FBMC) transceivers have drawn a lot of attention as a benefit of circumventing several OFDM drawbacks. Wen *et al.* [72] designed a LDS-FBMC scheme, which applies LDS for constructing FBMC signals. Additionally, a joint sparse graph (JSG) based FBMC transceiver termed as JSG-FBMC was proposed for combining the single graphs of LDS, a low-density weight matrix, and LDPC codes, which represent popular NOMA, multicarrier modulation and channel coding techniques, respectively. Osamura *et al.* [73] proposed a new multi-user scheme for mitigating the multi-user interference, in which the codeword of each user is randomly punctured and the punctured bits represent idle slots, hence, only a small random set of users are active at each time. This constraint imposed on the number of concurrent users significantly reduces the multi-user detection complexity. As a further advance, Denno *et al.* [74] proposed 'phase-only' based transmit precoding in support of multiple user terminals having a single antenna.

As a further advance, Zhao *et al.* [75] designed an energy interleaver and constellation rotation-based modulator by exploiting the NOMA concept for improving the energy transfer efficiency of wirelessly powered systems. Similarly, Özyurt and Kucur [76] designed a low-complexity multiple access method for single-antenna nodes by exploiting the concept of signal space diversity by relying on the power-domain NOMA philosophy for reducing both the BER and the number of SIC iterations.

B. CONTRIBUTION

Compared to the design of conventional dense spreading sequences for classic CDMA, designing the LDS sequences for NOMA systems is more complicated, since the design should be implemented under the sparsity constraint of the signature matrix. In the literature, there is a paucity of optimal signature matrix designs exhibiting maximum minimum code distance.

Against this background, we study a range of different distance metrics and the properties of a sophisticated signature matrix. Table 1 boldly and explicitly contrasts the novelty of our design to the family of state-of-the-art LDS code set designs. Explicitly, our new contributions are summarized as follows:

(1) We propose a novel iterative LDS design algorithm for maximizing the signal-to-interference-noise ratio (SINR) of each individual user of interest which jointly maps the user-signals to REs in a sparse manner and applies constellation shaping tp tje non-zero entries.
(2) We demonstrate that the code sets having the highest minimum distance are also optimal in terms of the BER criterion for transmission over Gaussian channels. Furthermore, when the code sets have the same minimum distance, those associated with higher average Gaussian separability tend to exhibit better BER performance. We show that our improved LDS code set outperforms the existing LDS designs in terms of its BER performance for BPSK and 4QAM transmissions over AWGN, non-dispersive and frequency-selective fading channels.
(3) Moreover, we design both a minimum mean-square estimation (MMSE) based and a parallel interference cancellation (PIC) (MMSE-PIC) aided detector [84], both which exhibit a comparable BER performance to that of the high-complexity ML detector.

The rest of the paper is organized as follows. In Section II, we discuss the system model, followed by the specific properties and design criteria of the spreading codes in Section III. Our improved iterative LDS sequence design is presented in Section IV, followed by our detection method proposed for AWGN, non-dispersive and frequency selective fading channels in Section V. After illustrating our simulation results in Section VIII, our conclusion and design guidelines are drawn in Section IX.

The following notations are used in this paper. All boldface lower case letters indicate column vectors and upper case letters indicate matrices, $()^T$ denotes transpose operation, sgn denotes the sign function, $|.|$ is the scalar magnitude, $||\cdot||_p$ denotes ℓ_p norm, $||\cdot|| \triangleq ||\cdot||_2$ is vector norm and $\mathbb{E}\{\cdot\}$ denotes expected value.

II. SYSTEM MODEL

First of all, perfect chip synchronization among all the transmitters is assumed. This provides the best-case estimate of the performance of what is in reality a fully asynchronous system, which only requires chip synchronization between the source transmitter and the target receiver. The spreading sequence $\mathbf{c}_k \in \mathbb{C}^{L\times 1}$ is considered to be s-sparse, when s coefficients are non-zero and $(L-s)$ are zeros, with the non-zero coefficients located in $\mathcal{I}_k \subset \{1, 2, ..., L\}$. In the scope of LDS design $\mathbf{c}_k$ can be considered sparse if the cardinality of non-zero entries obeys $|\mathcal{I}_k| \leq L/2$. However, the sparsity metric is also discussed further in the next section.

A. AWGN CHANNEL

We assume that the data stream is partitioned into length-Q subsequences, $\mathbf{b}_k \triangleq [b_{k,1}, b_{k,2}, \ldots, b_{k,Q}]$, of k-th user bits $b_{k,i} \in \{0, 1\}$, for $1 \leq j \leq Q$. The modulator maps each subsequence $\mathbf{b}_k$ to a symbol x_k from the M-ary symbol alphabet $\mathcal{X}_k = \{x_{k,1}, x_{k,2}, \ldots, x_{k,M}\}$, where, $x_{k,m} \in \mathbb{C}$ corresponds to the bit pattern $\mathbf{b}_k(m) = [b^m_{k,1}, b^m_{k,2}, \ldots, b^m_{k,Q}]$ and $M = 2^Q$. Let the modulator's bijective mapping ψ_k, representing the binary-to-symbol conversion of user k be defined as

$$\psi_k : \mathbf{b}_k(m) \in \{0, 1\}^{Q\times 1} \mapsto a_m \in \mathcal{X}_k, \ \forall m, \qquad (2)$$

and vice versa, its inverse operation be represented by $\mathbf{b}_k(m) = \psi_k^{-1}(a_m)$, $b^m_{k,i} = a^i_m$, where a^i_m denotes the i-th bit of the binary vector $\psi_k^{-1}(a_m)$. Then, the users' symbols are multiplexed after spreading them using the LDS codes. Mathematically, we can formulate the system model as

$$\begin{aligned} \mathbf{y} &= \sum_{k=1}^{K} \mathbf{c}_k d_k x_k + \mathbf{n} \\ &= \mathbf{CDx} + \mathbf{n}, \end{aligned} \qquad (3)$$

where K is the number of the users, d_k is the k-th user's amplitude, $x_k \in \mathcal{X}_k$ is the k-th user's symbol to be transmitted from the constellation alphabet, $\mathcal{X}_k$,

$\mathbf{C} = [\mathbf{c}_1, \mathbf{c}_2, \dots, \mathbf{c}_K] \in \mathbb{C}^{L\times K}$ is the column-normalized LDS code matrix, $||\mathbf{c}_k|| = 1$ for $1 \le k \le K$, $\mathbf{n} \in \mathbb{C}^{L\times 1}$ is an L-dimensional complex-valued AWGN vector with variance of σ^2 and $\mathbf{D}$ is a diagonal matrix hosting the users' amplitude, which is given as

$$\mathbf{D} = \begin{bmatrix} d_1 & 0 & \cdots & 0 \\ 0 & d_2 & 0 & \vdots \\ \vdots & 0 & \ddots & 0 \\ 0 & \dots & 0 & d_k \end{bmatrix}. \tag{4}$$

We assume that the constellation alphabet of each user is identical, i.e., $\mathcal{X}_k = \mathcal{X}$, $\forall k$ and the cardinality of the constellation is $M = |\mathcal{X}|$. The block diagram of the LDS transmitter is shown in Fig. 4. Note that for the AWGN channel, we assume that $h_k = 1$ for $1 \le k \le K$.

B. NON-DISPERSIVE FADING CHANNEL

A channel is said to exhibit flat or non-dispersive Rayleigh fading if the coherence bandwidth of the channel is higher than the bandwidth of the signal. In this case, all of the received multipath components arrive within a delay that is much smaller than the symbol duration; where the symbol is defined as one chip in the case of LDS spread signals. These channel coefficients are circularly symmetric complex Gaussian random variables with zero mean and unit variance. The magnitudes of the channel gains are Rayleigh distributed. The model of the flat or non-dispersive fading channel can be represented as

$$\begin{aligned} \mathbf{y} &= \sum_{k=1}^{K} \mathbf{c}_k h_k d_k x_k + \mathbf{n} \\ &= \mathbf{CHDx} + \mathbf{n}, \end{aligned} \tag{5}$$

where h_k is the k-th user's channel coefficient and $\mathbf{H}$ is a diagonal matrix with channel coefficients as shown below,

$$\mathbf{H} = \begin{bmatrix} h_1 & 0 & \cdots & 0 \\ 0 & h_2 & 0 & \vdots \\ \vdots & 0 & \ddots & 0 \\ 0 & \dots & 0 & h_k \end{bmatrix}. \tag{6}$$

The block diagram of the transmitter model of an LDS system in non-dispersive fading channels is shown in Fig. 4.

C. FREQUENCY-SELECTIVE FADING CHANNEL

A channel is said to exhibit frequency-selective fading, if the coherence bandwidth of the channel is lower than the bandwidth of the signal. In other words, it occurs whenever the received multipath components of a symbol extend beyond the symbol's time duration. The multipath channel can be modeled by a tap delay line based finite impulse response (FIR) filter of length L_p [85]. The system model for uplink communication over the frequency-selective fading channel can be written as

$$\begin{aligned} \mathbf{y} &= \sum_{k=1}^{K} \mathbf{h}_k * (\mathbf{c}_k d_k x_k) + \mathbf{n} \\ &= \sum_{k=1}^{K} \bar{\mathbf{H}}_k \mathbf{c}_k d_k x_k + \mathbf{n}, \end{aligned} \tag{7}$$

where $\mathbf{h}_k = \frac{1}{\sqrt{L_p}}[h_{k,1}, h_{k,2}, \dots, h_{k,L_p}]^T$ is the k-th user's channel impulse response (CIR), $*$ is the convolution operator and $\bar{\mathbf{H}}_k$ is a channel matrix with the size of $(L + L_p - 1) \times L$ and is expressed as,

$$\bar{\mathbf{H}} = \begin{bmatrix} h_{k,L_p} & 0 & \cdots & \cdots & \cdots & \cdots & 0 \\ \vdots & \ddots & \ddots & \ddots & \ddots & \ddots & \vdots \\ h_{k,2} & \cdots & h_{k,L_p} & 0 & \cdots & \cdots & 0 \\ h_{k,1} & h_{k,2} & \cdots & h_{k,L_p} & 0 & \cdots & 0 \\ 0 & h_{k,1} & h_{k,2} & \cdots & h_{k,L_p} & \cdots & 0 \\ \vdots & \ddots & \ddots & \ddots & \ddots & \ddots & \vdots \\ 0 & \cdots & 0 & h_{k,1} & h_{k,2} & \cdots & h_{k,L_p} \\ 0 & \cdots & \cdots & 0 & h_{k,1} & \cdots & h_{k,L_p-1} \\ \vdots & \ddots & \ddots & \ddots & \ddots & \ddots & \vdots \\ 0 & \cdots & \cdots & \cdots & \cdots & \cdots & h_{k,1} \end{bmatrix}. \tag{8}$$

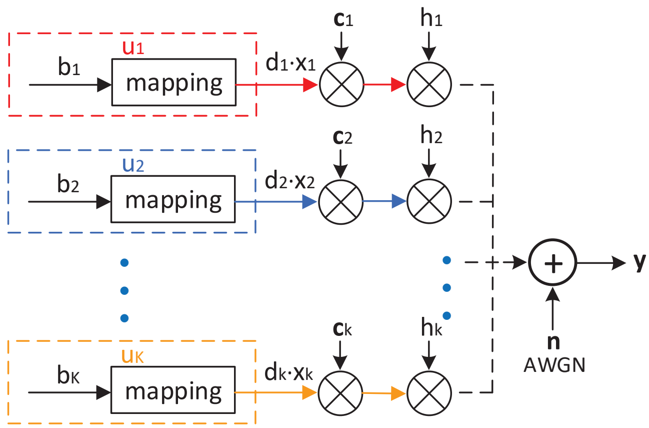

FIGURE 4. Transmitter of an LDS system communicating over non-dispersive fading channels.

The Gaussian random variables $h_{k,i}$ where $i = 1, 2, \dots, L_p$ have a zero mean and unit variance, while the factor $\frac{1}{\sqrt{L_p}}$ ensures that the channel gain experienced by the transmitted signal on average is unity. Here, we assume that the CIRs between users are independent from one another. The block diagram of the transmitter model of an LDS system for uplink communication over frequency-selective fading channel is shown in Fig. 5.

III. CODE PROPERTIES AND DESIGN CRITERIA

In this section, we first present some of the distance metrics that will be used in the development of an iterative algorithm with the intention of finding the improved LDS signature sets. Given the channel and receiver design specifics, the overall system performance is determined by the specific selection of the user signature set. One of the signature set metrics of interest is the minimum distance. The larger the distance, the better the performance in terms of BER. We recall that the minimum distance for the BPSK constellation $\mathcal{X} = \{\pm 1\}$ is 2 [ii].

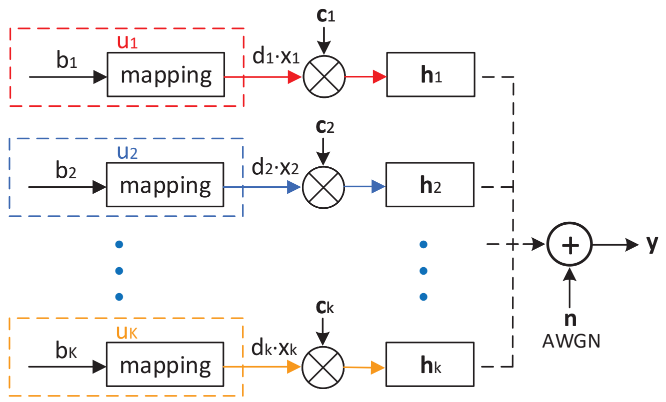

FIGURE 5. Transmitter of an LDS system communicating over frequency-selective fading channels.

A. DISTANCE METRICS

Definition III.1. The Euclidean distance of two L-dimensional vectors $\mathbf{y}_i$ and $\mathbf{y}_j$ for $i \neq j$ is given by

$$d_E(\mathbf{y}_i, \mathbf{y}_j) = ||\mathbf{y}_i - \mathbf{y}_j||_2, \tag{9}$$

where $\mathbf{y}_i = \mathbf{C}\mathbf{x}_i$, $\mathbf{y}_j = \mathbf{C}\mathbf{x}_j$, $\mathbf{x}_i, \mathbf{x}_j \in \mathcal{X}^{K\times 1}$ and $\mathbf{x}_i \neq \mathbf{x}_j$.

The minimum distance of the received vectors for a given code set can be formulated by

$$d_{E,min}(\mathbf{C}) = \underset{\substack{\mathbf{x}_i, \mathbf{x}_j \in \mathcal{X}^{K\times 1} \notin \{0\}^{K\times 1} \\ \mathbf{y}_i = \mathbf{C}\mathbf{x}_i, \mathbf{y}_j = \mathbf{C}\mathbf{x}_j}}{\operatorname{argmin}} d_E(\mathbf{y}_i, \mathbf{y}_j). \tag{10}$$

Theorem 1. *Let $\mathcal{C} \in \mathbb{C}^{L\times K}$ represent the set of all distinct sparse normalized column LDS matrices. Then $d_{E,min}(\mathcal{C})$ is equal to 2 when $\mathcal{X} = \{\pm 1\}$.*

Proof. Assume that $\mathbf{c}_i^T \mathbf{c}_j = 0$ for all $\mathcal{I}_i = \mathcal{I}_j$, $i \neq j$. Let $d_{E,min}(\mathcal{C}) = d_E(\mathbf{y}_n, \mathbf{y}_m)$, where $\mathbf{y}_n = \mathcal{C}\mathbf{x}_n$ and $\mathbf{y}_m = \mathcal{C}\mathbf{x}_m$. The difference vector $\mathbf{y} = \mathbf{y}_n - \mathbf{y}_m = \mathcal{C}(\mathbf{x}_n - \mathbf{x}_m) = \mathcal{C}\bar{\mathbf{x}}$ must have one non-zero element $\bar{x}_t \neq 0$, $x_{n,t} \neq x_{m,t}$, and $L-1$ zeros $\bar{x}_z = 0$, $x_{n,z} = x_{m,z}$ for $z \neq t$ to achieve $d_{E,min}$. Then $\bar{x}_t$ can only be 2 or -2, since we have $x_{n,t}, x_{m,t} \in \{\pm 1\}$. Therefore, the Euclidean distance obeys $||\mathbf{y}|| = ||\mathcal{C}\bar{\mathbf{x}}|| = ||2\mathbf{c}_t|| = 2||\mathbf{c}_t|| = 2$. □

Definition III.2. The product distance of two L-dimensional vectors $\mathbf{y}_i$ and $\mathbf{y}_j$ for $i \neq j$ is expressed by

$$d_P(\mathbf{y}_i, \mathbf{y}_j) = \prod_{t\in\mathcal{I}_{i,j}} |y_{i,t} - y_{j,t}|, \tag{11}$$

where $y_{i,t} - y_{j,t} \neq 0$ for all $t \in I_{i,j} \subset \{1, ..., L\}$. Let $d_{P,min}$ be the minimum product distance of the code set $\mathbf{C}$.

Definition III.3. The Manhattan distance [86] of two L-dimensional vectors $\mathbf{y}_i$ and $\mathbf{y}_j$ for $i \neq j$ is defined as

$$d_M(\mathbf{y}_i, \mathbf{y}_j) = ||\mathbf{y}_i - \mathbf{y}_j||_1. \tag{12}$$

Let $d_{M,min}$ be the minimum Manhattan distance of the code set $\mathbf{C}$.

B. CODE PROPERTIES

Another signature set metric of interest includes the total squared correlation, which can be linked to the MAI power associated with a code set.

Definition III.4. The total squared correlation (TSC) of $\mathbf{C}$ is the sum of the squared magnitudes of all inner products between signatures, which is expressed as

$$TSC(\mathbf{C}) = \sum_{i=1}^{K}\sum_{j=1}^{K} |\mathbf{c}_i^H \mathbf{c}_j|^2. \tag{13}$$

Let us denote, the number of bits per symbol x_k of user k by ρ_k. Then, there exists a K-dimensional capacity region $\Phi \subset \mathbb{R}^{K\times 1}$ for which each set of the number of bits/symbol also termed as the rate $\boldsymbol{\rho} = (\rho_1, \ldots, \rho_K)$ within this region can be achieved, while maintaining an infinitesimally low BER for every user, provided that the codeword length tends to infinity. In particular, the sum capacity C_{sum} over Φ is defined as

$$C_{sum} = \max_{\boldsymbol{\rho}\in\Phi} \sum_{k}^{K} \rho_k. \tag{14}$$

Definition III.5. The total sum capacity $C_{sum}(\mathbf{C}, \gamma)$ [87]–[89] in bits/symbol, defined as the maximum possible sum of the users' transmission rates attained, while still maintaining reliable reception of the signatures in an AWGN channel is expressed as

$$C_{sum}(\mathbf{C}, \gamma) = \log_2 |\mathbf{I}_L + \gamma \mathbf{C}\mathbf{P}\mathbf{C}^H|, \tag{15}$$

where we have $\mathbf{P} = \mathbf{D}\mathbb{E}\{\mathbf{x}\mathbf{x}^H\}\mathbf{D}^H$, γ is the received SNR of each user's signal[iii] and $\mathbf{I}_L$ is the $(L\times L)$-element identity matrix.

Definition III.6. The root-mean-square (RMS) cross-correlation and the maximum cross-correlation amplitude are expressed as

$$I_{rms}(\mathbf{C}) = \sqrt{\frac{1}{K(K-1)} \sum_{i=1}^{K}\sum_{j\neq i}^{K} |\mathbf{c}_i^H \mathbf{c}_j|^2}, \tag{16}$$

$$I_{max}(\mathbf{C}) = \max_{1\leq i<j\leq K} |\mathbf{c}_i^H \mathbf{c}_j|. \tag{17}$$

[ii] In signal space representation with the constellation points $\pm\sqrt{E_b/T_b}$ the minimum distance is expressed as $2\sqrt{E_b/T_b}$.

[iii] Here we assume identical received SNR for all user's signals.

Lemma 1. *The Welch Lower Bound [90] for any code set* $\mathbf{C}$*, with* $L \leq K$*, is expressed as*

$$I_{rms}(\mathbf{C}) \geq \sqrt{\frac{K-L}{(K-1)L}}, \tag{18}$$

with equality if and only if $\sum_{i=1}^{K} \mathbf{c}_i \mathbf{c}_i^H = \frac{K}{L}\mathbf{I}_L$*. Furthermore,*

$$I_{max}(\mathbf{C}) \geq \sqrt{\frac{K-L}{(K-1)L}}, \tag{19}$$

with equality if and only if

$$|\mathbf{c}_i^H \mathbf{c}_j| = \sqrt{\frac{K-L}{(K-1)L}} \quad \forall i \neq j. \tag{20}$$

The detailed proof of a well-known performance index that assesses the cross-correlation of the code matrix can be found in [90]. The spreading sequence $\mathbf{C}$ constitutes a Welch-bound-equality (WBE) and/or a maximum-Welch-bound-equality (MWBE) code matrix, when equality is satisfied in (18). Then I_{rms} meets the Welch bound and/or (19) meets the Welch bound on I_{max}. Since the MWBE is a stricter bound than the WBE, a MWBE code matrix is said to be a WBE matrix, but not vice versa. The Welch bound (19) is tight for smaller values of K, but becomes quite loose for larger K. It is a challenge to find $\mathbf{C}$ associated with an arbitrary L and K that can satisfy the Welch bound on I_{max}, (19). As an example, it is widely recognized that there is no $\mathbf{C}$ that satisfies the Welch bound on I_{max} when $K > L^2$ in the complex case, $\mathbf{C} \in \mathbb{C}^{L\times K}$, or when $K > L(L+1)/2$ in the real case $\mathbf{C} \in \mathbb{R}^{L\times K}$. Note that the expressions for the WBE and MWBE bounds for s-sparse matrices $\mathbf{C}$ are a bit different from the ones defined in (18) and (19).

Definition III.7. Let all of the users be defined as $\mathcal{U} = \{1, 2, \ldots, K\}$. The k-th symbol is considered to be Gaussian separable [48], if for all small variances, $\sigma_d^2 \to 0$, we have

$$\mathbf{c}_k^H \mathbf{R}_k^{-1} \mathbf{c}_k > \sum_{j\in\mathcal{U}-k} |\mathbf{c}_k^H \mathbf{R}_k^{-1} \mathbf{c}_j|, \tag{21}$$

where

$$\mathbf{R}_k = \sum_{j\in\mathcal{U}-k} \mathbf{c}_j \mathbf{c}_j^H + \sigma_d^2 \mathbf{I}_L, \tag{22}$$

and the parameters

$$\Delta_k = \mathbf{c}_k^H \mathbf{R}_k^{-1} \mathbf{c}_k - \sum_{j\in\mathcal{U}-k} |\mathbf{c}_k^H \mathbf{R}_k^{-1} \mathbf{c}_j|, \tag{23}$$

$$\Delta_{ave}(\mathbf{C}) = \frac{1}{K}\sum_{k=1}^{K} \Delta_k, \tag{24}$$

are called the Gaussian margin and average Gaussian margin of the matrix $\mathbf{C}$, respectively.

Linear detectors rely on a decision-boundary partitioning the composite multiuser signal-space into subspaces uniquely and unambiguously identified by the users' signatures. Therefore the existence of these hyperplanes that partition the projection subspace of the binary user signals into two sets for each user in the absence of channel noise, is a prerequisite for a high performance. This geometrical perspective allows us to formally state a separability criterion for linear detectors. As for this linear classifier, upon assuming that the underlying classes follow a Gaussian distribution, it was shown in [48] the optimal ML decision relies on this hyperplane which partitions the decision-space into a pair of L-dimensional subspaces. Therefore, the linear decision rule for user K is said to be Gaussian separable, if the probability of error tends to zero when the noise variance tends to zero.

Definition III.8. There are many metrics of vector sparsity, as described in [91], but we will define the general Hoyer sparseness measure of a vector $\mathbf{c}_i$ based on the relationship between the ℓ_m and ℓ_n norms as follows,

$$S_{m,n}(\mathbf{c}_i) = \frac{\frac{L^{(1/m)}}{L^{(1/n)}} - \frac{||\mathbf{c}_i||_m}{||\mathbf{c}_i||_n}}{\frac{L^{(1/m)}}{L^{(1/n)}} - 1}. \tag{25}$$

The average sparseness of a matrix $\mathbf{C}$ can be expressed as,

$$S_{m,n,ave}(\mathbf{C}) = \frac{1}{K}\sum_{k=1}^{K} S_{m,n}(\mathbf{c}_k). \tag{26}$$

Interesting special cases are those, when $m = 1$, $n = 2$, which are known as the Hoyer sparseness measure [91] and $m = 1$, $n = \infty$.

IV. PROPOSED LDS CODE DESIGN

In the following section, we describe the proposed iterative algorithm, which is used for designing the LDS code matrix $\mathbf{C}$. For the sake of simplicity let us assume that $d_k = 1$ for $1 \leq k \leq K$ and rewrite (3) as

$$\mathbf{y} = \mathbf{c}_k x_k + \sum_{i\neq k}^{K} \mathbf{c}_i x_i + \mathbf{n}, \tag{27}$$

$$= \mathbf{c}_k x_k + \mathbf{i}_k + \mathbf{n}, \tag{28}$$

where $\mathbf{y} \in \mathbb{C}^{L\times 1}$ and $\mathbf{i}_k \in \mathbb{C}^{L\times 1}$ denotes the colored interference imposed by the other users, when the autocorrelation matrix is given by $\mathbf{R}'_k \triangleq \mathbb{E}\{\mathbf{i}_k \mathbf{i}_k^H\}$. Let us define the overall perturbation, $\mathbf{g}_k = \mathbf{i}_k + \mathbf{n}$, and the autocorrelation as $\mathbf{R}_k \triangleq \mathbb{E}\{\mathbf{g}_k \mathbf{g}_k^H\} = \mathbf{R}'_k + \sigma^2 \mathbf{I}_L$. The detection of the information bit of user k can be achieved via max-SINR filtering (or, equivalently, min-TSC filtering, linear MMSE filtering). The filter that exhibits the maximum output SINR for user-k is a scaled version of e.g., $\mathbf{w}_{SINR,k}(\mathbf{c}_k) \triangleq \mathbf{R}_k^{-1}\mathbf{c}_k$. Then the corresponding maximum post-filtering SINR output of the filter $\mathbf{w}_{SINR,k}$ is given by

$$SINR(\mathbf{c}_k) = \frac{\mathbb{E}\left\{|\mathbf{w}_{SINR,k}^H(\mathbf{c}_k x_k)|^2\right\}}{\mathbb{E}\left\{|\mathbf{w}_{SINR,k}^H(\mathbf{i}_k + \mathbf{n})|^2\right\}} \tag{29}$$

$$= \mathbf{c}_k^H \mathbf{Q}_k \mathbf{c}_k, \tag{30}$$

where $\mathbf{Q}_k \triangleq \mathbf{R}_k^{-1}$. Our objective is to find the specific s-sparse complex signature $\mathbf{c}_k$ that maximizes (29), namely:

$$\mathbf{c}^{(s)}_{k,maxSINR} = \underset{\substack{\mathbf{c}\in\mathcal{C}^{L\times 1},||\mathbf{c}||=1\\|\mathcal{I}_k|=s}}{\operatorname{argmax}} \quad \mathbf{c}^H\mathbf{Q}_k\mathbf{c}. \tag{31}$$

The superscript (s) indicates that $\mathbf{c}^{(s)}_{k,maxSINR}$ is s-sparse with $|\mathcal{I}_k| = s$. To tackle the problem, we now propose to relax the sparseness constraint of (31) and proceed by solving the following problem instead,

$$\mathbf{c}_{k,maxSINR} = \underset{\mathbf{c}\in\mathcal{C}^{L\times 1},||\mathbf{c}||=1}{\operatorname{argmax}} \quad \mathbf{c}^H\mathbf{Q}_k\mathbf{c}. \tag{32}$$

Let $\{\mathbf{q}_{k,1},\mathbf{q}_{k,2},\cdots,\mathbf{q}_{k,L}\}$ be the L eigenvectors of $\mathbf{Q}_k$ with corresponding eigenvalues $\lambda_{k,1} \geq \lambda_{k,2} \geq \cdots \geq \lambda_{k,L}$. The sequence $\mathbf{c}$ that maximizes (32) is well known and it is equal to the eigenvector that corresponds to the maximum eigenvalue of the matrix $\mathbf{Q}_k$, i.e.,

$$\mathbf{c}_{k,maxSINR} = \underset{\mathbf{c}\in\mathcal{C}^{L\times 1},||\mathbf{c}||=1}{\operatorname{argmax}} \quad \mathbf{c}^H\mathbf{Q}_k\mathbf{c} = \mathbf{q}_{k,1}. \tag{33}$$

Alternatively, we can design the code set $\mathbf{C}$ based on the TSC criterion that is defined in Section III. Let us now demonstrate the iterative method used for minimizing the $TSC(\mathbf{C})$. We rewrite (13) as

$$\begin{aligned} TSC(\mathbf{C}) &= \sum_{i\neq k}^{K}\sum_{j\neq k}^{K}|\mathbf{c}_i^H\mathbf{c}_j|^2 + |\mathbf{c}_k^H\mathbf{c}_k|^2 + 2\sum_{i\neq k}^{K}|\mathbf{c}_k^H\mathbf{c}_i|^2 \\ &= TSC(\mathbf{C}_{[k]}) + 1 + 2\mathbf{c}_k^H\left(\sum_{i\neq k}^{K}\mathbf{c}_i\mathbf{c}_i^H\right)\mathbf{c}_k \\ &= TSC(\mathbf{C}_{[k]}) + 1 + 2\mathbf{c}_k^H\bar{\mathbf{R}}_k\mathbf{c}_k, \end{aligned} \tag{34}$$

where $\mathbf{C}_{[k]}$ denotes the preexisting code set except for the k-th column of the code set $\mathbf{C}$ and $\bar{\mathbf{R}}_k = \sum_{i\neq k}^{K}\mathbf{c}_i\mathbf{c}_i^H$ denotes the autocorrelation of the matrix $\mathbf{C}_{[k]}$, respectively. It becomes clear from (34) that the conditional minimization of $TSC(\mathbf{C})$ with respect to $\mathbf{c}_k$ for fixed (min-TSC-valued) $TSC(\mathbf{C}_{[k]})$ reduces to

$$\mathbf{c}^{(s)}_{k,minTSC} = \underset{\substack{\mathbf{c}\in\mathcal{C}^{L\times 1},||\mathbf{c}||=1\\|\mathcal{I}_k|=s}}{\operatorname{argmin}} \quad \mathbf{c}^H\bar{\mathbf{R}}_k\mathbf{c}. \tag{35}$$

The sequence $\mathbf{c}$ that minimizes the relaxed problem (35) is well known and it is equal to the eigenvector, $\mathbf{r}_{k,\upsilon}$, that corresponds to the minimum non-zero eigenvalue υ of the matrix $\bar{\mathbf{R}}_k$, i.e.,

$$\mathbf{c}_{k,minTSC} = \underset{\mathbf{c}\in\mathcal{C}^{L\times 1},||\mathbf{c}||=1}{\operatorname{argmin}} \quad \mathbf{c}^H\bar{\mathbf{R}}_k\mathbf{c} = \mathbf{r}_{k,\upsilon}. \tag{36}$$

Similarly, since our construction of spreading codes is restricted to unit energy, i.e., $\mathbf{c}_k^H\mathbf{c}_k = 1$, the underlying problem of minimizing (34) does not change, if we add $2\sigma^2\mathbf{c}_k^H\mathbf{c}_k$ and subtract $2\sigma^2$ from (34) to obtain

$$TSC(\mathbf{C}) = TSC(\mathbf{C}_{[k]}) + 1 + 2\mathbf{c}_k^H\mathbf{R}_k\mathbf{c}_k - 2\sigma^2, \tag{37}$$

where $\mathbf{R}_k$ is defined in (22). The normalized MMSE filter for user k [92], is

$$\mathbf{s}_{k,MMSE} = \frac{\mathbf{R}_k^{-1}\mathbf{c}_k}{(\mathbf{c}_k^H\mathbf{R}_k^{-1}\mathbf{c}_k)^{1/2}}. \tag{38}$$

Therefore, the results of (36), (38) can be used in Step 7 of the iterative construction of our proposed LDS design algorithm, as shown in Table 2. In other words, instead of computing $\mathbf{q}_{k,1}$, we compute $\mathbf{r}_{k,\upsilon}$ or $\mathbf{s}_{k,MMSE}$. We are now ready to present our proposed algorithm, which is shown in Table 2,

TABLE 2.

LDS design algorithm

Input: L, K, δ, σ_d, s-sparse
1: Initialize : $\Delta'_{ave} \leftarrow 0, \epsilon \leftarrow 0.2, \epsilon' \leftarrow 10^2$;
2: **while** $\Delta'_{ave} < \delta$
3: Initialize : $\mathbf{C}^{\text{iv}}$;
4: **while** $\epsilon' > \epsilon$
5: $\mathbf{C}' \leftarrow \mathbf{C}$
6: **for** $k \in \{1,\ldots,K\}$
7: Compute $\mathbf{q}_{k,1}$ in (33), or (36), or (38)
8: $\mathbf{c}_k \leftarrow \mathbf{q}^{[n]}_{k,1}$
9: $\epsilon' \leftarrow ||\mathbf{C}-\mathbf{C}'||_F$
10: Compute $\Delta'_{ave}(\mathbf{C})$ in (24)
Output: $\mathbf{C}$

where $\mathbf{q}^{[n]}_{k,1}$ denotes the s-sparse vector with only those s elements of $\mathbf{q}_{k,1}$ that have the largest absolute values. The scalar values δ and σ_d are design parameters, respectively. Note that the non-zero complex values of the sparse columns $\mathbf{c}_i$ are not necessarily unimodular, i.e., $\mathbf{c}_i = \{c_{i,j} \in \mathbb{C} : |c_{i,j}| = 1, j \in \mathcal{I}_i\}$, for $1 \leq i \leq K$, [93]. Unimodular s-sparse vectors have equal Hoyer sparsity, i.e., $S_{1,2}(\mathbf{c}_i) = \frac{L^{(1/2)}-s^{(1/2)}}{L^{(1/2)}-1}$.

A. CONVERGENCE OF THE ALGORITHM

The proposed algorithm converges to a locally optimal solution with an s-sparse matrix $\mathbf{C}$ that has one of the specific structures $\mathcal{A}$, where we have $\mathcal{A}_{i,j} = \{|c_{i,j}|_0 : 1 \leq i \leq L, 1 \leq j \leq K\}$. For a size of 4×6 and for the random initialization of $\mathbf{C}$ the algorithm converges to one of the three structures (e.g., $\mathcal{A}^1$, $\mathcal{A}^2$ and $\mathcal{A}^3$), which is described as follows,

$$\mathcal{A}^1 = \begin{bmatrix} 1 & 0 & 1 & 0 & 0 & 1 \\ 1 & 0 & 1 & 0 & 0 & 1 \\ 0 & 1 & 0 & 1 & 1 & 0 \\ 0 & 1 & 0 & 1 & 1 & 0 \end{bmatrix}, \tag{39}$$

$$\mathcal{A}^2 = \begin{bmatrix} 0 & 1 & 1 & 0 & 0 & 1 \\ 1 & 0 & 0 & 1 & 1 & 0 \\ 0 & 1 & 1 & 0 & 0 & 1 \\ 1 & 0 & 0 & 1 & 1 & 0 \end{bmatrix}, \tag{40}$$

[iv] Randomly generate $\mathbf{C} \in \mathbb{C}^{L\times K}$, where $||\mathbf{c}_i|| = 1, \forall\ 1 \leq i \leq K$.

$$\mathcal{A}^3 = \begin{bmatrix} 1 & 1 & 1 & 0 & 0 & 0 \\ 0 & 0 & 0 & 1 & 1 & 1 \\ 0 & 0 & 0 & 1 & 1 & 1 \\ 1 & 1 & 1 & 0 & 0 & 0 \end{bmatrix}, \tag{41}$$

where the order of the columns of all of the three structures can be arbitrarily ordered and not necessarily as shown above. The output structure of the matrix of the algorithm depends mainly on the initialization of the matrix $\mathbf{C}$. Specifically, if we arbitrarily initialize a 4×6 matrix that possesses one of the structures (e.g., $\mathcal{A}^1$, $\mathcal{A}^2$ and $\mathcal{A}^3$), the output of the algorithm will have the same structure as that of the initialization matrix. Therefore, to speed up the convergence of the algorithm in Table 2 we may choose to initialize the matrix $\mathbf{C}$ with one of the known structures.

B. UPWARD SCALING DESIGN FOR LDS

The algorithm proposed in Table 2 may potentially be considered for an upward scaling design for a given optimum LDS sequence. The underlying requirement is to develop a subset of the sparse matrix with the given optimal LDS code set for ensuring that the resultant LDS code set still maintains optimality. Appending spreading codes to a given LDS set may require complete redesign/reassignment of the resultant LDS code set. Mathematically, we wish to design an s-sparse code set $\mathbf{C}_K^{k'+1} = [\mathbf{c}_{k'+1}, \mathbf{c}_{k'+2}, \ldots, \mathbf{c}_K]$ matrix, where $\mathbf{c}_i = \{c_{i,j} \in \mathbb{C} : j \in \mathcal{I}_i\}$, for $i \in \mathcal{K} = \{k'+1, k'+2, \ldots, K\}$ that can be appended to a given code set $\mathbf{C}_{k'}^1 = [\mathbf{c}_1, \mathbf{c}_2, \ldots, \mathbf{c}_{k'}]$, where $\mathbf{c}_i = \{c_{i,j} \in \mathbb{C} : j \in \mathcal{I}_i\}$, for $i \in \mathcal{K}' = \{1, 2, \ldots, k'\}$ to result in an improved LDS code matrix $\mathbf{C} = [\mathbf{C}_{k'}^1, \mathbf{C}_K^{k'+1}]$. The only constraint imposed on the proposed algorithm while generating the LDS sequence is that the input matrix $\mathbf{C}_{k'}^1$ must obey one of the convergent structures discussed in Section IV-A above. Therefore, the resultant algorithm can be applied for designing s-sparse spreading codes that are appended to an input optimal LDS sequence with the aid of a small modification.

$$\mathcal{A} = \begin{bmatrix} 1 & 0 & 0 & 1 & 0 & 0 & 1 & 0 & 0 \\ 1 & 0 & 0 & 1 & 0 & 0 & 0 & 0 & 0 \\ 0 & 1 & 0 & 0 & 1 & 0 & 0 & 1 & 0 \\ 0 & 1 & 0 & 0 & 1 & 0 & 0 & 0 & 1 \\ 0 & 0 & 1 & 0 & 0 & 1 & 0 & 0 & 0 \\ 0 & 0 & 1 & 0 & 0 & 1 & 0 & 0 & 0 \end{bmatrix}.$$

In Step 3, we randomly initialize $\mathbf{C}_K^{k'+1}$ and form $\mathbf{C} = [\mathbf{C}_{k'}^1, \mathbf{C}_K^{k'+1}]$ instead of randomly initializing $\mathbf{C}$. In Step 6, we use $k \in \mathcal{K}$ instead of $k \in \{1, 2, \ldots, K\}$ as shown in Table 2. To illustrate one of the sample LDS outputs of size 6×9 from the modified algorithm, we first arbitrarily generate an orthogonal 2-sparse 6×6 matrix, which belongs to one of the convergent structure discussed in Section IV-A and use that as an input to the modified algorithm. The resultant LDS sequence structure is shown in Fig. 42. Observe that that in Fig. 42 the $\mathbf{C}_9^7$ matrix is 1-sparse and since the columns have unit energy, the elements are simply 1. We will characterize the performance of such code sets in our simulations. The proposed receiver is presented in the next section.

C. COMPLEXITY OF THE PROPOSED LDS CONSTRUCTION

The main complexity contribution of the proposed algorithm is associated with updating $\mathbf{q}_{k,1}$ either in (33), or in (36), or alternatively in (38). Direct calculations of $\mathbf{R}_k^{-1}$ for each user is expensive. However, with the aid of efficient numerical techniques such as the Sherman-Morrison-Woodbury formula, we can compute its inverse, i.e., $\mathbf{R}_k^{-1}$, at a complexity order of $\mathcal{O}(K^2)$. This process is repeated K times for obtaining all K users' LDS waveforms. On the other hand, the number of iterations in the 'while' loops in lines 4 and 2 depends on the thresholds ϵ and δ, respectively. The smaller the thresholds the longer it takes to complete the process. With our design parameters, the number of iterations on average was about 3 and 10 for the 'while' loops in lines 4 and 2, respectively. Therefore, the overall complexity is $\mathcal{O}(c \cdot K^3) = \mathcal{O}(K^3)$ where c is a constant, e.g., $c = 3 \cdot 10 = 30$.

V. MULTIUSER DETECTION

It is widely recognized that obtaining the ML solution is generally NP-hard [46]. Various suboptimal low-complexity detection techniques have already been proposed for conventional dense spreading based CDMA systems. These suboptimal approaches can be classified into two categories: linear and non-linear MUDs. Linear MUDs include among others, matched filtering (MF), MMSE, and zero-forcing (ZF) based schemes. In a non-linear successive interference cancellation aided detector the interference is first estimated and then it is subtracted from the received signal before detection. The cancellation process can then be carried out either successively (SIC) [94], or in parallel (PIC) [95]–[97]. In non-linear iterative detectors [98]–[102], PDA [48] aims for suppressing the MAI in each iteration in order to improve the overall error performance. Suboptimal so-called polynomial-time detectors that are based on the geometric approach are studied in [103], [104].

In comparison to dense CDMA, sparse CDMA or LDS is capable of substantially reducing the computational complexity of MUDs. This is a benefit of the sparse nature of LDS sequences that enables both the MPA and belief propagation (BP) algorithms to be applied at a lower complexity than the optimum MUD. In terms of reducing the complexity of the MPA algorithm even further without much performance erosion, Du *et al.* [105] proposed a detection scheme based on a dynamic factor graph by exploiting the channel state information. Another solution conceived by Tian *et al.* [106] reduces the complexity by restricting the search region of the superimposed multiuser constellation to a quadrant-like part of it. Razavi *et al.* [107] proposed a beneficial receiver component activation scheduling for iterative MUD in order to reduce its complexity by utilizing the LDPC codes for an LDS-OFDM system.

The relationship between the optimal performance and the performance achieved by iterative BP has been established by Guo and Wang in [108] in the CDMA context. Their study demonstrated that for about a hundred users, the theoretical performance limit of large systems is approached as a result of the central-limit theorem. Those studies are normally performed under the assumption of a large system, where both the number of users and the spreading factor tend towards infinity, while their ratio is kept constant. As an example, Takeuchi *et al.* [109] characterized the family of BP receivers via density evolution (DE) in the dense limit after assuming the large-system limit. In those studies the specific way the MPA is implemented played a significant role. The user's data detection based on the MPA and on the optimal ML detection using turbo-style processing is reported by Razavi *et al.* [23]. In contrast to this, it is shown in [110] that a joint detection and decoding approach based on an optimised sparse graph of the multiuser channel and the LDPC codes outperforms the iterative receiver of LDS-OFDM systems. Wen and Su [111] showed both numerically and analytically that the JSG-CDMA, which combines multiple access using LDS-CDMA and LDPC forward error correcting techniques, attains a satisfactory performance under rank-deficient conditions and outperforms conventional CDMA, LDS-CDMA as well as iterative detection aided LDS-CDMA. The detailed analysis is presented in [112].

Nevertheless, the BP and MPA detection methods still have exponential by increased computational complexity as a function of the number of users. The trade-off between the computational complexity and bandwidth efficiency at different user-load is studied by Raymond in [113]. Near-suboptimal detectors tend to strike a compelling performance as complexity trade-off compared to an MPA detector. Therefore, by taking full advantage of the LDS scheme, which has a lower MAI than dense CDMA systems, we consider an attractive low-complexity detector, which is based on the MMSE criterion and on PIC (MMSE-PIC) based detection [84] that has an even lower complexity than the MPA based detector, whilst achieving the same spectral efficiency. Fantuz and D'Amours [84] showed that the BER performance of MMSE-PIC is very close to that of the MPA detector for LDS systems communicating over AWGN, non-dispersive and frequency selective fading channels.

A. MMSE-PIC DETECTOR

The MMSE-PIC detector of Fig. 6 is constituted by a beneficial amalgam of the MMSE and PIC detectors which will be characterized for transmission over AWGN, non-dispersive and frequency-selective fading channels, respectively. For the sake of simplicity, the derivation of the detector is provided for BPSK and 4QAM, constellations of $\mathcal{X} = \{-1, +1\}$ and $\mathcal{X} = \{-1-j, -1+j, +1-j, +1+j\}/\sqrt{2}$. However, it should be noted that similar derivations can be readily provided for higher-order constellations, such as 8QAM, 16QAM, 32QAM, etc.

1) AWGN Channel

The despreading is performed by multiplying the received vector in (3) by the LDS code as follows,

$$\mathbf{r} = \mathbf{C}^H\mathbf{y} = \mathbf{RDx} + \mathbf{C}^H\mathbf{n}, \tag{42}$$

where we have $\mathbf{r} \in \mathbb{C}^{K\times 1}$ and the correlation matrix obeys $\mathbf{R} = \mathbf{C}^H\mathbf{C} \in \mathbb{C}^{K\times K}$. The optimal receiver achieves the minimum probability of error $Pr(\mathbf{x} \neq \widehat{\mathbf{x}})$ for each symbol vector $\mathbf{x}$, which is arranged by estimating $\widehat{\mathbf{x}}$ upon maximizing the *a posteriori* probability (APP) $Pr(\mathbf{x}|\mathbf{r})$'s given the observed despread sequence $\mathbf{r}$, which is formulated as

$$\widehat{\mathbf{x}} = \underset{\mathbf{x}\in\mathcal{X}^{K\times 1}}{\operatorname{argmax}}\, Pr(\mathbf{x}|\mathbf{r}). \tag{43}$$

This decision criterion is commonly referred to as the MAP [114] algorithm. It is widely known that the MAP detector has an exponentially increased complexity by the number of users K, which makes its application somewhat unrealistic even for moderate values of K. In practice it is more convenient to work with log-likelihood ratios (LLRs) than with probabilities. The LLRs for each symbol a_m, where $a_m \in \mathcal{X}$ for $1 \leq m \leq M$, of the k-th user can be written as

$$\Lambda_k(a_m) = \log\frac{\sum_{\mathbf{x}\in\mathcal{A}_{x_k}^{a_m}} Pr(\mathbf{r}|\mathbf{x})Pr(\mathbf{x})}{\sum_{\bar{\mathbf{x}}\in\mathcal{A}_{x_k}^{\overline{a_m}}} Pr(\mathbf{r}|\bar{\mathbf{x}})Pr(\bar{\mathbf{x}})}, \tag{44}$$

with $\mathcal{A}_{x_k}^{a_m} \subset \mathcal{A}_x$, $\mathcal{A}_{x_k}^{\overline{a_m}} \subset \mathcal{A}_x$ representing the set of all symbol vectors $\mathbf{x} \in \mathcal{A}_x$ in which we have $x_k = a_m$ and $x_k \neq a_m$ for the k-th user. Furthermore, we have $\mathcal{A}_x = \mathcal{X}^{K\times 1}$ and

$$Pr(\mathbf{r}|\mathbf{x}) = \frac{1}{\pi^K|\mathbf{\Sigma}|}\exp[-f^H(\mathbf{x})\mathbf{\Sigma}^{-1}f(\mathbf{x})], \tag{45}$$

where $f : \mathbf{x} \mapsto \mathbf{r} - \mathbf{R}_C\mathbf{x}$ represents a linear mapping of $\mathbf{R}_C = \mathbf{RD}$, the covariance matrix obey $\mathbf{\Sigma} = \sigma^2\mathbf{C}^H\mathbf{C}$ and $|\mathbf{\Sigma}|$ denotes the determinant of $\mathbf{\Sigma}$. If we assume that all symbol vectors have the same probability distribution of $Pr(\mathbf{x}) = \mathbf{1}/M^K$, then the log-sum approximation of (44) can be expressed as

$$\Lambda_k(a_m) \approx \min_{\mathbf{x}\in\mathcal{A}_{x_k}^{a_m}} ||\mathbf{\Sigma}^{-\frac{1}{2}}f(\mathbf{x})||^2 - \min_{\bar{\mathbf{x}}\in\mathcal{A}_{x_k}^{\overline{a_m}}} ||\mathbf{\Sigma}^{-\frac{1}{2}}f(\bar{\mathbf{x}})||^2. \tag{46}$$

The computational complexity is increased exponentially versus the number of users K because the LLRs in (46) are calculated jointly for all the users hence requiring the computation of M^K norm values. By contrast, the popular family of minimum mean square error detectors minimize the error-variance between the transmitted symbol and the filtered signal at the user level and they are more desirable in terms of complexity. Therefore, the per-user LLRs are computed separately. After MMSE filtering, our goal is to estimate the users' symbols independently. Therefore, the MMSE detector's action can be expressed in this form

$$\mathbf{u} = \mathbf{W}_{\text{MMSE}}\mathbf{r} \in \mathbb{C}^{K\times 1}, \tag{47}$$

where $\mathbf{u}$ represents the decision variables after the MMSE detector. The MMSE filter, weight-matrix $\mathbf{W}_{\text{MMSE}} \in \mathbb{C}^{K\times K}$

is found by minimizing the mean-square error between the estimated symbols and the true transmitted symbol $\mathbf{x}$, which is expressed as

$$\mathbf{W}_{\text{MMSE}} = \underset{\mathbf{W}\in\mathbb{C}^{K\times K}}{\operatorname{argmin}} \ \mathbb{E}\{|\mathbf{x}-\mathbf{Wr}|^2\}. \tag{48}$$

Under the reasonable assumption that each user's symbols are independent and identically distributed (i.i.d.) with unit energy, when we have $\mathbb{E}\{\mathbf{xx}^H\} = \mathbf{I}_K$, the solution of (48) is given by

$$\mathbf{W}_{\text{MMSE}} = \mathbf{R}_C^H\left(\mathbf{R}_C\mathbf{R}_C^H + \mathbf{\Sigma}\right)^{\dagger}, \tag{49}$$

where $(\cdot)^{\dagger}$ denotes the Moore-Penrose pseudoinverse operation [115]. The MMSE decision variables $\mathbf{u}$ are then processed to obtain the log likelihood ratios. The MMSE decision variable for the k-th user can be written as

$$\begin{aligned} u_k &= \mathbf{w}_k\mathbf{r} \\ &= \mathbf{w}_k\mathbf{R}_C^k x_k + \sum_{\substack{i=1\\ i\neq k}}^{K}\mathbf{w}_k\mathbf{R}_C^i x_i + \mathbf{w}_k\mathbf{Cn} \\ &= \beta_{k,k}x_k + \sum_{\substack{i=1\\ i\neq k}}^{K}\beta_{k,i}x_i + \mathbf{w}_k\mathbf{Cn}, \end{aligned} \tag{50}$$

where $\mathbf{w}_k \in \mathbb{C}^{1\times K}$ is the k-th row vector of $\mathbf{W}_{\text{MMSE}}$, $\mathbf{R}_C^k \in \mathbb{C}^{K\times 1}$ is the k-th column of $\mathbf{R}_C$, $x_k \in \mathcal{X}$ is the k-th symbol of the vector $\mathbf{x}$ and $\beta_{k,i} = \mathbf{w}_k\mathbf{R}_C^i \in \mathbb{C}$. Since the direct evaluation of $Pr(x_k = a_m|\mathbf{u})$ is computationally prohibitive, the PDA detector attempts to estimate it by using the Gaussian - "forcing" idea of [116] by approximating $Pr[x_k = a_m|\mathbf{u}, \{\mathbf{p}(j)\}_{\forall j\neq k}]$, that can serve as the updated value for $p_m(k)$. The vector $\mathbf{p}(k)$ is associated to x_k, whose m-th element $p_m(k)$, is the current estimate of *a posteriori* probability of $x_k = a_m$. In contrast to the PDA detector, MMSE detector attempts to estimate it by making a reasonable assumption on conceiving the *a priori* probability distribution of $Pr(x_k)$, namely that it is i.i.d. having an expected value of unity. If we model the residual MAI after the MMSE detector by a complex Gaussian random variable which is independent of the noise, then u_k is Gaussian as well. Let

$$\alpha_m(k) = -\frac{|u_k - \beta_{k,k}a_m|^2}{\sigma_k^2}, \tag{51}$$

where we have $\sigma_k^2 = \sum_{\substack{i=1\\ i\neq k}}^{K}|\beta_{k,i}|^2\mathbb{E}\{|x_i|^2\} + \mathbf{w}_k\mathbf{\Sigma}\mathbf{w}_k^H$, $\mathbb{E}\{|x_i|^2\} = 1$ since the x_i values are i.i.d. random variable. Provided that all the transmitted symbols have identical *a priori* probabilities, the *a posteriori* symbol probability is given by

$$\begin{aligned} Pr(x_k = a_m|u_k) &= \frac{Pr(u_k|x_k = a_m)Pr(x_k = a_m)}{\sum_{a_m\in\mathcal{X}} Pr(u_k|x_k = a_m)Pr(x_k = a_m)} \\ &= \frac{\exp[\alpha_m(k)]}{\sum_j \exp[\alpha_j(k)]}, \end{aligned} \tag{52}$$

where we have $Pr(u_k|x_k = a_m) = \frac{1}{\pi\sigma_k^2}\exp[\alpha_m(k)]$. The *a posteriori* probabilities of the symbols a_m can also be expressed in terms of their LLR's as follows,

$$\begin{aligned} \Lambda_k^{\text{MMSE}}(a_m) &= \log\frac{Pr(x_k = a_m|u_k)}{Pr(x_k \neq a_m|u_k)} \\ &= \log\frac{\exp[\alpha_m(k)]}{\sum_{j\neq m}\exp[\alpha_j(k)]}. \end{aligned} \tag{53}$$

Furthermore, to simplify the avaluation of (53), the log-sum approximation can be used:

$$\begin{aligned} \Lambda_k^{\text{MMSE}}(a_m) &\approx \max \log\exp[\alpha_m(k)] \\ &\quad - \max_{j\neq m} \log\exp[\alpha_j(k)] \\ &\approx \alpha_m(k) - \max_{j\neq m} \alpha_j(k). \end{aligned} \tag{54}$$

In the case of BPSK, (53) simplifies to:

$$\begin{aligned} \Lambda_k^{\text{MMSE}}(a_1) &= \log\frac{\exp[\alpha_1(k)]}{\exp[\alpha_2(k)]} \\ &= \alpha_1(k) - \alpha_2(k) \\ &= \frac{2\beta_{k,k}u_k}{\sigma_k^2}, \end{aligned} \tag{55}$$

where $a_1 = +1$ and $a_2 = -1$. Note that the *a posteriori* probability $Pr(x_k = a_m|u_k)$ in (52) can be expressed in terms of the LLRs of (53) as follows,

$$Pr[x_k = a_m|\Lambda_k^{\text{MMSE}}(a_m)] = \frac{1}{2}(1 + \tanh[\frac{1}{2}\Lambda_k^{\text{MMSE}}(a_m)]). \tag{56}$$

In practice, binary channel decoders require bit-level LLRs. Even though Gray-coding is used for QAM, which imposes correlation, for simplicity we assume the independence of the bits. Hence, if we assume the coded bits to be i.i.d., the log-likelihood ratio of a bit $b_{k,i}$ can be formulated as,

$$\begin{aligned} \Lambda_k^{\text{MMSE}}(b_i) &= \log\frac{Pr(b_{k,i} = 1|u_k)}{Pr(b_{k,i} = 0|u_k)} \\ &= \log\frac{\sum_{a_j\in\mathcal{X}_i^1} Pr(x_k = a_j|u_k)}{\sum_{a_j\in\mathcal{X}_i^0} Pr(x_k = a_j|u_k)} \\ &= \log\frac{\sum_{j|a_j\in\mathcal{X}_i^1}\exp[\alpha_j(k)]}{\sum_{j|a_j\in\mathcal{X}_i^0}\exp[\alpha_j(k)]}, \end{aligned} \tag{57}$$

where $b_{k,i}$ represents the i-th bit of the symbol x_k, $\mathcal{X}_i^{\lambda} = \{a_j \in \mathcal{X}|\mathbf{b}(j) = \psi^{-1}(a_j), b_i^j = \lambda\}$, and $\lambda = \{1, 0\}$. Note that the probability of having $b_{k,i} = 1$ can be expressed in terms of $\Lambda_k^{\text{MMSE}}(b_i)$ as:

$$Pr(b_{k,i} = 1|u_k) = \frac{\exp[\Lambda_k^{\text{MMSE}}(b_i)]}{1 + \exp[\Lambda_k^{\text{MMSE}}(b_i)]}. \tag{58}$$

The complexity of (57) can be reduced by using the log-sum approximation, which is expressed as

$$\begin{aligned} \Lambda_k^{\text{MMSE}}(b_i) &\approx \max_{j|a_j\in\mathcal{X}_i^1} \log\exp[\alpha_j(k)] \\ &\quad - \max_{j|a_j\in\mathcal{X}_i^0} \log\exp[\alpha_j(k)] \\ &\approx \max_{j|a_j\in\mathcal{X}_i^1} \alpha_j(k) - \max_{j|a_j\in\mathcal{X}_i^0} \alpha_j(k). \end{aligned} \tag{59}$$

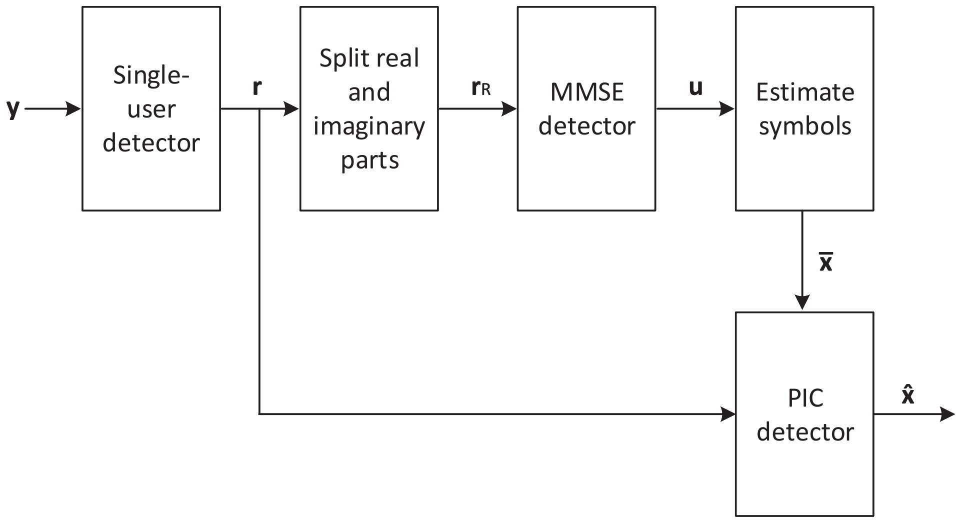

FIGURE 6. Block diagram of MMSE-PIC detector [84].

Given the bit-level LLRs $\Lambda_k^{\text{MMSE}}(b_i)$, the *a posteriori* probabilities can be expressed as follows,

$$Pr(x_k = a_j|\Lambda_k^{\text{MMSE}}(\mathbf{b})) = \prod_{i=1}^{Q} Pr[b_{k,i} = a_j^i|\Lambda_k^{\text{MMSE}}(b_i)],$$

where we have:

$$Pr(b_{k,i} = \lambda|\Lambda_k^{\text{MMSE}}(b_i)) = \frac{1}{2}(1 + \tilde{b}_{k,i}\mathsf{tanh}[\frac{1}{2}\Lambda_k^{\text{MMSE}}(b_i)]), \tag{60}$$

and

$$\tilde{b}_{k,i} = \begin{cases} +1, & \text{if } b_{k,i} = 1 \\ -1, & \text{if } b_{k,i} = 0 \end{cases}, \tag{61}$$

while $\Lambda_k^{\text{MMSE}}(\mathbf{b}) = [\Lambda_k^{\text{MMSE}}(b_1), \ldots, \Lambda_k^{\text{MMSE}}(b_Q)]^T$. The MMSE-PIC algorithm approximates the estimates $\bar{x}_k$ of the transmitted symbols x_k of user k by its mean value, which is formulated as,

$$\begin{aligned} \bar{x}_k &= \mathbb{E}\{x_k\} \\ &= \sum_{a_j \in \mathcal{X}} a_j \cdot Pr[x_k = a_j|\Lambda_k^{\text{MMSE}}(a_j)] \\ &= \sum_{a_j \in \mathcal{X}} a_j \cdot Pr[x_k = a_j|\Lambda_k^{\text{MMSE}}(\mathbf{b})], \end{aligned} \tag{62}$$

for $k = 1, \ldots, K$. Alternatively, the soft-decision of the estimates of $\bar{x}_k$ can be expressed as

$$\bar{x}_k = \underset{a_j \in \mathcal{X}}{\text{argmax}}\ Pr[x_k = a_j|\Lambda_k^{\text{MMSE}}(a_j)]. \tag{63}$$

In case of QAM, (62) can be expressed in terms of $\Lambda_k^{\text{MMSE}}(a_j)$ as

$$\begin{aligned} \bar{x}_k = \frac{1}{2\sqrt{2}}(&-\mathsf{tanh}[\frac{1}{2}\Lambda_k^{\text{MMSE}}(a_1)] - \mathsf{tanh}[\frac{1}{2}\Lambda_k^{\text{MMSE}}(a_2)] \\ &+\mathsf{tanh}[\frac{1}{2}\Lambda_k^{\text{MMSE}}(a_3)] + \mathsf{tanh}[\frac{1}{2}\Lambda_k^{\text{MMSE}}(a_4)] \\ &+j(-\mathsf{tanh}[\frac{1}{2}\Lambda_k^{\text{MMSE}}(a_1)] + \mathsf{tanh}[\frac{1}{2}\Lambda_k^{\text{MMSE}}(a_2)] \\ &-\mathsf{tanh}[\frac{1}{2}\Lambda_k^{\text{MMSE}}(a_3)] + \mathsf{tanh}[\frac{1}{2}\Lambda_k^{\text{MMSE}}(a_4)])), \end{aligned}$$

where $a_1 = \{-1 - j\}/\sqrt{2}$, $a_2 = \{-1 + j\}/\sqrt{2}$, $a_3 = \{+1-j\}/\sqrt{2}$, and $a_4 = \{+1+j\}/\sqrt{2}$. In terms of $\Lambda_k^{\text{MMSE}}(\mathbf{b})$, (62) can be expressed as

$$\bar{x}_k = \frac{1}{\sqrt{2}}(\mathsf{tanh}[\frac{1}{2}\Lambda_k^{\text{MMSE}}(b_1)] + j\mathsf{tanh}[\frac{1}{2}\Lambda_k^{\text{MMSE}}(b_2)]), \tag{64}$$

and the estimates of the transmitted symbol vector $\mathbf{x}$ of all users can be written as

$$\bar{\mathbf{x}} = \frac{1}{\sqrt{2}}(\mathsf{tanh}[\frac{1}{2}\Lambda^{\text{MMSE}}(\mathbf{b}_1)] + j\mathsf{tanh}[\frac{1}{2}\Lambda^{\text{MMSE}}(\mathbf{b}_2)]), \tag{65}$$

where $\Lambda^{\text{MMSE}}(\mathbf{b}_\eta) = [\Lambda_1^{\text{MMSE}}(b_\eta), \ldots, \Lambda_K^{\text{MMSE}}(b_\eta)]^T$ and $\eta \in \{1, 2\}$. In case of BPSK, (62) can be expressed in terms of $\Lambda_k^{\text{MMSE}}(a)$ as

$$\bar{x}_k = \mathsf{tanh}[\frac{1}{2}\Lambda_k^{\text{MMSE}}(a)], \tag{66}$$

where $a = \{-1, +1\}$ and the estimates of the transmitted symbol vector $\mathbf{x}$ of all users can be written as

$$\bar{\mathbf{x}} = \mathsf{tanh}[\frac{1}{2}\Lambda^{\text{MMSE}}(\mathbf{a})], \tag{67}$$

where $\Lambda^{\text{MMSE}}(\mathbf{a}) = [\Lambda_1^{\text{MMSE}}(a), \ldots, \Lambda_K^{\text{MMSE}}(a)]^T$.

The PIC stage of the detector produces the final decision variables according to

$$u_{\text{PIC},k} = u_k - \sum_{i \neq k}^{K} R_{C,k,i}\bar{x}_i, \tag{68}$$

where $R_{C,k,i}$ is the element in the k-th row and i-th column of $\mathbf{R}_C$, while u_k is the k-th element of $\mathbf{u}$. The estimates in (68) can be used as *a priori* probabilities for the channel decoder. If no channel coding is used, then hard-decision detection can be employed, which is formulated as

$$\hat{x}_k = \underset{a_j \in \mathcal{X}}{\text{argmin}} \; ||u_{\mathsf{PIC},k} - a_j||^2, \;\; \forall k. \tag{69}$$

In case of BPSK, the hard-decision bits may be then estimated by

$$\hat{\mathbf{x}} = \text{sgn}\left(\Re\{\mathbf{u}_{\mathsf{PIC}}\}\right), \tag{70}$$

where we have $\mathbf{u}_{\mathsf{PIC}} = [u_{\mathsf{PIC},1}, u_{\mathsf{PIC},2}, \ldots, u_{\mathsf{PIC},K}]^T$. After computing $u_{\mathsf{PIC},k}$ using $\overline{\mathbf{x}}$ in (68), we can recompute the LLRs in (53) by using the $u_{\mathsf{PIC},k}$ values instead of u_k obtained after the MMSE filter for improving the detection performance.

In order to take advantage of the potential diversity gain of the multi-dimensional signal space, we will exploit it by converting the Cartesian product of the complex plane to the real space, which will double the number of dimensions. Since detection of complex symbols (e.g., QAM) is equivalent to estimating the real and the imaginary parts of the complex symbols in parallel, this simplifies the detection process and reduces the decoding complexity as well. We then split the vectors and matrices in (42) into their real and imaginary components, as follows:

$$\mathbf{r}_R = \mathbf{R}_R \mathbf{x}_R + \mathbf{C}_R \mathbf{n}_R, \tag{71}$$

where we have $\mathbf{r}_R \in \mathbb{R}^{2K\times 1}$, $\mathbf{R}_R \in \mathbb{R}^{2K\times 2K}$, $\mathbf{C}_R \in \mathbb{R}^{2K\times 2L}$, $\mathbf{n}_R \in \mathbb{R}^{2L\times 1}$ and the subscript R, $\Re\{\}$ and $\Im\{\}$ represent the real domain as well as the real and imaginary parts of a complex number,

$$\mathbf{r}_R = \begin{bmatrix} \Re\{\mathbf{r}\} \\ \Im\{\mathbf{r}\} \end{bmatrix}, \mathbf{x}_R = \begin{bmatrix} \Re\{\mathbf{x}\} \\ \Im\{\mathbf{x}\} \end{bmatrix}, \mathbf{R}_R = \begin{bmatrix} \Re\{\mathbf{RD}\} & -\Im\{\mathbf{RD}\} \\ \Im\{\mathbf{RD}\} & \Re\{\mathbf{RD}\} \end{bmatrix},$$

$$\mathbf{C}_R = \begin{bmatrix} \Re\{\mathbf{C}^H\} & -\Im\{\mathbf{C}^H\} \\ \Im\{\mathbf{C}^H\} & \Re\{\mathbf{C}^H\} \end{bmatrix}$$

and

$$\mathbf{n}_R = \begin{bmatrix} \Re\{\mathbf{n}\} \\ \Im\{\mathbf{n}\} \end{bmatrix},$$

respectively. We treat the elements of $\mathbf{x}_R$ as independent multivariate random variables, where the i-th element, $x_{R,i}$, is a member of one of two possible sets,

$$x_{R,i} \in \begin{cases} \Re\{x_k = a_m | a_m \in \mathcal{X}\}, & i \in [1, K] \\ \Im\{x_k = a_m | a_m \in \mathcal{X}\}, & i \in [K+1, 2K], \end{cases} \tag{72}$$

where $k \in \{i, i-K\}$. The noise $\mathbf{n}_R$ has the variance matrix of $\mathbf{\Sigma}_R = \frac{\sigma^2}{2}\mathbf{C}_R\mathbf{C}_R^H$. Note that for BPSK transmission $\mathbf{x} \in \{\pm 1\}^{K\times 1}$ is real-valued, which results in its imaginary part being a zero vector. Then (71) can be simplified to:

$$\mathbf{r}_R = \begin{bmatrix} \Re\{\mathbf{RD}\} \\ \Im\{\mathbf{RD}\} \end{bmatrix} \mathbf{x} + \begin{bmatrix} \Re\{\mathbf{C}^H\} & -\Im\{\mathbf{C}^H\} \\ \Im\{\mathbf{C}^H\} & \Re\{\mathbf{C}^H\} \end{bmatrix} \begin{bmatrix} \Re\{\mathbf{n}\} \\ \Im\{\mathbf{n}\} \end{bmatrix}. \tag{73}$$

The separation of the real and imaginary parts provides an extra dimension for the detector in order to have a better estimate of each user's symbol. Therefore, the MMSE detector can be expressed as

$$\mathbf{u} = \mathbf{W}_{\mathsf{MMSE}} \mathbf{r}_R \in \mathbb{R}^{2K\times 1}, \tag{74}$$

where the MMSE filter, $\mathbf{W}_{\mathsf{MMSE}} \in \mathbb{R}^{2K\times 2K}$, is found by minimizing the mean-square error between the estimated symbols and the true transmitted symbol $\mathbf{x}_R$, which is expressed as

$$\mathbf{W}_{\mathsf{MMSE}} = \underset{\mathbf{W}\in\mathbb{R}^{2K\times 2K}}{\text{argmin}} \; \mathbb{E}\{||\mathbf{x}_R - \mathbf{W}\mathbf{r}_R||^2\}. \tag{75}$$

The solution of (75) is given by

$$\mathbf{W}_{\mathsf{MMSE}} = \mathbf{R}_R^T \left(\mathbf{R}_R \mathbf{R}_R^T + \mathbf{\Sigma}_R\right)^{\dagger}. \tag{76}$$

Note that in case of BPSK, we have $\mathbf{W}_{\mathsf{MMSE}} \in \mathbb{R}^{K\times 2K}$, $\mathbf{u} \in \mathbb{R}^{K\times 1}$ and $\mathbf{x}_R = \mathbf{x}$. The MMSE decision variable for the i-th element can be written as

$$\begin{aligned} u_i &= \mathbf{w}_i \mathbf{r}_R \\ &= \mathbf{w}_i \mathbf{R}_R^i x_{R,i} + \sum_{\substack{j=1 \\ j\neq i}}^{2K} \mathbf{w}_i \mathbf{R}_R^j x_{R,j} + \mathbf{w}_i \mathbf{C}_R \mathbf{n}_R \\ &= \beta_{i,i} x_{R,i} + \sum_{\substack{j=1 \\ j\neq i}}^{2K} \beta_{i,j} x_{R,j} + \mathbf{w}_i \mathbf{C}_R \mathbf{n}_R, \end{aligned} \tag{77}$$

where $\mathbf{w}_i \in \mathbb{R}^{1\times 2K}$ is the i-th row vector of $\mathbf{W}_{\mathsf{MMSE}}$, $\mathbf{R}_R^i \in \mathbb{R}^{2K\times 1}$ is the i-th column of $\mathbf{R}_R$, and $\beta_{i,j} = \mathbf{w}_i \mathbf{R}_R^j \in \mathbb{R}$. Expression (51) in the real domain can be expressed as

$$\alpha_m(i) = -\frac{(u_i - \beta_{i,i} a_m)^2}{2\sigma_i^2}, \tag{78}$$

where $a_m \in \mathcal{X}_R$ for $1 \le m \le 2M$, $\mathcal{X}_R = \{\Re\{\mathcal{X}\}, \Im\{\mathcal{X}\}\}$, $\sigma_i^2 = \sum_{\substack{j=1 \\ i\neq i}}^{2K} \beta_{i,j}^2 \mathbb{E}\{x_{R,j}^2\} + \mathbf{w}_i \mathbf{\Sigma}_R \mathbf{w}_i^T$ and $\mathbb{E}\{x_{R,j}^2\} = 1$ since the $x_{R,j}$s are i.i.d. random variables. Based on (78), the LLRs for each symbol a_m, defined as $\Lambda_i^{\mathsf{MMSE}}(a_m) = \log(Pr(x_{R,i} = a_m|u_i)/Pr(x_{R,i} \neq a_m|u_i)$, can be calculated by (53) as in the complex formulation scenario. All the other LLRs and *a posterior* probabilities are computed in a similar way to the complex formulation case, except that now we have to perform for $1 \le i \le 2K$ elements and $a_m \in \mathcal{X}_R$, $1 \le m \le 2M$ symbols with the exception of the BPSK case. In the PIC stage of (68), we substitute $R_{R,j,i}$ instead of $R_{C,k,i}$. In the case of QAM, the decision variable for user k can be computed as $u_{\mathsf{PIC},k} = u_{R,\mathsf{PIC},k} + ju_{R,\mathsf{PIC},k+K}$ and the hard-decision is given by $\hat{x}_k = \hat{x}_{R,k} + j\hat{x}_{R,k+K}$, for $1 \le k \le K$.

2) Non-dispersive Fading Channel

In addition to the despreading operation the decision variables u_ks are multiplied by the corresponding channel gains as follows,

$$\begin{aligned} \tilde{r}_k &= h_k^* \mathbf{c}_k^H \mathbf{y} \\ &= |h_k|^2 d_k x_k + \sum_{i=1, i\neq k}^{K} R_{k,i} h_k^* h_i d_i x_i + h_k^* \mathbf{c}_k^H \mathbf{n}, \end{aligned} \tag{79}$$

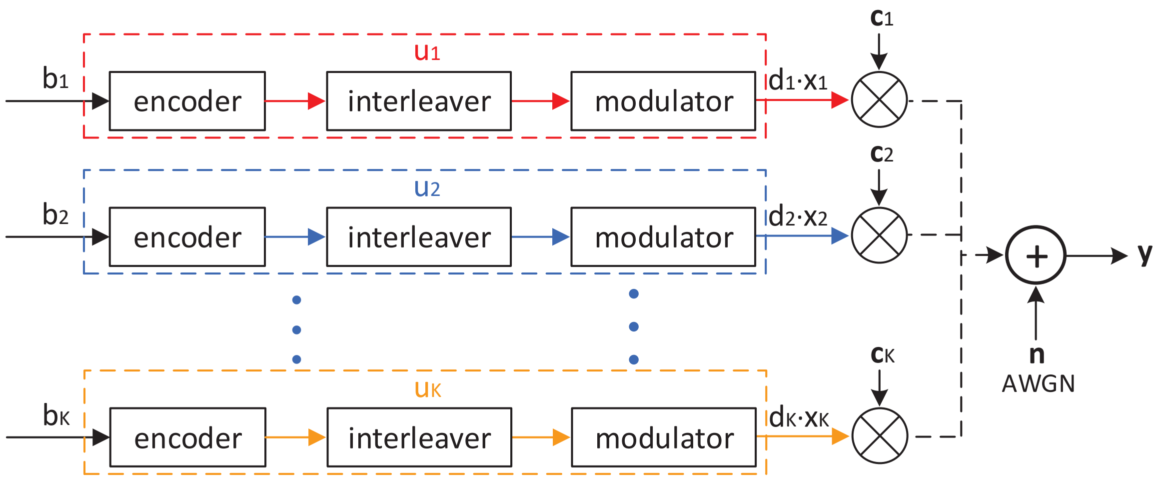

FIGURE 7. Block diagram of our BICM transmitter.

where the superscript * denotes the complex conjugate. The vector of decision variables can be expressed as

$$\begin{aligned}\tilde{\mathbf{r}} &= \mathbf{H}^H\mathbf{C}^H\mathbf{y}\\ &= \mathbf{H}^H\mathbf{C}^H\mathbf{C}\mathbf{H}\mathbf{D}\mathbf{x}+\mathbf{H}^H\mathbf{C}^H\mathbf{n}\\ &= \mathbf{H}^H\mathbf{R}\mathbf{H}\mathbf{D}\mathbf{x}+\mathbf{H}^H\mathbf{C}^H\mathbf{n}. \end{aligned}\tag{80}$$

The vectors and matrices in (80) are then split into real and imaginary components, as shown below:

$$\tilde{\mathbf{r}}_R = \tilde{\mathbf{R}}_R\mathbf{x}_R + \tilde{\mathbf{C}}_R\mathbf{n}_R, \tag{81}$$

where

$$\tilde{\mathbf{r}}_R=\begin{bmatrix}\Re\{\tilde{\mathbf{r}}\}\\ \Im\{\tilde{\mathbf{r}}\}\end{bmatrix}, \tilde{\mathbf{R}}_R=\begin{bmatrix}\Re\{\mathbf{H}^H\mathbf{R}\mathbf{H}\mathbf{D}\} & -\Im\{\mathbf{H}^H\mathbf{R}\mathbf{H}\mathbf{D}\}\\ \Im\{\mathbf{H}^H\mathbf{R}\mathbf{H}\mathbf{D}\} & \Re\{\mathbf{H}^H\mathbf{R}\mathbf{H}\mathbf{D}\}\end{bmatrix},$$

$$\tilde{\mathbf{C}}_R = \begin{bmatrix}\Re\{\mathbf{H}^H\mathbf{C}^H\} & -\Im\{\mathbf{H}^H\mathbf{C}^H\}\\ \Im\{\mathbf{H}^H\mathbf{C}^H\} & \Re\{\mathbf{H}^H\mathbf{C}^H\}\end{bmatrix},$$

respectively. The PIC-MMSE detector design for non-dispersive fading channel is very similar to that of the AWGN channel, except that the transmitted signal is subjected to the complex-valued gains. Nonetheless, the difference is that the correlation matrix $\tilde{\mathbf{R}}$ and the LDS sequence matrix $\tilde{\mathbf{C}}$ are defined above, as opposed to the correlation matrix $\mathbf{R}$ and LDS sequence matrix $\mathbf{C}$ used for AWGN channel.

3) Frequency-Selective Fading Channel

There has been extensive research on LDS and/or SCMA systems communicating over AWGN [22], [32]–[34], [39], [41] and non-dispersive fading channels [25], [35], [36], [40]. Most of the studies are dedicated to frequency-selective channels relying on LDS-OFDM [67], or MC-CDMA [83]. LDS-OFDM is eminently suitable for frequency-selective channels, since its subcarriers bandwidth is narrower than the channels coherence bandwidth [84]. Traditional CDMA tends to mitigate the multipath effects by using RAKE receivers [117], [118]. A whole suite of fading-mitigation techniques were conceived in Hanzo *et al.* [119] ; Hanzo *et al.* [120]. By contrast, here we employ a transmit pre-coding scheme for overcoming the multipath channel effect as proposed by Fantuz and D'Amours, which is detailed in [84]. Briefly, this transmit precoding scheme exploits the knowledge of the CIR for transforming the multipath channel into a single-path non-dispersive channel. More explicitly, it transforms (7) to (5), which is equivalent to over non-dispersive Rayleigh fading channel model. Therefore, the MMSE-PIC detector derived for non-dispersive fading channels can be directly applied to frequency-selective channels with the aid of the transmit precoding scheme of [84].

B. PDA DETECTOR

The PDA [116], [121] has been widely applied by low-complexity design alternative of the optimal maximum *a posteriori* (MAP) symbol decoders/detectors, as a benefit of its near-optimal detection performance in rank-deficient CDMA systems [48], [116]. Explicitly, its complexity increases no faster than $\mathcal{O}(K^3)$. The PDA detector was originally conceived in 2001 for CDMA [116] and its generalized version [122] can be directly applied to our LDS system designed for BPSK and QAM transmissions. In the case of QAM, Yang *et al.* [123] presented a unified bit-based PDA detection approach, which transforms a high-order rectangular QAM based multiuser system into a BPSK multiuser system. By contrast, in [124] an SCMA scheme is converted to a BPSK modulated CDMA system. More explicitly, we can convert (3) into a BPSK system as follows,

$$\mathbf{y} = \mathbf{C}\mathbf{D}\mathbf{W}\mathbf{b}+\mathbf{n} \tag{82}$$
$$= \mathbf{Q}\mathbf{b}+\mathbf{n}, \tag{83}$$

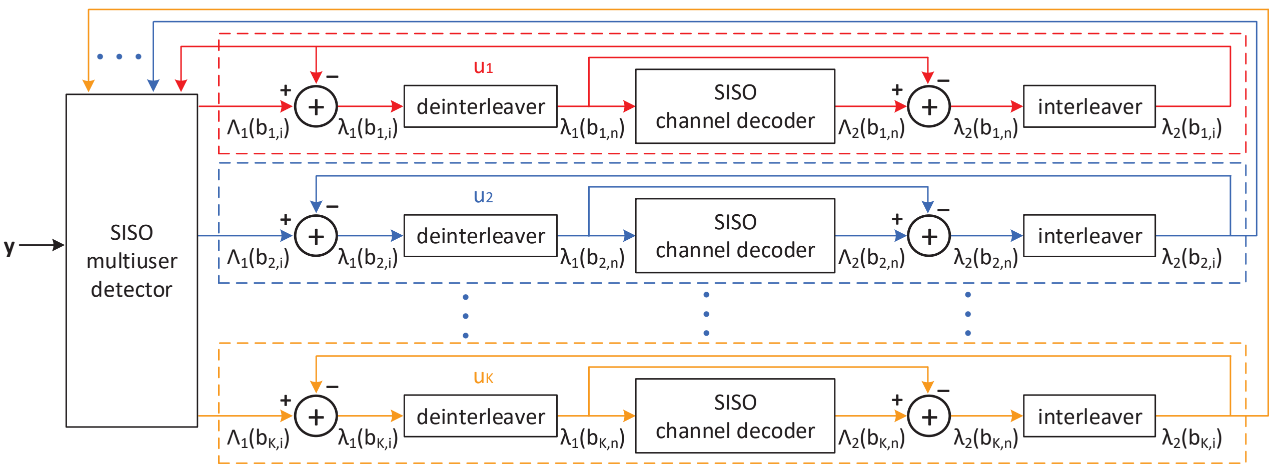

FIGURE 8. Block diagram of our iterative turbo MUD [99].

where we have $\mathbf{W} = \mathbf{I}_K \otimes \mathbf{s}^T$, $\mathbf{Q} = \mathbf{CDW}$, $\mathbf{s} = [j, 1]^T$ and $\otimes$ is a Kronecker operator. In SectionVIII we will present the BER performance of PDA detectors for transmission over AWGN, non-dispersive, and frequency-selective channels.

VI. CHANNEL ENCODING

In his groundbreaking work [125] Shannon beautifully laid out the fundamental limit of communications known as channel capacity. However, the early design of communication systems has focused on separate modulation and error correcting codes. Yet the solution to the problem of increasing the transmission rate without bandwidth expansion is to use a high-order constellation transmitting with spectral efficiency η where $1 \leq \eta \leq \log_2|\mathcal{X}|$ bits/symbol. Shannon also introduced [125] the idea of combining coding with nonbinary modulation using high-order constellations, for coded modulation (CM) [125]. In this context we emphasize that both the specific choice of coding as well as the mapping of coded bits to constellation points is influential in terms of determining the attainable performance.

The first practical CM scheme, namely the so-called multilevel coded modulation (MLCM) arrangement was introduced by Imai and Hirakawa in 1977 [126], [127]. Then in 1982 Unberboeck and Csajka developed the so-called the trellis-coded modulation (TCM) scheme that was specifically designed for increasing the Euclidean distance (ED) between the transmitted codewords because this is the most important criterion, when communicating over AWGN channels [128]. Later, CM inspired by the turbo principle has led to the so-called turbo trellis-coded modulation (TTCM) concept [129], [130].

Another important technique, namely the so-called bit-interleaved coded modulation (BICM) was conceived by Zhavi for fading channels [131]. Although BICM is inferior to TCM in terms of its ED, it outperforms TCM for transmission over fading channels as a benefit of its diversity gain. The original motivation of involving bit-interleavers was to improve the performance for transmission over fast-fading channels, because for such fading channels, the most important parameter of the code is its diversity gain rather than its ED. Morever, BICM exhibited very good performance for transmission over AWGN channels as well. This is the primary reason why BICM gained interest among researchers, but it also exhibits substantial flexibility in terms of its code design. In contrast to both TCM and TTCM, where the coding rate of $n/(n+1)$ must be carefully matched to the modulation constellation, BICM allows the constellation and the encoder to be designed more independently. The block diagram of a BICM transmitter is shown in Fig. 7 for a b_k-bit QAM scheme, while the matching SISO turbo multiuser detector [99] portrayed in Fig. 8.

VII. COMPLEXITY OF DETECTORS

The computational complexity of the existing MMSE-PIC, MPA, and PDA algorithms is compared in Table 3.

TABLE 3. Computational Complexity Comparison

Algorithms	Complexity	Main procedures
MMSE-PIC	$\mathcal{O}(K^2)$	multiplication, addition
MPA	$\mathcal{O}(M^{d_f})$	multiplication, addition
PDA	$\mathcal{O}(K^3)$	multiplication, addition

In the MMSE-PIC detector the MMSE filter, which requires matrix inversion, does not have to update the filter for every signaling interval when transmitting over AWGN channels, since there are no changes in the channel conditions. Explicitly, it can be computed before communications, given the prior knowledge of the spreading sequence of each user and the noise variance. By contrast, for non-dispersive

TABLE 4. LDS spreading code set coefficients for 4×6

	a_0	a_1	a_2	a_3	a_4	a_5	a_6	a_7	a_8	a_9	a_{10}	a_{11}
$\mathbf{C}$	1	e^{j60°	e^{j120°									
$\mathbf{C}^4$	1	e^{j30°	e^{j60°									
$\mathbf{C}^3$	1	$e^{j0.143\pi}$	$e^{j0.202\pi}$	$e^{j0.313\pi}$	$e^{j0.574\pi}$	$e^{j0.377\pi}$	$e^{j0.394\pi}$	$e^{j0.267\pi}$	$e^{j0.308\pi}$			
$\mathbf{C}^p$	0.223 $e^{j0.841\pi}$	0.975 $e^{-j0.455\pi}$	0.975 $e^{j0.455\pi}$	0.223 $e^{j0.159\pi}$	0.519 $e^{-j0.024\pi}$	0.855 $e^{-j0.943\pi}$	0.855 $e^{j0.943\pi}$	0.519 $e^{-j0.976\pi}$	0.339 $e^{-j0.964\pi}$	0.941 1	0.941 $e^{j0.036\pi}$	0.339 1
$\mathbf{C}^2$	0.646 $e^{-j0.073\pi}$	0.764 1	0.679 $e^{j0.655\pi}$	0.734 $e^{-j0.004\pi}$	0.852 $e^{-j0.639\pi}$	0.524 $e^{j0.027\pi}$	0.729 $e^{-j0.740\pi}$	0.684 1	0.743 $e^{j0.590\pi}$	0.670 1	0.594 $e^{-j0.010\pi}$	0.829 $e^{j0.024\pi}$

Note that a_0 coefficient of $\mathbf{C}^P$ can be read as $a_0 = 0.223e^{j0.841\pi}$.

and frequency-selective channels, it needs updating of the correlation matrix, as and when the channel gain changes. To avoid the regular recomputation of the filter coefficients, adaptive algorithms may be used, such as the recursive least squares or least mean squares techniques [132] for directly updating the inverse. Additionally, both the MPA and the PDA algorithms will also require some additional processing to adapt to the channel conditions [84].

In contrast to the MMSE-PIC, the MPA does not need to perform any matrix inversion, but its complexity increases exponential by both with the size of the symbol alphabet M and number of non-zero positions of the spreading waveform d_f [133]. Finally, the PDA requires matrix inversion, but fortunately this can be carried out quite efficiently with the aid of the Sherman–Morrison–Woodbury formula at an overall complexity order of $\mathcal{O}(K^3)$ [116].

VIII. COMPARISONS WITH OTHER LDS DESIGNS

In this section, we evaluate the performance of the proposed LDS code sequences generated by the algorithm of Table 2 for the LDS sequence designs of sizes 4×6 and 6×9.

A. UNCODED LDS

Simulations are performed for transmission over the complex AWGN channel using an identical transmission power for each user, whilst relying on unit-energy LDS sequences and no channel encoding. In the first experiment, we compare the LDS code matrices, of (84) and (85) that are generated by our proposed algorithm to the code matrices derived in [32], and shown in (87) and (88). The proposed algorithm is ran using the following parameters $L = 4$, $K = 6$, $\delta = 1.9$, $\sigma_d^2 = 0.5$ and $s = 2$. The initialization of the matrix $\mathbf{C}$ was performed, as discussed in Section IV-A, which results in a code set described as follows,

$$\mathbf{C}^p = \begin{bmatrix} a_0 & 0 & a_4 & 0 & 0 & a_{10} \\ a_1 & 0 & a_5 & 0 & 0 & a_{11} \\ 0 & a_2 & 0 & a_6 & a_8 & 0 \\ 0 & a_3 & 0 & a_7 & a_9 & 0 \end{bmatrix}, \tag{84}$$

where all the corresponding coefficients a_i are described in Table 4. We run again the algorithm, but this time with the random initialization of the matrix $\mathbf{C}$ with $\delta = 1.7$, which outputs the following code set,

$$\mathbf{C}^2 = \begin{bmatrix} 0 & a_2 & a_4 & 0 & 0 & a_{10} \\ a_0 & 0 & 0 & a_6 & a_8 & 0 \\ 0 & a_3 & a_5 & 0 & 0 & a_{11} \\ a_1 & 0 & 0 & a_7 & a_9 & 0 \end{bmatrix}, \tag{85}$$

where all the corresponding coefficients a_i are described in Table 4. For fair comparison, we take the existing LDS code sets presented in [32], [39], and [35] and label them as $\mathbf{C}$, $\mathbf{C}^3$, and $\mathbf{C}^4$, which are then normalized as follows,

$$\mathbf{C} = \frac{1}{\sqrt{2}} \begin{bmatrix} a_0 & a_1 & a_2 & 0 & 0 & 0 \\ a_0 & 0 & 0 & a_1 & a_2 & 0 \\ 0 & a_0 & 0 & a_1 & 0 & a_2 \\ 0 & 0 & a_0 & 0 & a_1 & a_2 \end{bmatrix}, \tag{86}$$

$$\mathbf{C}^3 = \frac{1}{\sqrt{2}} \begin{bmatrix} a_0 & a_1 & a_2 & 0 & 0 & 0 \\ a_0 & 0 & 0 & a_3 & a_5 & 0 \\ 0 & a_1 & 0 & a_4 & 0 & a_7 \\ 0 & 0 & a_2 & 0 & a_6 & a_8 \end{bmatrix}, \tag{87}$$

$$\mathbf{C}^4 = \frac{1}{\sqrt{2}} \begin{bmatrix} a_0 & a_1 & a_2 & 0 & 0 & 0 \\ a_0 & 0 & 0 & a_1 & a_2 & 0 \\ 0 & a_0 & 0 & a_1 & 0 & a_2 \\ 0 & 0 & a_0 & 0 & a_1 & a_2 \end{bmatrix}, \tag{88}$$

where all the corresponding coefficients a_i derived for each code set are described in Table 4. The properties of the matrices in our comparisons are summarized at a glance in Table 5.

TABLE 5. Comparisons ($\mathbf{C}_{4\times6}$)

Metric	$\mathbf{C}$	$\mathbf{C}^p$	$\mathbf{C}^2$	$\mathbf{C}^3$	$\mathbf{C}^4$
$d_{E,min}$	2.00	2.00	2.00	1.83	1.47
Δ_{ave}	1.49	**1.90**	1.75	1.10	1.16
$d_{P,min}$	2.00	0.76	0.04	0.11	0.29
$d_{M,min}$	2.83	2.40	2.38	2.83	2.83
C_{sum}	4.95	5.23	5.29	4.99	4.99
$S_{1,2,ave}$	0.59	**0.72**	0.60	0.59	0.59
$MWBE$	No	No	Yes	No	No

As seen in Fig. 9, $\mathbf{C}^p$ outperforms the other candidates (e.g., $\mathbf{C}$, $\mathbf{C}^3$ and $\mathbf{C}^4$), when ML detection is used. Although our proposed matrices, $\mathbf{C}^p$ and $\mathbf{C}^2$, have the same d_{min}, they have a higher value of Δ_{ave} compared to $\mathbf{C}$, $\mathbf{C}^3$ and $\mathbf{C}^4$. Furthermore, $\mathbf{C}^2$ is considered to be a MWBE matrix, whereas all the other candidates are not. However, the code set $\mathbf{C}^p$ exhibits better BER performance than $\mathbf{C}^2$.

Therefore, we surmise that the BER performance depends not only on the minimum distance (e.g., d_{min}), but also on the average Gaussian separability margin Δ_{ave}. We also note that the average sparsity of our proposed matrix $\mathbf{C}^p$ defined in (26) is higher than that of its counterparts, which is shown in bold in Table 5. In the case of the code sets having dimensions of 6×9, we illustrate the code sets generated by Table 2 $\mathbf{C}^p$, $\mathbf{C}^3$, $\mathbf{C}^4$ and $\mathbf{C}^5$. The initialization of matrix $\mathbf{C}$ is performed as discussed in Section IV-A using $\delta = 1.8$, which results in the following code set,

$$\mathbf{C}^p = \begin{bmatrix} a_0 & a_2 & 0 & 0 & 0 & 0 & 0 & a_{12} & 0 \\ a_1 & a_3 & 0 & 0 & 0 & 0 & a_{12} & 0 & 0 \\ 0 & 0 & a_4 & a_6 & 0 & 0 & 0 & 0 & 0 \\ 0 & 0 & a_5 & a_7 & 0 & 0 & 0 & 0 & 0 \\ 0 & 0 & 0 & 0 & a_8 & a_{10} & 0 & 0 & 0 \\ 0 & 0 & 0 & 0 & a_9 & a_{11} & 0 & 0 & a_{12} \end{bmatrix}, \tag{89}$$

Note in our simulations, 'off-line' computation is assumed, however 'on-line' computation can be performed upon any changes such as channel conditions, L and s-sparseness, etc.

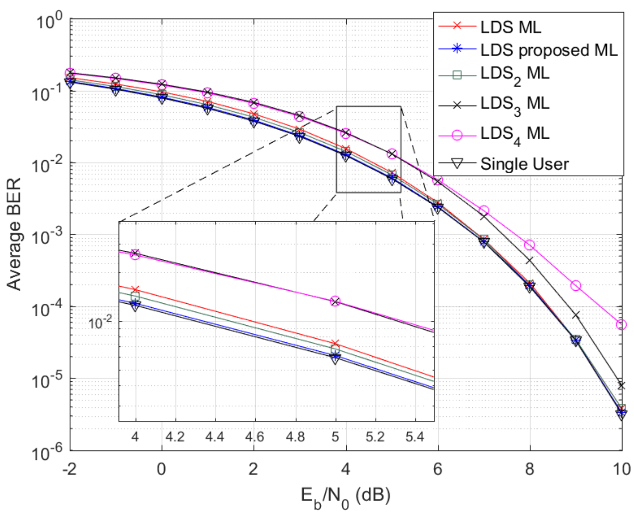

FIGURE 9. Uncoded BPSK case comparisons of $\mathbf{C}_{4\times 6}$ with labels LDS [32], LDS3 [39], LDS4 [35].

We run the algorithm once again, but this time with random initialization of the matrix $\mathbf{C}$, in conjunction with $\delta = 1.7$, $\delta = 1.65$ and $\delta = 1.65$, which outputs the following code sets,

$$\mathbf{C}^3 = \begin{bmatrix} a_0 & 0 & 0 & a_6 & 0 & 0 & a_{12} & 0 & 0 \\ a_1 & 0 & 0 & a_7 & 0 & 0 & a_{13} & 0 & 0 \\ 0 & a_2 & 0 & 0 & a_8 & 0 & 0 & a_{14} & 0 \\ 0 & a_3 & 0 & 0 & a_9 & 0 & 0 & a_{15} & 0 \\ 0 & 0 & a_4 & 0 & 0 & a_{10} & 0 & 0 & a_{16} \\ 0 & 0 & a_5 & 0 & 0 & a_{11} & 0 & 0 & a_{17} \end{bmatrix}, \tag{90}$$

$$\mathbf{C}^4 = \begin{bmatrix} a_0 & 0 & 0 & a_6 & 0 & 0 & a_{12} & 0 & 0 \\ 0 & a_2 & 0 & 0 & a_8 & 0 & 0 & a_{14} & 0 \\ 0 & 0 & a_4 & 0 & 0 & a_{10} & 0 & 0 & a_{16} \\ a_1 & 0 & 0 & a_7 & 0 & 0 & a_{13} & 0 & 0 \\ 0 & a_3 & 0 & 0 & a_9 & 0 & 0 & a_{15} & 0 \\ 0 & 0 & a_5 & 0 & 0 & a_{11} & 0 & 0 & a_{17} \end{bmatrix}, \tag{91}$$

$$\mathbf{C}^5 = \begin{bmatrix} a_0 & 0 & 0 & a_6 & 0 & 0 & a_{12} & 0 & 0 \\ 0 & a_2 & 0 & 0 & a_8 & 0 & 0 & a_{14} & 0 \\ a_1 & 0 & 0 & a_7 & 0 & 0 & a_{13} & 0 & 0 \\ 0 & a_3 & 0 & 0 & a_9 & 0 & 0 & a_{15} & 0 \\ 0 & 0 & a_4 & 0 & 0 & a_{10} & 0 & 0 & a_{16} \\ 0 & 0 & a_5 & 0 & 0 & a_{11} & 0 & 0 & a_{17} \end{bmatrix}, \tag{92}$$

where all the corresponding coefficients a_i for each code set are described in Table 6. For comparison we consider the existing LDS sequence sets proposed in [32] and label them as $\mathbf{C}$ and $\mathbf{C}^2$, which are then normalized as follows,

$$\mathbf{C} = \frac{1}{\sqrt{2}} \begin{bmatrix} 0 & 0 & a_2 & 0 & 0 & 0 & a_1 & 0 & a_0 \\ 0 & a_2 & 0 & a_1 & 0 & 0 & a_0 & 0 & 0 \\ 0 & 0 & a_1 & a_0 & 0 & a_2 & 0 & 0 & 0 \\ a_0 & 0 & 0 & 0 & a_1 & 0 & 0 & 0 & a_2 \\ a_2 & 0 & 0 & 0 & 0 & a_0 & 0 & a_1 & 0 \\ 0 & a_1 & 0 & 0 & a_0 & 0 & 0 & a_2 & 0 \end{bmatrix}, \tag{93}$$

$$\mathbf{C}^2 = \frac{1}{\sqrt{2}} \begin{bmatrix} 0 & 0 & a_0 & 0 & 0 & 0 & a_1 & 0 & a_2 \\ 0 & a_0 & 0 & a_1 & 0 & 0 & a_2 & 0 & 0 \\ 0 & 0 & a_0 & a_1 & 0 & a_2 & 0 & 0 & 0 \\ a_0 & 0 & 0 & 0 & a_1 & 0 & 0 & 0 & a_2 \\ a_0 & 0 & 0 & 0 & 0 & a_1 & 0 & a_2 & 0 \\ 0 & a_0 & 0 & 0 & a_1 & 0 & 0 & a_2 & 0 \end{bmatrix}, \tag{94}$$

where all the corresponding coefficients a_i for each code set are described in Table 6. Table 7 shows the comparison metric of all the LDS sequences. Similar to the case of the 4×6 code set, observe in Fig. 10 that the proposed $\mathbf{C}^p$ outperforms other LDS sequences in terms of its BER performance.

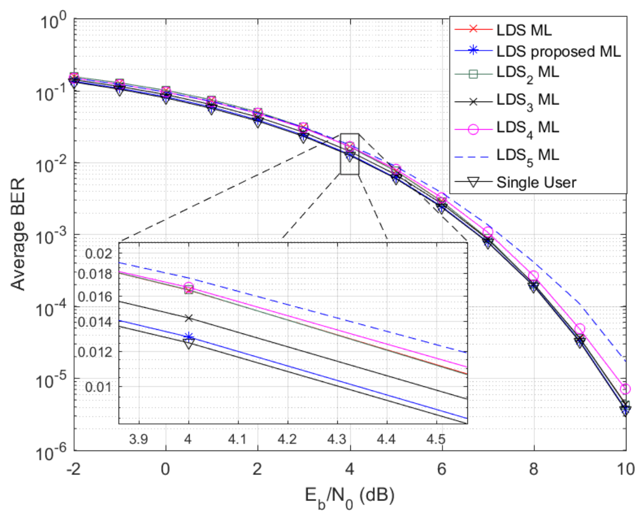

FIGURE 10. Uncoded BPSK case comparisons of $\mathbf{C}_{6\times 9}$ code sets with [32] labeled as LDS.

We again observe that the average Gaussian separability value, Δ_{ave}, and the average sparsity, $S_{1,2,ave}$, are higher for the matrix $\mathbf{C}^p$ compared the other matrices. In order to further characterize the performance, we performed simulations using channel encoding, as discussed in the next section.

B. CODED LDS

Compared to the LDS designs conceived in [32], [35], [39], the sum rate C_{sum} of our proposed codes is higher by about 0.30 bits per channel use. Hence it is expected that there is a channel code for our proposed LDS sequences that can produce a higher coded sum rate than those advocated in [32], [35], [39].

Therefore, to illustrate this hypothesis, we performed simulations using LDPC, turbo and polar encoding to compare

TABLE 6. LDS spreading code set coefficients for 6×9

	a_0	a_1	a_2	a_3	a_4	a_5	a_6	a_7	a_8	a_9	a_{10}	a_{11}	a_{12}	a_{13}	a_{14}	a_{15}	a_{16}	a_{17}
$\mathbf{C}$	1	e^{j60°	e^{j120°															
$\mathbf{C}^2$	1	e^{j60°	e^{j120°															
$\mathbf{C}^p$	0.951	0.310	0.310	0.951	0.473	0.881	0.881	0.473	0.783	0.622	0.622	0.783	1.000					
	−0.450	−0.682	0.682	−0.550	−0.870	−0.941	0.941	−0.130	0.416	−0.367	0.367	0.584	0.000					
$\mathbf{C}^3$	0.875	0.484	0.600	0.800	0.862	0.510	0.658	0.753	0.841	0.541	0.664	0.748	0.547	0.837	0.658	0.753	0.562	0.827
	−0.234	0.000	−0.778	0.000	−0.441	0.000	0.440	0.000	−0.130	0.000	0.888	0.000	−0.853	0.000	0.532	0.000	0.189	0.000
$\mathbf{C}^4$	0.351	0.937	0.785	0.620	0.865	0.502	0.865	0.502	0.615	0.789	0.419	0.908	0.793	0.609	0.711	0.704	0.760	0.651
	−1.000	0.000	0.046	−0.981	0.595	0.000	−0.448	−0.020	0.400	0.030	−0.818	0.000	0.340	0.000	−0.300	0.000	−0.140	0.000
$\mathbf{C}^5$	0.317	0.949	0.953	0.302	0.743	0.670	0.780	0.626	0.500	0.866	0.710	0.705	0.890	0.457	0.583	0.812	0.667	0.745
	0.023	1.000	−0.197	0.000	0.187	1.000	0.706	1.000	0.362	0.000	−0.145	0.000	−0.482	−1.000	−0.841	0.000	0.527	0.000

Note that a_0 and a_{12} coefficients of $\mathbf{C}^P$ can be interpreted as $a_0 = 0.951e^{-j0.450\pi}$ and $a_{12} = 1.000$.

our proposed LDS sequences to the ones advocated in [32], [35], [39].

TABLE 7. Comparisons ($\mathbf{C}_{6\times 9}$)

Metric	$\mathbf{C}$	$\mathbf{C}^p$	$\mathbf{C}^2$	$\mathbf{C}^3$	$\mathbf{C}^4$	$\mathbf{C}^5$
$d_{E,min}$	2.00	2.00	2.00	2.00	1.81	1.60
Δ_{ave}	1.34	**1**.88	1.34	1.76	1.62	1.64
$d_{P,min}$	2.00	1.10	2.00	0.03	0.26	0.02
$d_{M,min}$	2.83	2.00	2.83	2.37	2.13	1.85
C_{sum}	7.35	7.75	7.39	7.93	7.93	7.93
$S_{1,2,ave}$	0.71	**0**.84	0.71	0.73	0.74	0.75
$MWBE$	No	No	No	No	Yes	Yes

We used three different error control codes. The first is a custom semi-random parity check matrix generator for the LDPC code as described in [134]. The second, we used the long-term evolution (LTE) turbo code described in [135].

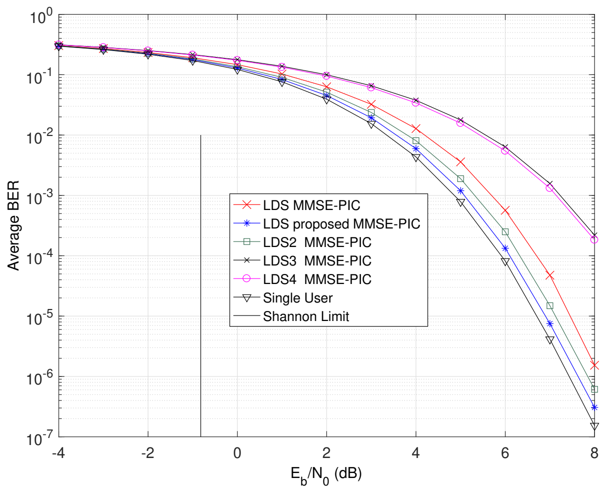

FIGURE 11. BPSK with LDPC encoding comparisons of $\mathbf{C}_{4\times 6}$ code sets with labels LDS [32], LDS3 [39], LDS4 [35].

The third we used the polar code for which we calculated the Bhattacharyya parameters for the bit channel construction method as described in [136]. The construction of the LTE turbo interleaver is based on the quadratic permutation polynomial (QPP) scheme of [135]. For all three channel encoding cases we used a code rate of $1/3$ with input message block lengths of 320 bits and the encoded code length of 972 for both the LDPC and LTE turbo codes. Furthermore, we used 340 input, and 1024 encoded code bits for polar coding. All of the output codewords the channel coders are then interleaved as in the BICM scheme discussed in Section VI.

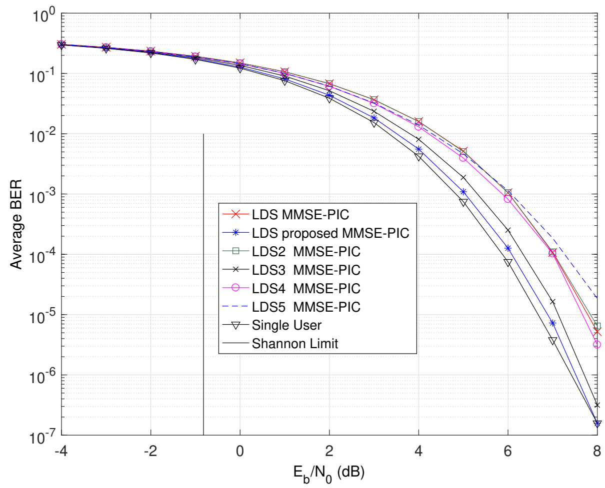

FIGURE 12. BPSK with LDPC encoding comparisons of $\mathbf{C}_{6\times 9}$ code sets with [32] labeled as LDS.

The BER performance of the LDS sequences shown in Figs. 11 - 14 for BPSK modulation shows that our proposed LDS code sets outperform the ones proposed in [32], [35], [39] for these coded cases. Thus trend is more clear when using LDPC encoding, as shown in Figs. 11 and 12 rather than LTE turbo encoding, shown in Figs. 13 and 14. In addition to the MMSE-PIC detector we applied both PDA [116] and SISO MMSE [99] detectors for BPSK modulation, which are characterized in Figs. 15 and 16. Our propsoed LDS based scheme outperforms the code set of [32] in terms of its BER performance for both the PDA and SISO MMSE detectors.

The complex PDA detector [122] was adopted for QAM, is characterized in Figs. 17-20. The SCMA scheme associated with a factor graph of 4×6 and $M = 4$ is compared to the LDS spreading matrix of size 4×6 using 4QAM in Figs. 18-20. We observe that the proposed LDS outperforms the SCMA arrangement using an MPA detector and the LDS of [32]. Similar results are also presented in Figs. 21 and 22 for bit-based PDA detection in [123].

C. LDS CODE SETS FOR 200% OVERLOAD FACTOR

In this section we evaluate the BER performance of our LDS sets for a normalized load factor of $\beta = K/L = 2$. More explicitly, we have constructed 4×8, 6×12 and 8×16 LDS code sets using our proposed algorithm presented in Table 2.

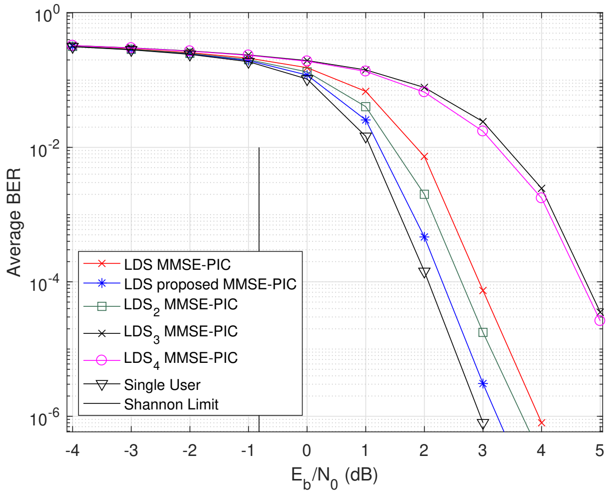

FIGURE 13. BPSK with turbo encoding comparisons of $\mathbf{C}_{4\times 6}$ code sets with labels LDS [32], LDS3 [39], LDS4 [35].

The resultant column vectors have only two non-zero values. For comparison purposes, we also included LDS sets associated with $\beta = K/L = 2$ from the designs found in [22] and [34]. The minimum Euclidean distance for the 4×8, and 6×12 LDS code sets of [22] are 1.17 and 1.43, whilst for the proposed sets they are 2.0, respectively.

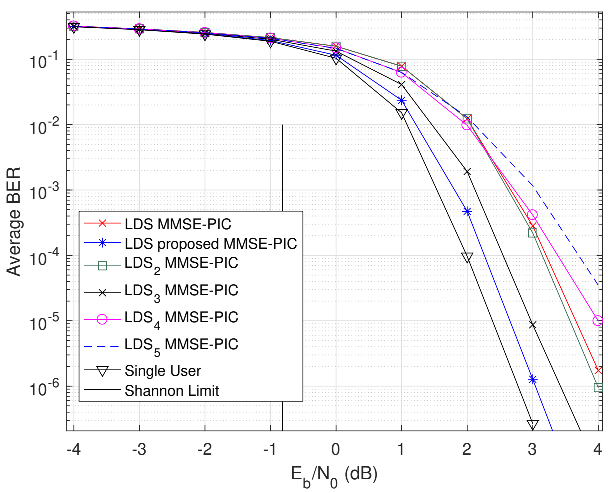

FIGURE 14. BPSK with turbo encoding comparisons of $\mathbf{C}_{6\times 9}$ code sets with [32] labeled as LDS.

Similarly, the average Gaussian separability margins for the 4×8, 6×12, and 8×16 LDS code sets of [22] are 0.96, 0.0 and 1.48, whilst for the proposed sets they are 1.79, 1.6 and 1.66, respectively.

The reason why the LDS code sets in [22] and [34] are selected as the benchmarks is because the BER performance of other LDS candidates is similar for the 200% normalized load factor scenarios.

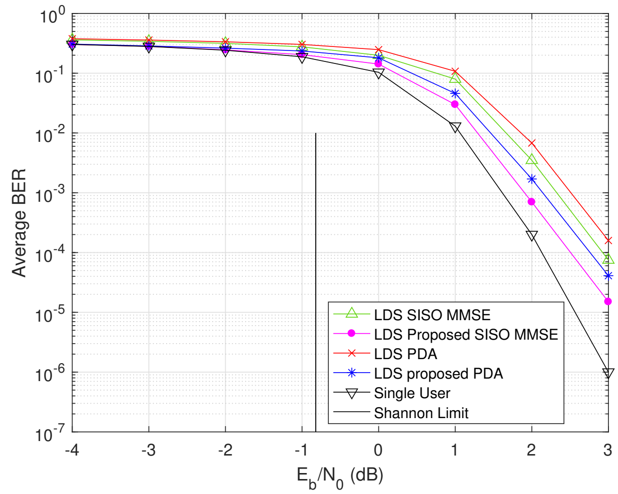

FIGURE 15. BPSK with turbo encoding comparisons of $\mathbf{C}_{4\times 6}$ code sets with [32] labeled as LDS.

Observe in Figs. 23, 27, 29 and Figs. 26, 28, 30 that our proposed LDS code sets designed both for uncoded and turbo coded scenarios outperform the LDS code sets of [22] and [34]. At the BER of 10^{-3} there is about $1-2$ dB SNR gain for the uncoded scenarios and a slighter smaller SNR gain is observed for coded scenarios.

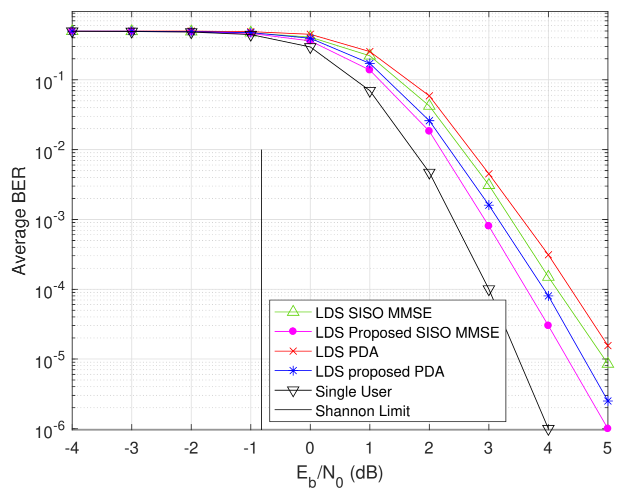

FIGURE 16. BPSK with polar encoding comparisons of $\mathbf{C}_{4\times 6}$ code sets with [32] labeled as LDS.

As seen in Figs. 23, 26-31, the proposed LDS code sets tend to approach the single-user BER. This is achieved as a benefit of the diversity gain obtained when splitting the complex vectors and matrices into real and imaginary parts, as discussed in the context of (73). For the BPSK case, our complex LDS matrix $\mathbf{C}$ of size $L \times K$ is transformed into $\mathbf{C}_R$ of size $2L \times K$ after splitting it into real and imaginary parts. In order to have an orthogonal matrix $\mathbf{C}_R$, the number of users should be $K = 2L$, hence we have $\beta = 2$.

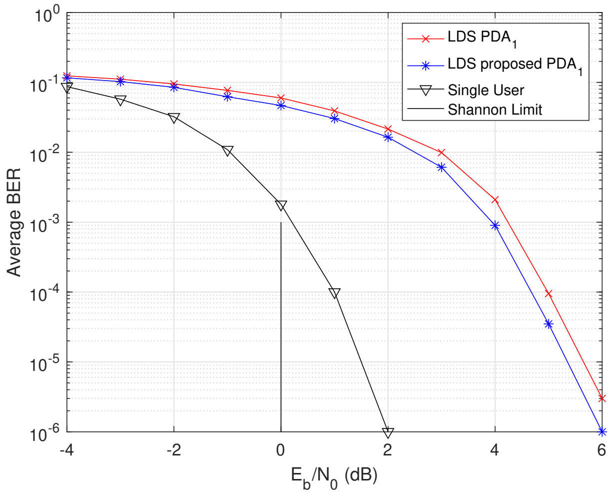

FIGURE 17. QAM with LDPC encoding, iteration number = 1, comparisons of $\mathbf{C}_{4\times6}$ code sets with [32] labeled as LDS.

The proposed LDS construction seen in Table 2 provides an LDS matrix, so that when we convert it into its real and imaginary parts, the resultant $\mathbf{C}_R$ matrix becomes near-orthogonal. This explains the reason for having a near-single-user BER performance for the proposed LDS, but we also observe that the BER performance deteriorates dramatically for scenarios of $K > 2L$. On the other hand in contrast to BPSK, for QAM signaling, the LDS matrix $\mathbf{C}$ is converted into $\mathbf{C}_R$ of size $2L \times 2K$ after the real and imaginary parts are split.

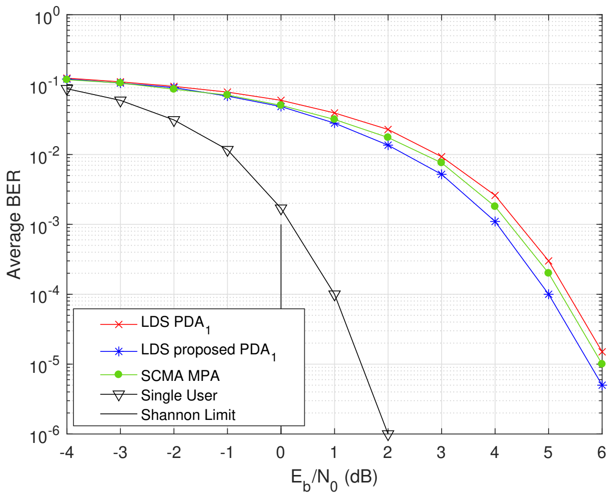

FIGURE 18. QAM with LDPC encoding, iteration number = 5, comparisons of $\mathbf{C}_{4\times6}$ code sets with [32] labeled as LDS.

Therefore, $\mathbf{C}_R$ cannot be orthogonal, unless we have $L = K$, as verified by our simulations.

Furthermore, the orthogonality of $\tilde{\mathbf{C}}_R$ in BPSK signalling can be further degraded, when no transmitter precoding is utilized for transmission over frequency-selective fading channels. The performance difference of LDS codes over non-dispersive and frequency-selective fading channels are portrayed in Figs. 32 and 33. In our simulations, we assumed $L_p = 7$ for the frequency-selective fading channel.

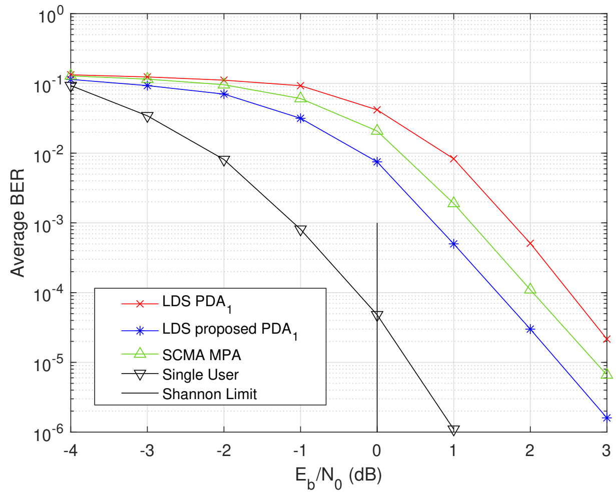

FIGURE 19. QAM with turbo encoding, iteration number = 1, comparisons of $\mathbf{C}_{4\times6}$ code sets with [32] labeled as LDS.

As for future research, we have to perform a detailed stochastic analysis of the legitimate LDS code sets for complex signal constellations to find the specific sets, which have the best performance. We also have to study the direct optimization of the matrix $\mathbf{C}_R$ in real domain in order to achieve near-orthogonality, instead of optimizing $\mathbf{C}$ in the complex domain under the constraint of keeping the non-zero locations of the real and imaginary parts identical.

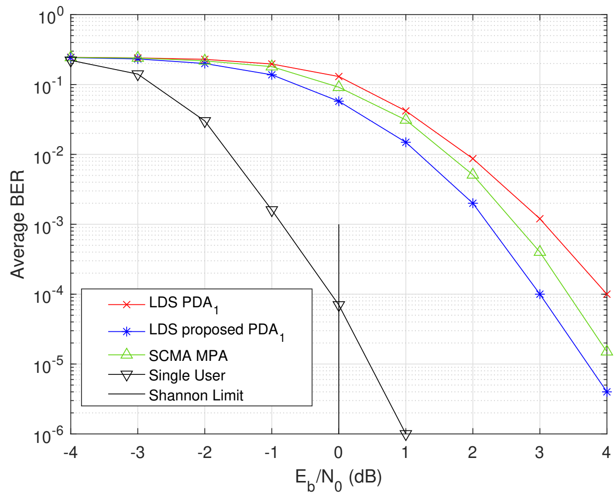

FIGURE 20. QAM with polar encoding, iteration number = 1, comparisons of $\mathbf{C}_{4\times6}$ code sets with [32] labeled as LDS.

As for QAM, we can investigate the design of matrices for the rank-deficient scenarios of $K > L$ in the real domain instead of the complex domain. Furthermore, we have to conceive LDS designs for ensuring that the resultant $\tilde{\mathbf{C}}_R$ is near-orthogonal even under fading channels.

D. SPECTRAL EFFICIENCY

One of the key performance metrics of LDS spreading code design is the resultant spectral efficiency, $\eta_{LDS}(\mathbf{C}, \gamma)$ (bits/s/Hz), which can be expressed as a function of either the SNR, γ or of the energy per bit E_b/N_o.

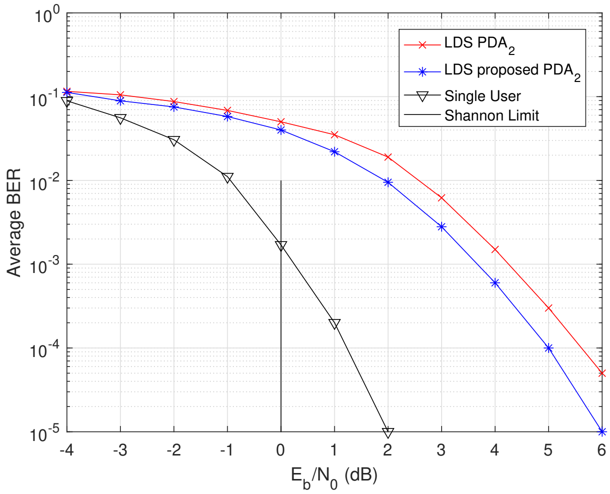

FIGURE 21. QAM with LDPC encoding, iteration number = 5, comparisons of $\mathbf{C}_{4\times 6}$ code sets with [32] labeled as LDS.

The spectral efficiency $\eta_{LDS}(\mathbf{C}, \gamma)$ is defined as the maximum mutual information between the symbol vector $\mathbf{x}$ and the observed L-dimensional vector $\mathbf{y}$ in (3) for a given $\mathbf{C}$ over distributions of $\mathbf{x}$ normalized to L.

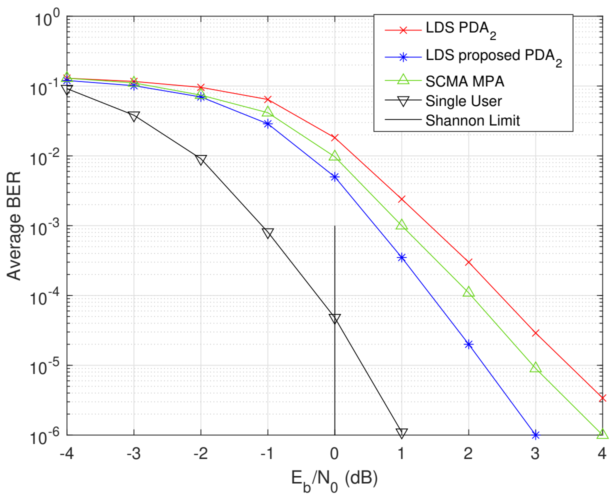

FIGURE 22. QAM with turbo encoding, iteration number = 1, comparisons of $\mathbf{C}_{4\times 6}$ code sets with [32] labeled as LDS.

Under the constraint of $\mathbb{E}\{\mathbf{x}\mathbf{x}^H\} = E_s\mathbf{I}_L$, the optimum detection for a given LDS $\mathbf{C}$ may be achieved; for a Gaussian distributed $\mathbf{x}$ the resultant spectral efficiency $\eta_{LDS}(\mathbf{C}, \gamma)$ can be expressed by [10]

$$\eta_{LDS}(\mathbf{C}, \gamma) = \frac{C_{sum}(\mathbf{C}, \gamma)}{L} = \frac{1}{L}\log_2 |\mathbf{I}_L + \gamma \mathbf{C}\mathbf{D}\mathbf{D}^H\mathbf{C}^H|, \tag{95}$$

where E_s denotes energy per symbol, $N_o\mathbf{I}_L$ is the noise covariance and the per-symbol SNR γ is given by [137]

$$\gamma = \frac{\frac{1}{K}\mathbb{E}\{|\mathbf{x}|^2\}}{\frac{1}{L}\mathbb{E}\{|\mathbf{n}|^2\}} = \frac{\frac{1}{K}E_b N_b}{\frac{1}{L}N_o L} = \frac{1}{\beta}\frac{E_b}{N_o}\frac{N_b}{L} = \frac{1}{\beta}\frac{E_b}{N_o}\eta_{LDS}, \tag{96}$$

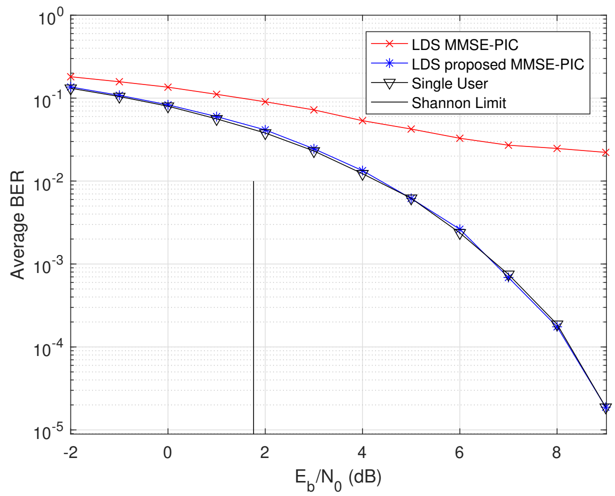

FIGURE 23. Uncoded BPSK transmission, $\mathbf{C}_{4\times 8}$ code sets with [22] labeled as LDS.

where we have $\mathbb{E}\{|\mathbf{x}|^2\} = N_b E_b$, $\mathbb{E}\{|\mathbf{n}|^2\} = LN_o$, N_b denotes the number of bits encoded in $\mathbf{x}$ for a capacity-achieving system, and N_b/L, which is expressed in bits per dimension, represents the spectral efficiency of (95). Since L denotes the number of complex dimensions in our system, $\eta_{LDS}(\mathbf{C}, \gamma)$, can be interpreted as the maximum number of bits per each complex dimension.

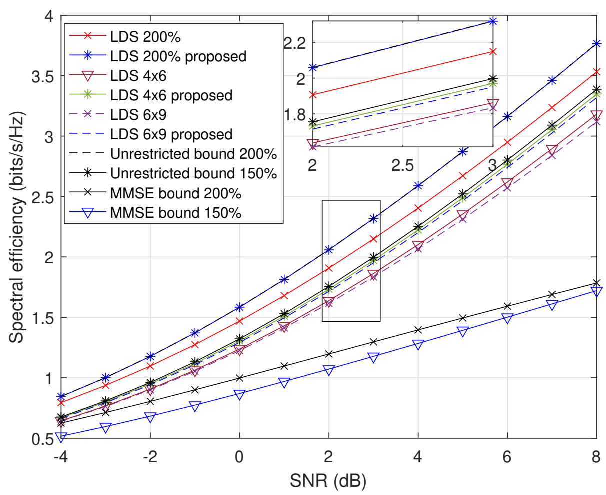

FIGURE 24. Spectral efficiency vs SNR of the AWGN channel for BPSK.

An upper bound on $\eta_{LDS}(\mathbf{C}, \gamma)$ can be considered as the spectral efficiency, when the LDS spreading sequence has a length of $L = 1$. This is equivalent of a K-user Gaussian multiple access channel and its spectral efficiency in the case of the average-energy-constraint is given by $\log_2(1 + \gamma d_{tot})$ bits/s/Hz per chip [87], where $d_{tot} = \mathbf{c}_1'\mathbf{c}_1'^H = \cdots =$

$\mathbf{c}'_L\mathbf{c}'^H_L$, and $\mathbf{c}'_{\mathbf{i}}$ are row vectors of $\mathbf{CD}$. We can show that $\eta_{LDS}(\mathbf{C},\gamma)$ is indeed capable of achieving the upper bound even when $L > 1$.

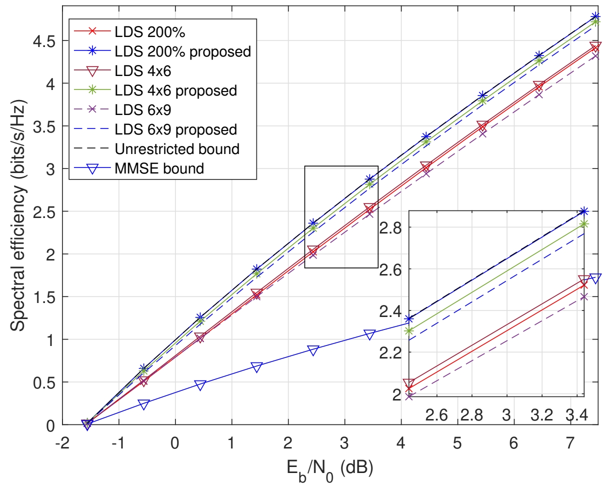

FIGURE 25. Spectral efficiency vs E_b/N_o of the AWGN channel for BPSK.

Proposition 1. *Let* $\mathbf{C}$ *be an LDS spreading matrix with* $\mathbf{D}$ *being the diagonal energy-constraint matrix and* $K > L$*. Then, we have:*

$$\eta_{LDS}(\mathbf{C},\gamma) \leq \log_2\left(1+\gamma d_{tot}\right). \tag{97}$$

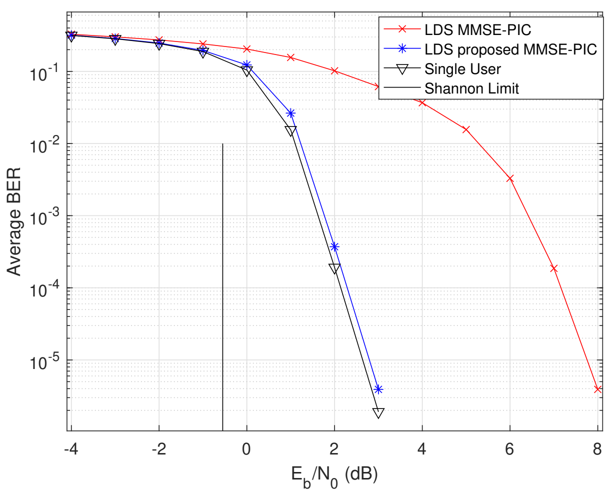

FIGURE 26. Turbo coded BPSK transmission, $\mathbf{C}_{4\times 8}$ code sets with [22] labeled as LDS.

The necessary and sufficient condition of attaining the spectral efficiency upper bound of the system dispensing with spreading when the LDS signature waveforms are WBE sequences, is that of satisfying the condition $\mathbf{CDD}^H\mathbf{C}^H = d_{tot}\mathbf{I}_L$ *[87].*

Proof. The proposition can be proved by first applying Hadamard's inequality [138] to the determinant in (95), yielding:

$$|\mathbf{I}_L + \gamma d_{tot}\mathbf{I}_L| \leq \prod_{i=1}^{L}(1+\gamma d_{tot}). \tag{98}$$

Indeed the above expression satisfies the condition of equality, since the determinant is a diagonal matrix. Then using Jensen's inequality, we have [138]:

$$\begin{aligned}\log_2|\mathbf{I}_L + \gamma d_{tot}\mathbf{I}_L| &= \log_2\prod_{i=1}^{L}(1+\gamma d_{tot})\\ &= \sum_{i=1}^{L}\log_2\left(1+\gamma d_{tot}\right)\\ &= L\log_2\left(1+\gamma d_{tot}\right).\end{aligned} \tag{99}$$

□

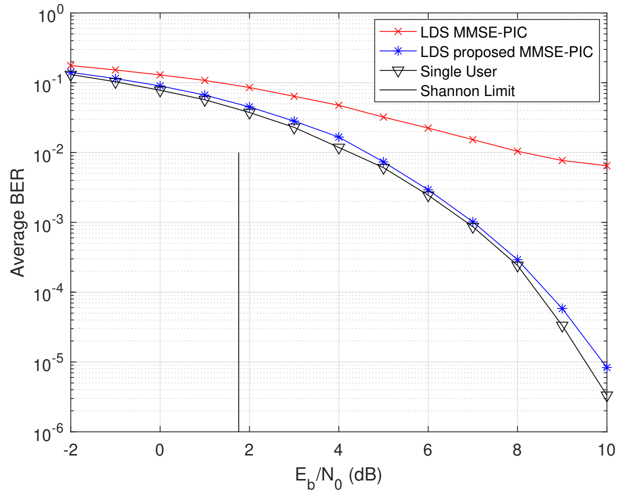

FIGURE 27. Uncoded BPSK transmission, $\mathbf{C}_{6\times 12}$ code sets with [22] labeled as LDS.

Since in our design the columns of $\mathbf{C}$ are of unit-length and $\mathbf{D} = \mathbf{I}_K$, the Frobenius norm of $\mathbf{CD}$ can be written as

$$||\mathbf{CD}||_F = \sum_{k=1}^{K}\mathbf{c}_k^H\mathbf{c}_k = \sum_{i=1}^{L}\mathbf{c}'_i\mathbf{c}'^H_i = K. \tag{100}$$

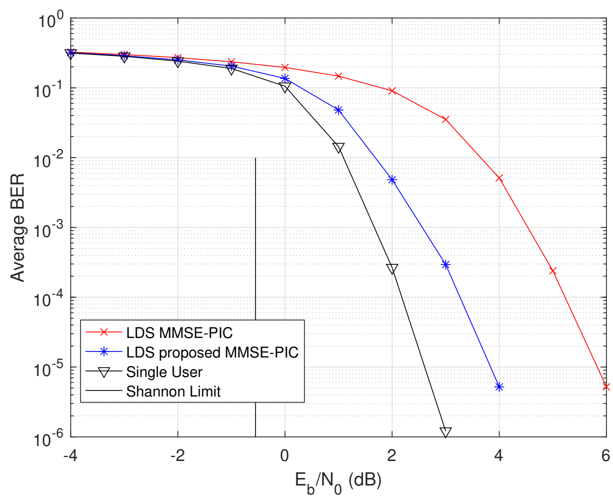

FIGURE 28. Turbo coded BPSK transmission, $\mathbf{C}_{6\times 12}$ code sets with [22] labeled as LDS.

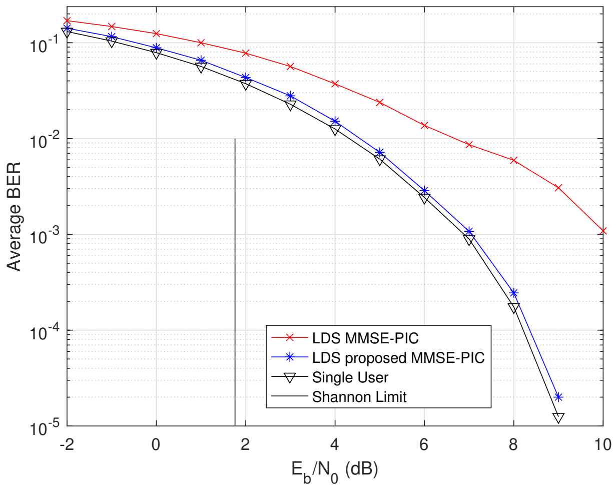

FIGURE 29. Uncoded BPSK transmission, $\mathbf{C}_{8\times16}$ code sets with [22] labeled as LDS.

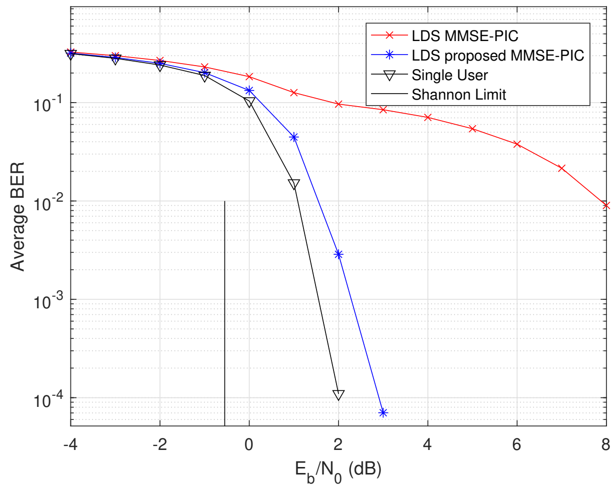

FIGURE 31. Turbo coded BPSK transmission, $\mathbf{C}_{8\times16}$ code sets with [34] labeled as LDS.

Therefore, we have $d_{tot} = K/L$ as $\mathbf{c}_1'\mathbf{c}_1'^H = \cdots = \mathbf{c}_L'\mathbf{c}_L'^H$. Note that if the K users do not have equal average-input-energy constraints, i.e., $\mathbf{D}\mathbf{D}^H \neq d'\mathbf{I}_L$, it is generally hard to design an LDS code set that maximizes $\eta_{LDS}(\mathbf{C},\gamma)$ in Proposition 1.

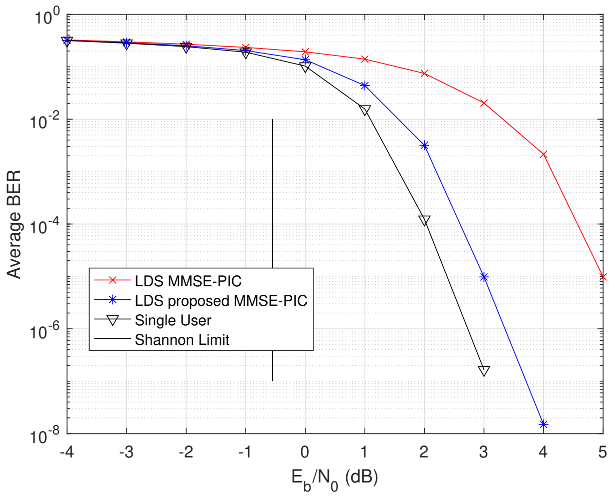

FIGURE 30. Turbo coded BPSK transmission, $\mathbf{C}_{8\times16}$ code sets with [22] labeled as LDS.

In all our BER performance plots, the information rates for LDS 4×6, 6×9, 4×8, 6×12 and 8×16 in case of BPSK are $\eta_{LDS} = N_b/L = 1.5$, $\eta_{LDS} = 1.5$, $\eta_{LDS} = 2$, $\eta_{LDS} = 2$, and $\eta_{LDS} = 2$ bits/s/Hz, respectively. Therefore, the corresponding unrestricted Shannon limits are calculated by using the upper bound $\log_2(1+\gamma\beta)$ (97) as $E_b/N_o = (2^{\eta_{LDS}}-1)/\eta_{LDS}$, $E_b/No = 1.219(0.86\text{dB})$ and $E_b/No = 1.5$ (1.76dB) for $\eta_{LDS} = 1.5$ and $\eta_{LDS} = 2$, respectively. In case of 4QAM (2 bits per symbol) the corresponding η_{LDS} is multiplied by 2 and for a channel coding rate of $1/3$ by $1/3$.

In addition to analysing the spectral efficiency of the optimal detection, a range of linear detectors, such as the single-user MF (SUMF), ZF, MMSE are derived in [64]. The spectral efficiency of these multiple access channels is given by [64]:

$$\begin{aligned} R_{\text{lds}}^{\text{sumf}}(\beta,\gamma) &= R_{\text{lds}}^{\text{zf}}(\beta,\gamma) = R_{\text{lds}}^{\text{mmse}}(\beta,\gamma) \\ &= \beta\sum_{k\geq0}\frac{\beta^k\exp(-\beta)}{k!}\log_2\left(1+\frac{\gamma}{k\gamma+1}\right) \end{aligned}$$

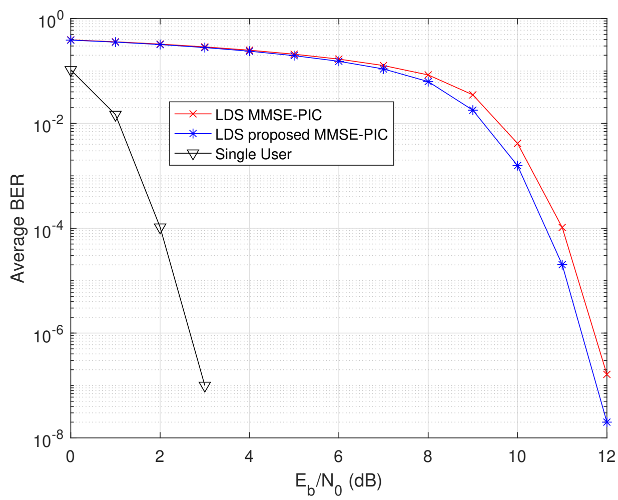

FIGURE 32. Turbo coded BPSK transmission over non-dispersive fading chananel, $\mathbf{C}_{8\times16}$ code sets with [22] labeled as LDS.

where ! denotes factorial. The proposed LDS design approaches the upper bound of the spectral efficiency, as shown in Figs. 24 and 25 for the case of optimal detection.

On average there is a 0.2 bits/s/Hz gap between our proposed scheme and the existing state-of-the-art LDS designs. According to Proposition 1 the proposed LDSs are WBE sequences or exhibit WBE-like properties, as they approach the upper bound. Having LDS code sets exhibiting optimal spectral efficiency inspires us to design low-complexity detectors such as the MMSE-PIC arrangement, which is capable of operating even beyond a normalized load factor of 200%.

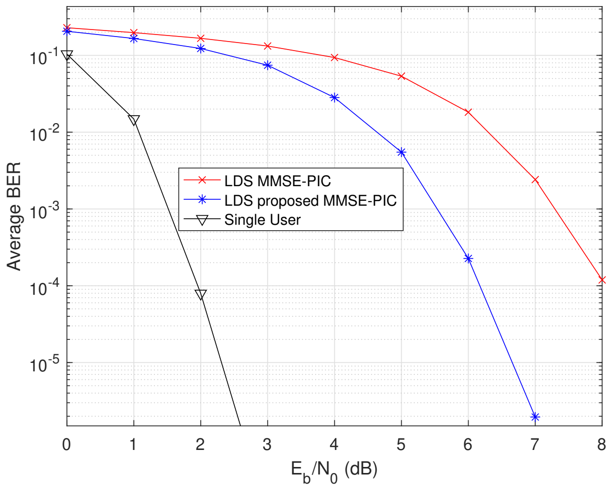

FIGURE 33. Turbo coded BPSK transmission over frequency-selective fading channel, $\mathbf{C}_{8\times16}$ code sets with [22] labeled as LDS.

IX. CONCLUSION AND DESIGN GUIDELINES

In this paper, we have provided a comprehensive literature review of LDS construction designs by considering the most recent developments. Both the design and application of LDS code sets have been described in Tables 2 and 3, respectively. Widely used design criteria conceived for developing the LDS matrices have also been presented. Moreover, we conceived an improved LDS sequence design based on the Gaussian separability criterion. We demonstrated that achieving the best BER performance depends not only on the minimum distance, but also on the average Gaussian separability margin.

Based on that criterion, we developed an iterative algorithm that is based on maximizing the SINR of each individual user of interest, which converges to the desired solution. We select the optimum candidates having the highest minimum distance and those associated with the highest average Gaussian separability, which perform well along with channel coding.

Our proposed LDS code set outperforms the existing LDS designs both for BPSK and 4QAM transmission in terms of its BER. We elaborate a little further on the design guidelines associated with the proposed algorithm and presented in Table 2. More explicitly, as portrayed in Figs. 9 and 10, our code design, conceived, for 4×6 and 6×9 constructions provides some, modest, power gain compared to other code designs without any increase in computational complexity when using our codes. A compelling BER performance is shown for the size of $K = 2L$. Our conclusion is that the Gaussian separability margin has to be considered when comparing code sets with equal minimum Euclidean distance or TSC properties. We can summarize our design guidelines as follows:

(1) For a given transmission channel, we have to determine the number of users K, the length L of the waveform sequence, the grade of sparseness, as well as the parameters δ and σ_d, which are obtained heuristically, as discussed in Section IV.
(2) The proposed designs jointly map the signals of the users to REs in a sparse manner, they perform constellation shaping and judiciously allocate the power to each spreading sequence.
(3) The proposed algorithm is iterative, hence whenever there is a change in the channel conditions and/or the number of users K, we can re-run our algorithm to produce new LDS codes. However, if for some reason one should avoid adapting to the channel environment, we suggest to use the average noise variance associated with the maximum number of users. If less users are present, using a subset of the LDS code sets is recommended.

Furthermore, we also proposed a low-complexity minimum mean-square estimation and parallel interference cancellation aided detector, which exhibited a comparable BER performance to that of ML detection. The MMSE-PIC algorithm has however much lower complexity than the MPA. In our future research we will conceive LDS designs for higher-order constellations for transmission over dispersive fading channels and the radical direct minimum BER optimization criterion of [139].

REFERENCES

[1] L. Dai, B. Wang, Z. Ding, Z. Wang, S. Chen, and L. Hanzo, "A survey of non-orthogonal multiple access for 5G," *IEEE Commun. Surveys & Tuts.*, vol. 20, no. 3, pp. 2294–2323, thirdquarter 2018.

[2] C. Bockelmann, N. K. Pratas, G. Wunder, S. Saur, M. Navarro, D. Gregoratti, G. Vivier, E. De Carvalho, Y. Ji, C. Stefanovic, P. Popovski, Q. Wang, M. Schellmann, E. Kosmatos, P. Demestichas, M. Raceala-Motoc, P. Jung, S. Stanczak, and A. Dekorsy, "Towards massive connectivity support for scalable mMTC communications in 5G networks," *IEEE Access*, vol. 6, pp. 28 969–28 992, May 2018.

[3] A. Ghosh, A. Maeder, M. Baker, and D. Chandramouli, "5G evolution: A view on 5G cellular technology beyond 3GPP release 15," *IEEE Access*, vol. 7, pp. 127 639–127 651, Sep. 2019.

[4] J. Ding, M. Nemati, C. Ranaweera, and J. Choi, "IoT connectivity technologies and applications: A survey," *IEEE Access*, vol. 8, pp. 67 646–67 673, Apr. 2020.

[5] L. Chettri and R. Bera, "A comprehensive survey on internet of things (IoT) toward 5g wireless systems," *IEEE Internet of Things Journal*, vol. 7, pp. 16–32, Jan. 2020.

[6] C. Kalalas and J. Alonso-Zarate, "Massive connectivity in 5G and beyond: Technical enablers for the energy and automotive verticals," in *Proc. 6G Wireless Summit (6G SUMMIT)*, Levi, Finland, May 2020, pp. 1–5.

[7] H. Kulhandjian, "A visible light communications framework for intelligent transportation systems," Mineta Transportation Institute Publications, Tech. Rep., Project No. 1911, August 2020.

[8] R. M. Marè, C. E. Cugnasca, C. L. Marte, and G. Gentile, "Intelligent transport systems and visible light communication applications: An overview," in *Proc. of IEEE International Conf. on Intelligent Transportation Systems (ITSC)*, Rio de Janeiro, Brazil, Nov. 2016, pp. 2101–2106.

[9] H. Sari, F. Vanhaverbeke, and M. Moeneclaey, "Extending the capacity of multiple access channels," *IEEE Commun. Mag.*, vol. 38, no. 1, pp. 74–82, Jan. 2000.

[10] S. Verdu and S. Shamai, "Spectral efficiency of CDMA with random spreading," *IEEE Trans. Inf. Theory*, vol. 45, no. 2, pp. 622–640, Mar. 1999.

[11] H. Sari, F. Vanhaverbeke, and M. Moeneclaey, "Multiple access using two sets of orthogonal signal waveforms," *IEEE Commun. Lett.*, vol. 4, no. 1, pp. 4–6, Jan. 2000.

[12] F. Vanhaverbeke, M. Moeneclaey, and H. Sari, "DS/CDMA with two sets of orthogonal spreading sequences and iterative detection," *IEEE Commun. Lett.*, vol. 4, no. 9, pp. 289–291, Sep. 2000.

[13] M. Kulhandjian and D. A. Pados, "Uniquely decodable code-division via augmented Sylvester-Hadamard matrices," in *Proc. IEEE Wireless Commun. and Network. Conf. (WCNC)*, Paris, France, Apr. 2012, pp. 359–363.

[14] M. Kulhandjian, C. D'Amours, and H. Kulhandjian, "Uniquely decodable ternary codes for synchronous CDMA systems," in *Proc. IEEE Pers., Indoor, Mobile Radio Conf. (PIMRC)*, Bologna, Italy, Sep. 2018, pp. 1–6.

[15] M. Kulhandjian, C. D'Amours, H. Kulhandjian, H. Yanikomeroglu, D. A. Pados, and G. Khachatrian, "Fast decoder for overloaded uniquely decodable synchronous CDMA," *arXiv:1806.03958 [eess.SP]*, Jun. 2018. [Online]. Available: https://arxiv.org/abs/1806.03958

[16] M. Kulhandjian, C. D'Amours, H. Kulhandjian, H. Yanikomeroglu, and G. Khachatrian, "Fast decoder for overloaded uniquely decodable synchronous optical CDMA," in *Proc. IEEE Wireless Commun. and Network. Conf. (WCNC)*, Marrakech, Morocco, Apr. 2019, pp. 1–7.

[17] M. Basharat, W. Ejaz, M. Naeem, A. Masood Khattak, and A. Anpalagan, "A survey and taxonomy on nonorthogonal multiple-access schemes for 5G networks," *Trans. on Emerging Telecommun. Technologies*, vol. 29, no. 1, p. e3202, Jun. 2017.

[18] Q. Wang, R. Zhang, L. Yang, and L. Hanzo, "Non-orthogonal multiple access: A unified perspective," *IEEE Wireless Commun.*, vol. 25, no. 2, pp. 10–16, Apr. 2018.

[19] N. Ye, H. Han, L. Zhao, and A.-H. Wang, "Uplink nonorthogonal multiple access technologies toward 5G: A survey," *Wireless Commun. and Mobile Comp.*, vol. 2018, no. article ID 6187580, pp. 1–26, Jun. 2018.

[20] M. B. Shahab, R. Abbas, M. Shirvanimoghaddam, and S. J. Johnson, "Grant-free non-orthogonal multiple access for IoT: A survey," *arXiv:1910.06529 [eess.SP]*, Oct. 2019. [Online]. Available: https://arxiv.org/abs/1910.06529

[21] L. Dai, B. Wang, Y. Yuan, S. Han, C. I, and Z. Wang, "Non-orthogonal multiple access for 5G: solutions, challenges, opportunities, and future research trends," *IEEE Commun. Mag.*, vol. 53, no. 9, pp. 74–81, Sep. 2015.

[22] R. Hoshyar, F. P. Wathan, and R. Tafazolli, "Novel low-density signature for synchronous CDMA systems over AWGN channel," *IEEE Trans. Signal Process.*, vol. 56, no. 4, pp. 1616–1626, Apr. 2008.

[23] R. Razavi, M. AL-Imari, M. A. Imran, R. Hoshyar, and D. Chen, "On receiver design for uplink low density signature OFDM (LDS-OFDM)," *IEEE Trans. Commun.*, vol. 60, no. 11, pp. 3499–3508, Nov. 2012.

[24] H. Nikopour and H. Baligh, "Sparse code multiple access," in *Proc. IEEE Pers., Indoor, Mobile Radio Conf. (PIMRC)*, London, U.K., Sep. 2013, pp. 332–336.

[25] L. Li, Z. Ma, P. Z. Fan, and L. Hanzo, "High-dimensional codebook design for the SCMA down link," *IEEE Trans. on Vehic. Tech.*, vol. 67, no. 10, pp. 10 118–10 122, Oct. 2018.

[26] S. Chen, B. Ren, Q. Gao, S. Kang, S. Sun, and K. Niu, "Pattern division multiple access - a novel nonorthogonal multiple access for fifth-generation radio networks," *IEEE Trans. on Vehic. Tech.*, vol. 66, no. 4, pp. 3185–3196, Apr. 2017.

[27] Z. Yuan, G. Yu, W. Li, Y. Yuan, X. Wang, and J. Xu, "Multi-user shared access for internet of things," in *Proc. IEEE Veh. Technol. Conf. (VTC Spring)*, Nanjing, China, May 2016, pp. 1–5.

[28] M. Vameghestahbanati, I. D. Marsland, R. H. Gohary, and H. Yanikomeroglu, "Multidimensional constellations for uplink SCMA systems—a comparative study," *IEEE Commun. Surveys & Tuts.*, vol. 21, no. 3, pp. 2169–2194, thirdquarter 2019.

[29] M. Mohammadkarimi, M. A. Raza, and O. A. Dobre, "Signature-based nonorthogonal massive multiple access for future wireless networks: Uplink massive connectivity for machine-type communications," *IEEE Veh. Technol. Magazine*, vol. 13, no. 4, pp. 40–50, Dec. 2018.

[30] J. Choi, "Low density spreading for multicarrier systems," in *Proc. IEEE Int. Symp. Spread Spectr. Techn. Appl. Programm. Book Abstracts (ISSSTA)*, Sydney, Australia, Aug. 2004, pp. 575–578.

[31] R. Hoshyar, F. P. Wathan, and R. Tafazolli, "Novel low-density signature structure for synchronous DS-CDMA systems," in *Proc. IEEE Global Telecommun. Conf. (GLOBECOM)*, San Francisco, U.S.A., Nov. 2006, pp. 1–5.

[32] J. van de Beek and B. M. Popović, "Multiple access with low-density signatures," in *Proc. IEEE Global Telecommun. Conf. (GLOBECOM)*, Honolulu, U.S.A., Nov. 2009, pp. 1–6.

[33] A. R. Safavi, A. G. Perotti, and B. M. Popović, "Ultra low density spread transmission," *IEEE Commun. Lett.*, vol. 20, no. 7, pp. 1373–1376, Jul. 2016.

[34] T. Qi, W. Feng, and Y. Wang, "Optimal sequences for non-orthogonal multiple access: A sparsity maximization perspective," *IEEE Commun. Lett.*, vol. 21, no. 3, pp. 636–639, Mar. 2017.

[35] T. Qi, W. Feng, Y. Chen, and Y. Wang, "When NOMA meets sparse signal processing: Asymptotic performance analysis and optimal sequence design," *IEEE Access*, vol. 5, pp. 18 516–18 525, Jul. 2017.

[36] C. Jiang and Z. Wu, "A novel uplink NOMA scheme based on low density superposition modulation," in *Proc. IEEE Veh. Technol. Conf. (VTC-Fall)*, Toronto, Canada, Sep. 2017, pp. 1–5.

[37] T. Qi, W. Feng, and Y. Wang, "On the sparsity of spreading sequences for NOMA with reliability guarantee and detection complexity limitation," in *Proc. IEEE Veh. Technol. Conf. (VTC-Spring)*, Sydney, Australia, Jun. 2017, pp. 1–6.

[38] J. Zhang, X. Wang, X. Yang, and H. Zhou, "Low density spreading signature vector extension (LDS-SVE) for uplink multiple access," in *Proc. IEEE Veh. Technol. Conf. (VTC-Fall)*, Toronto, Canada, Sep. 2017, pp. 1–5.

[39] G. Song, X. Wang, and J. Cheng, "Signature design of sparsely spread code division multiple access based on superposed constellation distance analysis," *IEEE Access*, vol. 5, pp. 23 809–23 821, Oct. 2017.

[40] H. Yu, Z. Fei, N. Yang, and N. Ye, "Optimal design of resource element mapping for sparse spreading non-orthogonal multiple access," *IEEE Wireless Commun. Lett.*, vol. 7, no. 5, pp. 744–747, Oct. 2018.

[41] K. Zhang, J. Xu, C. Yin, W. Tan, and C. Li, "A sparse superposition multiple access scheme and performance analysis for 5G wireless communication systems," in *Proc. IEEE/CIC Int. Conf. on Commun. in China (ICCC) Workshops*, Kansas City, U.S.A., May 2018, pp. 90–95.

[42] H. Wang, K. Xiao, B. Xia, and J. Wang, "Performance analysis and optimization for the LDPC-coded multi-carrier LDS system," in *Proc. IEEE Veh. Technol. Conf. (VTC-Spring)*, Kuala Lumpur, Malaysia, Apr. 2019, pp. 1–5.

[43] K. Lu and C. Jiang, "Optimized low density superposition modulation for 5G mobile multimedia wireless networks," *IEEE Access*, vol. 7, pp. 174 227–174 235, Dec. 2019.

[44] Z. Liu, P. Xiao, and Z. Mheich, "Power-imbalanced low-density signatures (LDS) from Eisenstein numbers," in *Proc. IEEE VTS Asia Pacific Wireless Commun. Symp. (APWCS)*, Singapore, Aug. 2019, pp. 1–5.

[45] Y. Sun, "Quasi-large sparse-sequence CDMA: Approach to single-user bound by linearly-complex LAS detector," in *Proc. IEEE Annual Conf. on Inf. Sci. and Systems*, Princeton, U.S.A., Mar. 2008, pp. 320–323.

[46] R. Lupas and S. Verdu, "Linear multiuser detectors for synchronous code-division multiple-access channels," *IEEE Trans. Inf. Theory*, vol. 35, no. 1, pp. 123–136, Jan. 1989.

[47] B. Hassibi and H. Vikalo, "On the sphere-decoding algorithm I. Expected complexity," *IEEE Trans. Signal Processing*, vol. 53, no. 8, pp. 2806–2818, Aug. 2005.

[48] G. Romano, F. Palmieri, P. K. Willett, and D. Mattera, "Separability and gain control for overloaded CDMA," in *Proc. of the Conf. on Inf. Sci. and Sys. (CISS)*, Princeton, NJ, USA, Mar. 2005, pp. 1–6.

[49] M. K. Varanasi, "Decision feedback multiuser detection: a systematic approach," *IEEE Trans. Inf. Theory*, vol. 45, no. 1, pp. 219–240, Jan. 1999.

[50] Y. Sun and J. Xiao, "Multicode sparse-sequence CDMA: Approach to optimum performance by linearly complex wslas detectors," *Wireless Pers. Commun.*, vol. 71, no. 2, pp. 1049–1056, Jul. 2013.

[51] P. G. Casazza, A. Heinecke, F. Krahmer, and G. Kutyniok, "Optimally sparse frames," *IEEE Trans. Inf. Theory*, vol. 57, no. 11, pp. 7279–7287, Nov. 2011.

[52] K. Xiao, B. Xia, Z. Chen, J. Wang, D. Chen, and S. Ma, "On optimizing multicarrier-low-density codebook for GMAC with finite alphabet inputs," *IEEE Commun. Lett.*, vol. 21, no. 8, pp. 1811–1814, Aug. 2017.

[53] X. Liu, H. Chen, M. Peng, and F. Yang, "Identical code cyclic shift multiple access—a bridge between CDMA and NOMA," *IEEE Trans. on Vehic. Tech.*, vol. 69, no. 3, pp. 2878–2890, Mar. 2020.

[54] C. Jiang and Y. Wang, "An uplink SCMA codebook design combining probabilistic shaping and geometric shaping," *IEEE Access*, vol. 8, pp. 76 726–76 736, Apr. 2020.

[55] G. Song, K. Cai, Y. Chi, J. Guo, and J. Cheng, "Super-sparse on-off division multiple access: Replacing repetition with idling," *IEEE Trans. Commun.*, vol. 68, no. 4, pp. 2251–2263, Apr. 2020.

[56] N. Ye, X. Li, H. Yu, L. Zhao, W. Liu, and X. Hou, "DeepNOMA: A unified framework for NOMA using deep multi-task learning," *IEEE Trans. Commun.*, vol. 19, no. 4, pp. 2208–2225, Apr. 2020.

[57] H. Xie, W. Xu, H. Q. Ngo, and B. Li, "Non-coherent massive MIMO systems: A constellation design approach," *IEEE Trans. Wireless Commun.*, vol. 19, no. 6, pp. 3812–3825, Jun. 2020.

[58] L. Lan, Y. Y. Tai, S. Lin, B. Memari, and B. Honary, "New constructions of quasi-cyclic LDPC codes based on special classes of BIBD's for the AWGN and binary erasure channels," *IEEE Trans. Commun.*, vol. 56, no. 1, pp. 39–48, Jan. 2008.

[59] Y. Wu, E. Attang, and G. E. Atkin, "A novel noma design based on Steiner system," in *Proc. IEEE Int. Conf. Electro/Inf. Technol. (EIT)*, Rochester, U.S.A., May 2018, pp. 0846–0850.

[60] J. H. Dinitz and J. C. Colbourn, *Handbook of Combinatorial Designs*, 2nd ed. Chapman & Hall, CRC, 2007.

[61] M. Yoshida and T. Tanaka, "Analysis of sparsely-spread CDMA via statistical mechanics," in *Proc. IEEE Int. Symp. Inf. Theory (ISIT)*, Seattle, U.S.A., Jul. 2006, pp. 2378–2382.

[62] A. Montanari and D. Tse, "Analysis of belief propagation for non-linear problems: The example of CDMA (or: How to prove Tanaka's formula)," in *Proc. IEEE Inf. Theory Workshop (ITW)*, Punta del Este, Uruguay, Mar. 2006, pp. 160–164.

[63] J. Raymond and D. Saad, "Sparsely spread CDMA—a statistical mechanics-based analysis," *IEEE Trans. Inf. Theory*, vol. 40, no. 41, pp. 12 315–12 333, Sep. 2007.

[64] M. T. P. Le, G. C. Ferrante, T. Q. S. Quek, and M. Di Benedetto, "Fundamental limits of low-density spreading NOMA with fading," *IEEE Trans. Wireless Commun.*, vol. 17, no. 7, pp. 4648–4659, Jul. 2018.

[65] S. Chen, K. Peng, Y. Zhang, and J. Song, "A comparative study on the capacity of SCMA and LDSMA," in *Proc. Int. Wireless Commun. Mobile Computing Conf. (IWCMC)*, Limassol, Cyprus, Jun. 2018, pp. 1099–1103.

[66] M. AL-Imari, M. A. Imran, R. Tafazolli, and D. Chen, "Performance evaluation of low density spreading multiple access," in *Proc. Int. Wireless Commun. and Mobile Computing Conf. (IWCMC)*, Limassol, Cyprus, Aug. 2012, pp. 383–388.

[67] R. Hoshyar, R. Razavi, and M. Al-Imari, "LDS-OFDM an efficient multiple access technique," in *Proc. IEEE Veh. Technol. Conf. (VTC Spring)*, Taipei, Taiwan, May 2010, pp. 1–5.

[68] M. Li and S. V. Hanly, "Precoding optimization for the sparse MC-CDMA downlink communication," in *Proc. IEEE Int. Conf. on Commun. (ICC)*, Syndney, Australia, Jun. 2014, pp. 2106–2111.

[69] N. Suraweera, S. V. Hanly, and P. Whiting, "Distributed beamforming for the multicell sparsely-spread MC-CDMA downlink," in *Proc. IEEE Veh. Technol. Conf. (VTC-Spring)*, Syndney, Australia, Jun. 2017, pp. 1–5.

[70] B. Fontana da Silva, C. A. A. Meza, D. Silva, and B. F. Uchôa-Filho, "Exploiting spatial diversity in overloaded MIMO LDS-OFDM multiple access systems," in *Proc. IEEE 9th Latin-American Conf. on Commun. (LATINCOM)*, Guatemala City, Guatemala, Nov. 2017, pp. 1–6.

[71] Y. Liu, L. Yang, and L. Hanzo, "Spatial modulation aided sparse code-division multiple access," *IEEE Trans. Wireless Commun.*, vol. 17, no. 3, pp. 1474–1487, Mar. 2018.

[72] L. Wen, P. Xiao, R. Razavi, M. A. Imran, M. Al-Imari, A. Maaref, and J. Lei, "Joint sparse graph for FBMC/OQAM systems," *IEEE Trans. Veh. Technol.*, vol. 67, no. 7, pp. 6098–6112, Jul. 2018.

[73] A. Osamura, G. Song, J. Cheng, and K. Cai, "Sparse multiple access and code design with near channel capacity performance," in *Proc. Int. Symp. Inf. Theory and Its Applic. (ISITA)*, Singapore, Oct. 2018, pp. 139–143.

[74] S. Denno, R. Sasaki, and Y. Hou, "Low density signature based packet access with phase only adaptive precoding," in *Proc. IEEE Veh. Technol. Conf. (VTC-Spring)*, Kuala Lumpur, Malaysia, Apr. 2019, pp. 1–5.

[75] Y. Zhao, J. Hu, Z. Ding, and K. Yang, "Joint interleaver and modulation design for multi-user SWIPT-NOMA," *IEEE Trans. Commun.*, vol. 67, no. 10, pp. 7288–7301, Oct. 2019.

[76] S. Özyurt and O. Kucur, "Quadrature NOMA: A low-complexity multiple access technique with coordinate interleaving," *IEEE Wireless Commun. Lett.*, vol. 9, no. 9, pp. 1452–1456, Sep. 2020.

[77] R. Razavi, R. Hoshyar, M. A. Imran, and Y. Wang, "Information theoretic analysis of LDS scheme," *IEEE Commun. Lett.*, vol. 15, no. 8, pp. 798–800, Aug. 2011.

[78] M. K. Varanasi and T. Guess, "Optimum decision feedback multiuser equalization with successive decoding achieves the total capacity of the Gaussian multiple-access channel," in *Proc. Asilomar Conf. on Signals, Systems and Computers*, vol. 2, Pacific Grove, CA, U.S.A., Nov. 1997, pp. 1405–1409.

[79] R. Razavi, M. Ali Imran, and R. Tafazolli, "EXIT chart analysis for turbo LDS-OFDM receivers," in *Proc. Int. Wireless Commun. and Mobile Computing Conf. (IWCMC)*, Istanbul, Turkey, Jul. 2011, pp. 354–358.

[80] O. Shental, B. M. Zaidel, and S. S. Shitz, "Low-density code-domain NOMA: Better be regular," in *Proc. IEEE Int. Symp. Inf. Theory (ISIT)*, Aachen, Germany, Jun. 2017, pp. 2628–2632.

[81] B. M. Zaidel, O. Shental, and S. S. Shitz, "Sparse NOMA: A closed-form characterization," in *Proc. IEEE Int. Symp. Inf. Theory (ISIT)*, Colorado, U.S.A., Jun. 2018, pp. 1106–1110.

[82] M. AL-Imari, M. A. Imran, and R. Tafazolli, "Low density spreading for next generation multicarrier cellular systems," in *Proc. Int. Conf. on Future Commun. Networks*, Baghdad, Iraq, Apr. 2012, pp. 52–57.

[83] M. Li, C. Liu, and S. V. Hanly, "Precoding for the sparsely spread MC-CDMA downlink with discrete-alphabet inputs," *IEEE Trans. Veh. Technol.*, vol. 66, no. 2, pp. 1116–1129, Feb. 2017.

[84] M. Fantuz and C. D'Amours, "Low complexity PIC-MMSE detector for LDS systems," in *Proc. IEEE Canadian Conf. on Electrical and Computer Engineering (CECE)*, Edmonton, Canada, May 2019.

[85] R. Price and P. E. Green, "A communication technique for multipath channels," *Proc. IRE*, vol. 46, no. 3, pp. 555–570, Mar. 1958.

[86] S. Craw, "Manhattan Distance," in *Encyclopedia of Machine Learning*, C. Sammut and G. I. Webb, Eds. Boston, MA: Springer US, 2010, pp. 639–639.

[87] M. Rupf and J. L. Massey, "Optimum sequence multisets for synchronous code-division multiple-access channels," *IEEE Trans. Inf. Theory*, vol. 40, no. 4, pp. 1261–1266, Jul. 1994.

[88] P. Viswanath and V. Anantharam, "Optimal sequences and sum capacity of synchronous CDMA systems," *IEEE Trans. Inf. Theory*, vol. 45, no. 6, pp. 1984–1991, Sep. 1999.

[89] F. Vanhaverbeke and M. Moeneclaey, "Sum capacity of the OCDMA/OCDMA signature sequence set," *IEEE Commun. Lett.*, vol. 6, no. 8, pp. 340–342, Aug. 2002.

[90] L. Welch, "Lower bounds on the maximum cross correlation of signals (Corresp.)," *IEEE Trans. Inf. Theory*, vol. 20, no. 3, pp. 397–399, May 1974.

[91] N. Hurley and S. Rickard, "Comparing Measures of Sparsity," *IEEE Trans. Inf. Theory*, vol. 55, no. 10, pp. 4723–4741, Oct. 2009.

[92] S. Ulukus and R. D. Yates, "Iterative construction of optimum signature sequence sets in synchronous CDMA systems," *IEEE Trans. Inf. Theory*, vol. 47, no. 5, pp. 1989–1998, Jul. 2001.

[93] M. Soltanalian and P. Stoica, "Designing unimodular codes via quadratic optimization," *IEEE Trans. on Signal Proc.*, vol. 62, no. 5, pp. 1221–1234, Mar. 2014.

[94] M. Kobayashi, J. Boutros, and G. Caire, "Successive interference cancellation with SISO decoding and EM channel estimation," *IEEE J. Sel. Areas Commun.*, vol. 19, no. 8, pp. 1450–1460, Aug. 2001.

[95] M. K. Varanasi and B. Aazhang, "Multistage detection in asynchronous code-division multiple-access communications," *IEEE Trans. Commun.*, vol. 38, no. 4, pp. 509–519, Apr. 1990.

[96] G. Xue, J. Weng, T. Le-Ngoc, and S. Tahar, "Adaptive multistage parallel interference cancellation for CDMA," *IEEE J. Sel. Areas Commun.*, vol. 17, no. 10, pp. 1815–1827, Oct. 1999.

[97] D. Guo, L. K. Rasmussen, S. Sun, and T. J. Lim, "A matrix-algebraic approach to linear parallel interference cancellation in CDMA," *IEEE Trans. Commun.*, vol. 48, no. 1, pp. 152–161, Jan. 2000.

[98] M. C. Reed, C. B. Schlegel, P. D. Alexander, and J. A. Asenstorfer, "Iterative multiuser detection for CDMA with FEC: near-single-user performance," *IEEE Trans. Commun.*, vol. 46, no. 12, pp. 1693–1699, Dec. 1998.

[99] X. Wang and H. V. Poor, "Iterative (turbo) soft interference cancellation and decoding for coded CDMA," *IEEE Trans. Commun.*, vol. 47, no. 7, pp. 1046–1061, Jul. 1999.

[100] S. Morosi, R. Fantacci, E. Del Re, and A. Chiassai, "Design of turbo-MUD receivers for overloaded CDMA systems by density evolution technique," *IEEE Trans. Wireless Commun.*, vol. 6, no. 10, pp. 3552–3557, Oct. 2007.

[101] P. Kumar and S. Chakrabarti, "An analytical model of iterative interference cancellation receiver for orthogonal/orthogonal overloaded DS-CDMA system," *Int. J. Wirel. Inf. Netw.*, vol. 17, no. 1-2, pp. 64–72, Jun. 2010.
[102] S. Sasipriya and C. S. Ravichandran, "An analytical model of iterative interference cancellation receiver for orthogonal/orthogonal overloaded DS-CDMA system," *Telecommun. Syst.*, vol. 56, no. 4, pp. 509–518, Aug. 2014.
[103] A. Najkha, C. Roland, and E. Boutillon, "A near-optimal multiuser detector for MC-CDMA systems using geometrical approach," in *Proc. IEEE Int. Conf. on Acoust., Speech, and Sig. Proc. (ICASSP)*, vol. 3, Philadelphia, U.S.A., Mar. 2005, pp. 877–880.
[104] G. Manglani and A. K. Chaturvedi, "Application of computational geometry to multiuser detection in CDMA," *IEEE Trans. Commun.*, vol. 54, no. 2, pp. 204–207, Feb. 2006.
[105] Y. Du, B. Dong, P. Gao, Z. Chen, J. Fang, and S. Wang, "Low-complexity LDS-CDMA detection based on dynamic factor graph," in *Proc. IEEE Global Telecommun. Conf. Workshops (GC Wkshps)*, Washington, U.S.A., Dec. 2016, pp. 1–6.
[106] L. Tian, J. Zhong, M. Zhao, and L. Wen, "An optimized superposition constellation and region-restricted MPA detector for LDS system," in *Proc. IEEE Int. Conf. on Commun. (ICC)*, Kuala Lumpur, Malaysia, May 2016, pp. 1–5.
[107] L. Wen, R. Razavi, P. Xiao, and M. A. Imran, "Fast convergence and reduced complexity receiver design for LDS-OFDM system," in *Proc. IEEE Pers., Indoor, Mobile Radio Conf. (PIMRC)*, Washington DC, U.S.A., Sep. 2014, pp. 918–922.
[108] D. Guo and C. Wang, "Multiuser detection of sparsely spread CDMA," *IEEE Journal on Selected Areas in Commun.*, vol. 26, no. 3, pp. 421–431, Apr. 2008.
[109] K. Takeuchi, T. Tanaka, and T. Kawabata, "Performance improvement of iterative multiuser detection for large sparsely spread CDMA systems by spatial coupling," *IEEE Trans. Inf. Theory*, vol. 61, no. 4, pp. 1557–9654, Apr. 2015.
[110] L. Wen, R. Razavi, M. A. Imran, and P. Xiao, "Design of joint sparse graph for OFDM system," *IEEE Trans. on Wireless Commun.*, vol. 15, no. 4, pp. 1823–1836, Apr. 2015.
[111] L. Wen and M. Su, "Joint sparse graph over GF(q) for code division multiple access systems," *IET Communications*, vol. 9, no. 5, pp. 707–718, Mar. 2015.
[112] L. Wen, J. Lei, and M. Su, "Improved algorithm for joint detection and decoding on the joint sparse graph for CDMA systems," *IET Communications*, vol. 10, no. 3, pp. 336–345, Feb. 2016.
[113] J. Raymond, "Optimal sparse CDMA detection at high load," in *Proc. Int. Symp. Modeling Optim. Mobile, Ad Hoc, Wireless Netw. (WiOpt)*, Seoul, South Korea, Jun. 2009, pp. 1–5.
[114] J. G. Proakis, *Digital Communications*, 5th ed. McGraw Hill, 2007.
[115] G. H. Golub and C. F. Van Loan, *Matrix Computations*, 4th ed. The Johns Hopkins University Press, 2013.
[116] J. Luo, K. R. Pattipati, and P. K. Willett, "Near-optimal multiuser detection in synchronous CDMA using probabilistic data association," *IEEE Commun. Lett.*, vol. 5, no. 9, pp. 361–366, Sep. 2001.
[117] G. L. Turin, "Introduction to spread-spectrum antimultipath techniques and their application to urban digital radio," *Proc. IEEE*, vol. 68, no. 3, pp. 328–353, Mar. 1980.
[118] C. D'Amours, M. Moher, and A. Yongacoglu, "Comparison of pilot symbol-assisted and differentially detected BPSK for DS-CDMA systems employing RAKE receivers in Rayleigh fading channels," *IEEE Trans. on Vehic. Tech.*, vol. 47, no. 4, pp. 1258–1267, Nov. 1998.
[119] L. Hanzo, M. Münster, B. Choi, and T. Keller, *OFDM and MC-CDMA for Broadband Multi-User Communications, WLANs and Broadcasting*. John Wiley & Sons, 2003.
[120] L. Hanzo, L.-L. Yang, E.-L. Kuan, and K. Yen, *Single- and Multi-Carrier DS-CDMA: Multi-User Detection, Space-Time Spreading, Synchronisation, Networking and Standards*. Wiley-IEEE Press, 2003.
[121] M. Kulhandjian, E. Bedeer, H. Kulhandjian, C. D'Amours, and H. Yanikomeroglu, "Low-complexity detection for faster-than-Nyquist signaling based on probabilistic data association," *IEEE Commun. Lett.*, pp. 1–6, Dec. 2019.
[122] D. Pham, K. R. Pattipati, P. K. Willett, and J. Luo, "A generalized probabilistic data association detector for multiple antenna systems," *IEEE Commun. Lett.*, vol. 8, no. 4, pp. 205–207, Apr. 2004.
[123] S. Yang, T. Lv, R. G. Maunder, and L. Hanzo, "Unified bit-based probabilistic data association aided MIMO detection for high-order QAM constellations," *IEEE Trans. on Vehic. Tech.*, vol. 60, no. 3, pp. 981–991, Mar. 2011.
[124] M. Kulhandjian and C. D'Amours, "Design of permutation-based sparse code multiple access system," in *Proc. IEEE Pers., Indoor, Mobile Radio Conf. (PIMRC)*, Montreal, Canada, Oct. 2017, pp. 1031–1035.
[125] C. E. Shannon, "A mathematical theory of communication," *The Bell Syst. Tech. Journal*, vol. 27, no. 4, pp. 623–656, Oct. 1948.
[126] H. Imai and S. Hirakawa, "A new multilevel coding method using error-correcting codes," *IEEE Trans. Inf. Theory*, vol. 23, no. 3, pp. 371–377, May 1977.
[127] ——, "Correction to 'A new multilevel coding method using error-correcting codes'," *IEEE Trans. Inf. Theory*, vol. 23, no. 6, pp. 784–784, Nov. 1977.
[128] G. Ungerboeck, "Channel coding with multilevel/phase signals," *IEEE Trans. Inf. Theory*, vol. 28, no. 1, pp. 55–67, Jan. 1982.
[129] ——, "Trellis-coded modulation with redundant signal sets Part I: Introduction," *IEEE Commun. Mag.*, vol. 25, no. 2, pp. 5–11, Feb. 1987.
[130] ——, "Trellis-coded modulation with redundant signal sets Part II: State of the art," *IEEE Commun. Mag.*, vol. 25, no. 2, pp. 12–21, Feb. 1987.
[131] E. Zehavi, "8-PSK trellis codes for a Rayleigh channel," *IEEE Trans. Commun.*, vol. 40, no. 5, pp. 873–884, May 1992.
[132] B. N. Thanh, V. Krishnamurthy, and R. J. Evans, "Detection-aided recursive least squares adaptive multiuser detection in DS/CDMA," *IEEE Signal Proc. Lett.*, vol. 9, no. 8, pp. 229–232, Aug. 2002.
[133] Y. Du, B. Dong, Z. Chen, J. Fang, and X. Wang, "A fast convergence multiuser detection scheme for uplink SCMA systems," *IEEE Wireless Commun. Lett.*, vol. 5, no. 4, pp. 388–391, Aug. 2016.
[134] Li Ping, W. K. Leung, and Nam Phamdo, "Low density parity check codes with semi-random parity check matrix," *Electronics Letters*, vol. 35, no. 1, pp. 38–39, Jan. 1999.
[135] H. Zarrinkoub, *Understanding LTE with MATLAB: From Mathematical Modeling to Simulation and Prototyping*, 1st ed. Wiley Publishing, 2014.
[136] H. Vangala, E. Viterbo, and Y. Hong, "A comparative study of polar code constructions for the AWGN channel," *arXiv:1501.02473 [cs.IT]*, Jan. 2015. [Online]. Available: https://arxiv.org/abs/1501.02473
[137] S. Verdu, "Spectral efficiency in the wideband regime," *IEEE Trans. Inf. Theory*, vol. 48, no. 6, pp. 1319–1343, Jun. 2002.
[138] T. M. Cover and J. A. Thomas, *Elements of Information Theory*. USA: Wiley-Interscience, 2006.
[139] Sheng Chen, A. K. Samingan, B. Mulgrew, and L. Hanzo, "Adaptive minimum-BER linear multiuser detection for DS-CDMA signals in multipath channels," *IEEE Trans. on Signal Proc.*, vol. 49, no. 6, pp. 1240–1247, Jun. 2001.

MICHEL KULHANDJIAN (M'18-SM'20) received his M.S. and Ph.D. degrees in Electrical Engineer from the State University of New York at Buffalo in 2007 and 2012, respectively. He had previously received his B.S. degree in Electronics Engineering and Computer Science (Minor), with "Summa Cum Laude" from the American University in Cairo (AUC) in 2005. He was employed at Alcatel-Lucent, in Ottawa, Ontario, in 2012. In the same year he was appointed as a Research Associate at EION Inc. He received Natural Science and Engineering Research Council of Canada (NSERC) Industrial R&D Fellowship (IRDF). He is currently a Research Scientist at the School of Electrical Engineering and Computer Science at the University of Ottawa. He is also employed as a senior embedded software engineer at L3Harris Technologies.

His research interests include wireless multiple access communications, adaptive coded modulation, waveform design for overloaded code-division multiplexing applications, channel coding, space-time coding, adaptive multiuser detection, statistical signal processing, covert communications, spread-spectrum steganography and steganalysis. He has served as a guest editor for Journal of Sensor and Actuator Networks (JSON). He actively serves as member of Technical Program Committee (TPC) of IEEE WCNC, IEEE GLOBECOM, IEEE ICC, and IEEE VTC.

HOVANNES KULHANDJIAN (S'14-M'15-SM'20) received the B.S. degree (magna cum laude) in electronics engineering from The American University in Cairo, Cairo, Egypt, in 2008, and the M.S. and Ph.D. degrees in electrical engineering from the State University of New York at Buffalo, Buffalo, NY, USA, in 2010 and 2014, respectively. From December 2014 to July 2015, he was an Associate Research Engineer with the Department of Electrical and Computer Engineering, Northeastern University, Boston, MA, USA. He is currently an Assistant Professor with the Department of Electrical and Computer Engineering, California State University, Fresno, Fresno, CA, USA. His current research interests include wireless communications and networking, with applications to underwater acoustic communications, visible light communications and applied machine learning. He has served as a guest editor for IEEE Access - Special Section Journal on Underwater Wireless Communications and Networking. He has also served as a Session Co-Chair for IEEE UComms 2020, Session Chair for ACM WUWNet 2019. He actively serves as a member of the Technical Program Committee for ACM and IEEE conferences such as IEEE GLOBECOM 2015-2020, UComms 2020, PIMRC 2020, WD 2019, ACM WUWNet 2019, ICC 2015-2018, among others.

CLAUDE D'AMOURS received the degrees of B.A.Sc, M.A.Sc. and Ph.D. in Electrical Engineering from the University of Ottawa in 1990, 1992 and 1995 respectively. In 1992 he was employed as a Systems Engineer at Calian Communications Ltd. In 1995 he joined the Communications Research Centre in Ottawa, Ontario, Canada, as a Systems Engineer. Later in 1995, he joined the Department of Electrical and Computer Engineering at the Royal Military College of Canada in Kingston, Ontario, Canada, as an Assistant Professor. He joined the School of Information Technology and Engineering (SITE), which has since been renamed as the School of Electrical Engineering and Computer Science (EECS), at the University of Ottawa as an Assistant Professor in 1999. From 2007-2011, he served as Vice Dean of Undergraduate Studies for the Faculty of Engineering and has been serving as the Director of the School of EECS at the University of Ottawa since 2013. His research interests are in physical layer technologies for wireless communications systems, notably in multiple access techniques and interference cancellation.

LAJOS HANZO (M'91-SM'92-F'04) (http://www-mobile.ecs.soton.ac.uk, https://en.wikipedia.org/wiki/Lajos_Hanzo) (FIEEE'04, Fellow of the Royal Academy of Engineering F(REng), of the IET and of EURASIP), received his Master degree and Doctorate in 1976 and 1983, respectively from the Technical University (TU) of Budapest. He was also awarded the Doctor of Sciences (DSc) degree by the University of Southampton (2004) and Honorary Doctorates by the TU of Budapest (2009) and by the University of Edinburgh (2015). He is a Foreign Member of the Hungarian Academy of Sciences and a former Editor-in-Chief of the IEEE Press. He has served several terms as Governor of both IEEE ComSoc and of VTS. He has published 1900+ contributions at IEEE Xplore, 19 Wiley-IEEE Press books and has helped the fast-track career of 123 PhD students. Over 40 of them are Professors at various stages of their careers in academia and many of them are leading scientists in the wireless industry.